ELECTRIC FIELDS AND SOLVATION IN MICRSCOPIC LIQUIDS

by

Daniel R. Martin

A Thesis Presented in Partial Fulfillment
of the Requirements for the Degree
Master of Science

ARIZONA STATE UNIVERSITY

August 2008

ELECTRIC FIELDS AND SOLVATION IN MICRSCOPIC LIQUIDS

by

Daniel R. Martin

has been approved

August 2008

Graduate Supervisory Committee

Dmitry V. Matyushov, Chair
Timothy Steimle
Arjan van der Vaart

ACCEPTED BY THE GRADUATE COLLEGE

ABSTRACT

The presentation of the results of an analytical model and simulations of the cavity, reaction, and local fields inside a dipolar liquid as well as studies of the solvation thermodynamics of dipolar or point-charge solutes show significant differences between simulation results and continuum solutions, as well as some distinct differences with the microscopic theory of solvation. The analytical microscopic theory shows that the equations of continuum electrostatics, *i.e.* Maxwell's cavity field, Onsager's local and reaction fields, and the Onsager and Born equations pertaining to electrostatic solvation theory, are not realized in the context of simulations. The analytical solution for the cavity field is shown to only be continuum like through a singularity in the microscopic response function representing a non-decaying longitudinal polarization wave, while the reaction field, although predicted quite well from the analytical theory, does not correspond to the continuum solution whatsoever. The continuum cavity field solutions obtained here depend on the order of continuum and thermodynamic limits taken in the microscopic equations. Fields in microscopic cavities are much different from macroscopic predictions approaching with increasing cavity size a new continuum expression derived from the microscopic equations. Numerical Monte Carlo simulations never reach the standard continuum limit and instead converge to a new continuum solution.

The presentation of the simulation results for the fluctuations of the electrostatic potential and electric field show significant differences from the corresponding continuum results. We found that the thermodynamics of polar solvation dramatically change from what is expected when the cavity size becomes about 4-5 times larger than the size of the liquid solvent particles. The range of small cavities can be reasonably understood within the framework of current solvation models. On the contrary, the regime of large

cavities is characterized by a significant softening of the cavity interface resulting in the decay of the fluctuation variances with the cavity size much faster than anticipated by both the continuum electrostatics and microscopic theories. For instance, the variance of potential decays with the cavity size approximately between one over the cavity radius to the fourth and sixth instead of the inverse of the cavity radius scaling expected from standard electrostatics. The results presented suggest that cores of non-polar molecular assemblies in polar liquids lose solvation strength much faster than is traditionally anticipated.

TABLE OF CONTENTS

Page

LIST OF TABLES

LIST OF FIGURES

CHAPTER 1

The Basics of Dielectrics and Polarization

There exists so much material on the properties of dielectrics that to make a simple overview of the subject is nearly impossible for even the most intelligent of scientists. For this reason only a very brief overview of the relevant material will be provided. Some of the literature about polarization and dielectrics exists only as sections of textbooks while a few complete textbooks have been written. The subject matter can be found in the included references [1, 2, 3, 4, 5, 6] along with many others. This chapter will be organized as to provide a conceptual understanding of dielectrics in Section I of this chapter, basics about continuum dielectrics and polarization in Section II of this chapter including the concepts of bound and free charge and the relationship between the Maxwell field and the bulk polarization. Section III will discuss some of the concepts pertaining to fields in dielectrics from a continuum point of view, while Section IV will discuss very briefly the statistical mechanical approach to treating dielectric material, specifically dealing with the Debye and Onsager equations and the Kirkwood factor. Finally, in Section V a more modern approach to dielectrics will be discussed and how it pertains to the dielectric constant through the longitudinal and transverse k-dependent structure factors.

I. Simple Explanation of Complex Phenomena

In the late 1800's Faraday noticed that if an insulator was placed between the plates of a parallel plate capacitor, the capacitance would increase compared to the capacitor without insulating material. He also noticed that the increase in the capacitance was dependent only on the properties of the insulating material. Eventually, this behavior was explained with the help of Maxwell and Lorentz. A simple idea to clarify their discoveries can be thought of by considering a bunch of atoms each isolated in their own separate perfectly conducting sphere, insulated between each atom and of a density of a liquid or solid at standard conditions. When these atoms are collectively placed into a plate capacitor the

'surface charge' on each sphere will orient itself so that the field inside is eliminated. This behavior results in an overall effective dipole sitting on each sphere. The collective reorientation described requires some energy and therefore results in the entire slab of insulating material storing energy, which explains why there is an increase in capacitance. This 'model' is, of course, not to be taken literally since molecules are not perfectly conducting spheres, but does allow for a relatively simple explanation of some very complicated behavior.

From a more modern perspective, we know that an atom is made of positively charged protons and negatively charge electrons. When an electric field is applied, as in the case of the parallel plate capacitor, the electrons become displaced from the positively charged atomic center. The displacement between the electrons and protons is what actually creates the dipole moment necessary in the above description to create the overall increase in capacitance. Since the individual dipole moment of each atom is a local property, it is nice to introduce the polarization of a material, which is defined as the average dipole moment of the entire system divided by its volume. As will be seen in the next section, the polarization can be related to the electric field inside a material through the static dielectric constant. Along with this idea, a mathematical introduction to the subject of dielectrics will be given in the following sections.

In the two cases given above, we have taken something from an atomic point of view and attempted to explain the overall behavior of the bulk system. We have gained insight into the 'microscopic' world by attempting to deduce information from what we know about physically observable properties in the 'macroscopic' world. This process is, of course, extremely important in the development of the subject even though there are times when it is possible to observe some behavior of a system without having any verifiability. This distinction will become more clear as we see differences in continuum dielectric theory

and the microscopic theories that are currently being developed.

II. Continuum Dielectrics and Polarization

In continuum theories of dielectrics a linear relationship is assumed (experimentally verifiable) to exist between the polarization and the Maxwell field. This relation is given by

$$\mathbf{P}(\mathbf{r}) \;=\; \frac{\epsilon - 1}{4\pi}\,\mathbf{E}(\mathbf{r})\,, \tag{1.1}$$

where ϵ is the static or frequency-dependent bulk dielectric constant while $\mathbf{E}(\mathbf{r})$ and $\mathbf{P}(\mathbf{r})$ are the respective Maxwell field and polarization vector. The well known expression given in Eq. (1.1) has a long history of understanding and can be physically interpreted after considering some basic electrostatics. In particular, consider the potential due to a dipolar system contained in a volume Ω'. This potential is given by

$$\begin{aligned} V(\mathbf{r}) &= \int_{\Omega'} \frac{\mathbf{P}(\mathbf{r}')\cdot(\mathbf{r}-\mathbf{r}')}{|\mathbf{r}-\mathbf{r}'|^3}\; d^3r' \\ &= \int_{\Omega'} \mathbf{P}(\mathbf{r}')\cdot\boldsymbol{\nabla}'\left(\frac{1}{|\mathbf{r}-\mathbf{r}'|}\right)\; d^3r'\,, \end{aligned} \tag{1.2}$$

where $\mathbf{P}(\mathbf{r})$ is the dipole moment per unit volume. Integration by parts yields

$$V(\mathbf{r}) \;=\; \int_{\Omega'} \left[\boldsymbol{\nabla}'\cdot\left(\frac{\mathbf{P}(\mathbf{r}')}{|\mathbf{r}-\mathbf{r}'|}\right) - \frac{1}{|\mathbf{r}-\mathbf{r}'|}\left(\boldsymbol{\nabla}'\cdot\mathbf{P}(\mathbf{r}')\right)\right]\; d^3r'\,. \tag{1.3}$$

After using the divergence theorem, *i.e.*

$$\int_V \boldsymbol{\nabla}\cdot\left(\mathbf{A}(\mathbf{r})\,f(r)\right)\,dV \;=\; \oint_\sigma f(r)\,\mathbf{A}(\mathbf{r})\cdot\hat{\boldsymbol{n}}\;d\sigma\,, \tag{1.4}$$

Eq. (1.3) becomes

$$V(\mathbf{r}) \;=\; \oint_{\partial\Omega'} \frac{1}{|\mathbf{r}-\mathbf{r}'|}\left(\mathbf{P}(\mathbf{r}')\cdot\hat{\boldsymbol{n}}'\right)\; d^2r' - \int_{\Omega'} \frac{1}{|\mathbf{r}-\mathbf{r}'|}\left(\boldsymbol{\nabla}'\cdot\mathbf{P}(\mathbf{r}')\right)\; d^3r'\,, \tag{1.5}$$

where the unit vector $\hat{\boldsymbol{n}}'$ is normal to the surface $\partial\Omega'$ which bounds the volume Ω'. After some consideration, one sees that Eq. (1.5) can be interpreted as the sum of the potentials

from two types of 'bound' charges. The first term can be interpreted as the potential due to the charge bound to the surface, while the second term is due to the charge density fixed inside the dielectric. These charge densities can be expressed as

$$\sigma_b(\mathbf{r}) \;=\; \mathbf{P}(\mathbf{r}) \cdot \hat{\boldsymbol{n}}\,, \tag{1.6}$$

and

$$\rho_b(\mathbf{r}) \;=\; -\boldsymbol{\nabla} \cdot \mathbf{P}(\mathbf{r})\,, \tag{1.7}$$

respectively.

The idea of bound charge in this context is used to physically interpret the terms in the potential given in Eq. (1.5), although the meaning does imply some real physics. Consider a bunch of dipoles fixed inside of a sample with a constant volume and subject to the force of an external field which is strong enough to align the dipoles on average head to tale. The result of this scenario is that the local field inside the sample will be canceled between the dipoles since the tale of one dipole will be on average at the head of another dipole. The surface of the sample will therefore have a net accumulation of either heads or tales depending on the direction of the external field. In more realistic terms, the electrons inside the atoms that make up a dielectric are not 'free' to move about as in a metal, but are physically bound to the atoms which in the presence of an external field can be polarized such that the positive and negative ends are aligned resulting in an accumulation of negative charge at one end and a lack of negative charge (positive) at the other end. In this context the idea of bound charge is not just used as a superficial tool for interpreting mathematics, but does give some physical insight into the average microscopic effects that make up microscopic dielectrics.

With the idea of bound and free charge, one can rewrite the total charge density in

Gauss's law as

$$\begin{aligned} \boldsymbol{\nabla} \cdot \mathbf{E}(\mathbf{r}) &= 4\pi\rho(\mathbf{r}) \\ &= 4\pi(\rho_b(\mathbf{r}) + \rho_f(\mathbf{r})) \\ &= 4\pi(-\boldsymbol{\nabla} \cdot \mathbf{P}(\mathbf{r}) + \rho_f(\mathbf{r}))\,, \end{aligned} \tag{1.8}$$

where ρ_f represents the 'free' charge. Rearranging Eq. (1.8) results in

$$\nabla \cdot (\mathbf{E}(\mathbf{r}) + 4\pi\mathbf{P}(\mathbf{r})) = 4\pi\rho_f(\mathbf{r})\,, \tag{1.9}$$

from which the electric displacement can be defined as the field created from the Maxwell field $\mathbf{E}(\mathbf{r})$ plus the field due to the accumulation of charge within the dielectric. The sum of these two contributions is called the electric displacement and is given by

$$\mathbf{D}(\mathbf{r}) \equiv \mathbf{E}(\mathbf{r}) + 4\pi\,\mathbf{P}(\mathbf{r})\,. \tag{1.10}$$

Finally, Gauss's law can be rewritten as

$$\nabla \cdot \mathbf{D}(\mathbf{r}) = 4\pi\rho(\mathbf{r})\,, \tag{1.11}$$

where the subscript f has been dropped for convenience. The right hand side of Eq. (1.11) for perfect insulators is zero indicating that the charge responsible for its electric properties is bound to the atoms within the substance, at least on average.

The components of the polarization vector $\mathbf{P}(\mathbf{r})$ can in general be written in a Taylor series in the Maxwell field $\mathbf{E}(\mathbf{r})$ with tensorial coefficients. Explicitly, this may look like

$$P_i = \chi^{(1)}_{ij}\,E_j + \chi^{(2)}_{ijk}\,E_j\,E_k + \cdots\,, \tag{1.12}$$

where the Einstein summation convention is used for repeated indices. Thus, for small fields the first term is leading and there exists a linear relationship between the polarization

and the Maxwell field. In fact, if **P** and **E** are taken to be parallel, the second rank tensor $\chi^{(1)} = \chi$ (referred to as the susceptibility) is diagonal. Furthermore, for an isotropic dielectric with no preferential direction, the three components of the susceptibility are equivalent, and the polarization may be written as

$$\mathbf{P}(\mathbf{r}) \;=\; \chi\,\mathbf{E}(\mathbf{r})\,. \tag{1.13}$$

Using Eq. (1.13) along with the relationship between the electric displacement and the Maxwell field given by $\mathbf{D}(\mathbf{r}) = \epsilon\,\mathbf{E}(\mathbf{r})$, one finds an expression relating the susceptibility and the dielectric constant given by

$$\chi \;=\; \frac{\epsilon - 1}{4\,\pi}\,. \tag{1.14}$$

Putting Eq. (1.14) into Eq. (1.13), we arrive at the expression given in Eq. (1.1),

$$\mathbf{P}(\mathbf{r}) \;=\; \frac{\epsilon - 1}{4\,\pi}\,\mathbf{E}(\mathbf{r})\,. \tag{1.15}$$

It must be noted here that even though the relationship is applicable in many circumstances, there does exist the generalization of Eq. (1.15) in Eq. (1.12) since the value of the susceptibility can, in general, depend on the spatial coordinates inside a dielectric. Also, this relationship is what will be used to calculate the fields in molecular dielectrics using hard sphere dipolar (DHS) system as the testing ground. Of course, we will need correct this response function since we will be concerned with the local properties of solutes and cavities of the dipolar system.

III. Fields Inside Dielectrics: Continuum Approach

To begin to understand the complication that may arise from looking at the detailed nature of dielectric materials, it is important to begin to understand the average effects of other atoms in the vicinity of the molecules that make up the dielectric. Throughout

this particular 'thermodynamic' approach to the subject matter, one must consider electric fields inside dielectrics both from a global, continuum point of view (a la Maxwell) and from the more modern approach of using statistical mechanics and microscopic solvation theory. In this section we will be mostly concerned with the continuum approach to dielectric a good understanding of the framework is imperative to understand the details of a more sophisticated theory. As will be seen, an understanding of the local field is required in order to understand the macroscopic properties of dielectrics and the general electric fields that are used in the experimental treatment of real molecules. The continuum approach considered here will therefore establish the conceptual understanding needed to move forward into the microscopic theory of dielectrics.

To give proper respect to all the wonderful texts on the subject of electrostatics and material Maxwell's equations, we will first consider a slab of dielectric material sandwiched between the plates of a parallel plate capacitor. This capacitor is connected to a battery of some sort that can be turned on and off, and varied as to control the electric field produced between the plates. When the applied field is turned on, there is an electric field induced inside the dielectric due to the charges being displaced and the surface charges that are produced. If we consider just a small rectangular section of the dielectric, then the electric field inside this section is equal to

$$\begin{aligned} \mathbf{E}_{in} &= \mathbf{E}_+ + \mathbf{E}_- \\ &= (-2\pi\sigma_+ + 2\pi\sigma_-)\hat{n} \\ &= -4\pi\sigma\hat{n} \;=\; -4\pi\mathbf{P}\,, \end{aligned} \tag{1.16}$$

where σ_+ and σ_- are the positive and negative surface charges on the respective surfaces and $\hat{n}$ is the unit vector pointing normal to the surface of the negatively charge plate to

the positively charged plate. Therefore, the total field inside the dielectric is the sum of the applied field and the field inside the dielectric due to the polarization,

$$\begin{aligned} \mathbf{E} &= \mathbf{E}_0 + \mathbf{E}_{in} \\ &= \mathbf{E}_0 - 4\pi\mathbf{P}\,. \end{aligned} \tag{1.17}$$

Using Maxwell's Displacement, $\mathbf{D} = \mathbf{E} + 4\pi\mathbf{P}$, we find that $\mathbf{D} = \mathbf{E}_0 = \epsilon\mathbf{E}$. Thus, the Maxwell field inside the dielectric can be expressed in terms of the applied field. This expression means that the relationship between electric field inside the material and the applied field is only dependent upon the nature of the material, *i.e.* the dielectric constant ϵ.

Now we can extend this picture by considering a sphere inside the dielectric. At this point there are two methods to create the sphere. A spherical cavity could be carved in the dielectric so that there is a vacuum inside the cavity. Using this picture and solving Laplace's equation, one finds the electric field at the center of the cavity to be

$$\begin{aligned} \mathbf{E}_c &= \frac{3\epsilon}{2\epsilon+1}\mathbf{E} \\ &= \frac{3}{2\epsilon+1}\mathbf{E}_0\,. \end{aligned} \tag{1.18}$$

The details of this calculation can be found in Appendix C, in particular, the discussion leading up to Eq. (C12).

An alternative approach in dealing with fields inside dielectric materials is to consider a virtual cavity in which there is still dielectric material inside the cavity. In this case when the external field is applied, the cavity becomes uniformly polarized and charges appear on the surface of the cavity. The field inside the cavity is given by

$$\mathbf{E}_c = \frac{\epsilon+2}{3\epsilon}\mathbf{E}_0\,. \tag{1.19}$$

This particular expression is know as the Lorentz field and can be derived by taking the negative of the field inside a polarized sphere given Appendix A as the internal field, using the relationship given in Eq. (1.15), and simply adding that result to the Maxwell field inside a dielectric.

Here the question then becomes which field should be used in defining the local field acting on a molecule inside a dielectric. Since the local field can be defined as the sum of the cavity field and the Onsager reaction field [12],

$$\mathbf{R} \;=\; \frac{2(\epsilon-1)}{2\epsilon+1}\frac{\mathbf{m}_0}{R_0^3}\,, \tag{1.20}$$

($\mathbf{m}_0$ is the on-site dipole moment) it is of great importance to thoroughly understand how these equations become realized in both microscopic and macroscopic theories of dielectrics. The derivation of the reaction field is also given in Appendix C.

The formulation of Maxwell's equations for dielectric materials is in its essence a boundary value problem and depends completely on the discontinuity of the dipolar polarization at the dielectric boundary. If the dielectric interface is different than what is assumed from Maxwell's equations, then the dielectric response could be completely different from that which is predicted by this type of continuum approach. This is, of course, only if the size of the cavity is not in some sense macroscopic. Thus, three size scales will be introduced; the macroscopic size, in which Maxwell's equations can be applied to predict the overall behavior, the microscopic size, in which molecular sizes become extremely significant and solvation surfaces can have great effects on the local behavior, and the mesoscopic size for which there is the possibility of a transition between the macroscopic and microscopic sizes.

IV. Statistical Mechanics Applied to Dielectrics

The detailed molecular structure of a typical dielectric material including electronic, dipolar and quadrupolar structures, make it very difficult to understand the full nature of a real dielectric, especially from a quantum mechanical point of view. What can be done is that from a statistical point of view. The previous sections have presented the ideas of dielectrics in terms of macroscopic quantities using arguments relating average microscopic effects. Even though these ideas were motivated within the context of individual molecules, the detailed microscopic viewpoint has not been fully considered. In doing so, the interactions of the individual molecules become important and must be considered. These interactions can be expressed as a potential that depends on the position and orientation of all the individual molecules. In the presence of an external field, the potential for a system of interacting, non-polarizable dipoles surrounded by a macroscopic dielectric with dielectric constant ϵ can be written as

$$V_N(\mathbf{r}_N, \mathbf{\Omega}_N; \mathbf{E}_0) \;=\; U(\mathbf{r}_N, \mathbf{\Omega}_N) - \sum_{i=1}^{N} \mathbf{m}(\mathbf{\Omega}_i) \cdot \mathbf{E}_0 \,, \tag{1.21}$$

where $\mathbf{E}_0$ is the external electric field, $\mathbf{m}$ is the permanent dipole moment of the N identical molecules, and $\mathbf{r}_N$ and $\mathbf{\Omega}_N$ are sets of their positions and orientations, respectively. The potential excluding the individual dipole interactions with the external field due to only the dipolar interactions of the individual molecules, $U(\mathbf{r}_N, \mathbf{\Omega}_N)$ in Eq. (1.21), may be explicitly written as [13]

$$\begin{aligned} U(\mathbf{r}_N, \mathbf{\Omega}_N) \;=\; & U_0(\mathbf{r}_N, \mathbf{\Omega}_N) - \frac{1}{2} \sum_{i=1}^{N} \sum_{j \neq i}^{N} \mathbf{m}(\mathbf{\Omega}_i) \cdot \mathbf{T}(\mathbf{r}_i, \mathbf{r}_j) \cdot \mathbf{m}(\mathbf{\Omega}_j) \\ & - \frac{1}{2} \sum_{i=1}^{N} \sum_{j=1}^{N} \mathbf{m}(\mathbf{\Omega}_i) \cdot \mathbf{R}(\mathbf{r}_i, \mathbf{r}_j, \epsilon) \cdot \mathbf{m}(\mathbf{\Omega}_j) \,, \end{aligned} \tag{1.22}$$

where $\mathbf{T}(\mathbf{r}_i, \mathbf{r}_j)$ is the usual dipole-dipole tensor,

$$\begin{aligned} \mathbf{T}_{ij} \equiv \mathbf{T}(\mathbf{r}_i, \mathbf{r}_j) &= \boldsymbol{\nabla}_i \boldsymbol{\nabla}_j \left(\frac{1}{r_{ij}} \right) \\ &= \frac{1}{r_{ij}^3} \left[3 \frac{\mathbf{r}_{ij} \mathbf{r}_{ij}}{r_{ij}^2} - \mathbf{I} \right] , \end{aligned} \tag{1.23}$$

($r_{ij} = |\mathbf{r}_i - \mathbf{r}_j|$), and $\mathbf{R}(\mathbf{r}_i, \mathbf{r}_j, \epsilon) \cdot \mathbf{m}(\boldsymbol{\Omega}_j) \equiv \mathbf{R}_{ij}(\epsilon) \cdot \mathbf{m}_j$ is the reaction field arising from the dipole being in the surrounding dielectric (the tensor $\mathbf{R}_{ij}(\epsilon)$ will be referred to as the reaction-dipole tensor). The potential function $U_0(\mathbf{r}_N, \boldsymbol{\Omega}_N)$ corresponds to the short-range interactions and will be assumed to consist of pair dependencies only.

The polarization density $\mathbf{P}$ can be written in terms of the average total dipole moment $\langle \mathbf{M} \rangle$ by realizing

$$\mathbf{P} = \frac{\langle \mathbf{M} \rangle}{V} , \tag{1.24}$$

where V is the volume of the sample under consideration. With this definition and Eq. (1.15), one can easily see that

$$\frac{\epsilon - 1}{4\pi} \mathbf{E} = \frac{\langle \mathbf{M} \rangle}{V} . \tag{1.25}$$

Thus, since the dielectric can be assumed at this point to be isotropic, $\langle \mathbf{M} \rangle$ and $\mathbf{E}$ will have the same direction and the calculation of the average of $\mathbf{M}$ in the direction of $\mathbf{E}$ will suffice. Hence,

$$\frac{\epsilon - 1}{4\pi} E = \frac{\langle \mathbf{M} \cdot \hat{\mathbf{e}} \rangle}{V} , \tag{1.26}$$

where the unit vector $\hat{\mathbf{e}}$ is defined by $\mathbf{E} = E \, \hat{\mathbf{e}}$ to be in the direction of the electric field.

To do the average of the total dipole moment, it is essential to understand some basic concepts of statistical mechanics. The statistical mechanical average of an observable

quantity A is given by the integral over phase space of this quantity weighted by the Boltzmann factor divided by the partition function. For our purposes, the momentum integrals will drop out of the average since U is independent of the momentum and the Hamiltonian will therefore be replaced by the potential. With this substitution, it is imperative that the phase space include both the positions and orientations of the dipoles since the potential is both spatially and orientationally dependent. With this in mind, the average of the quantity A is given by

$$\langle A \rangle = \frac{1}{Z} \int d(1) \cdots \int d(N) A e^{-\beta U} , \tag{1.27}$$

where the canonical partition function is simply

$$Z = \int d(1) \cdots \int d(N) e^{-\beta U} . \tag{1.28}$$

In both Eqs. (1.27) and (1.28) the integrations $d(i)$ refer to both the angular and spatial variables, *i.e.* $d(i) = d^3 r_i \, d\mathbf{\Omega}_i$. There are generally three orientational Euler angles in which $\int d\mathbf{\Omega}_i = 8\pi^2$, but for molecules with an axis of symmetry, $\int d\mathbf{\Omega}_i = 4\pi$.

Using Eq. (1.27) replacing A with $\mathbf{M} \cdot \hat{\mathbf{e}}$, one finds for the average of the total dipole moment

$$\begin{aligned}
\langle \mathbf{M} \cdot \hat{\mathbf{e}} \rangle &= \frac{1}{Z} \int d(1) \cdots \int d(N) (\mathbf{M} \cdot \hat{\mathbf{e}}) \, e^{-\beta U} \\
&= \frac{1}{Z} \int d(1) \cdots \int d(N) (\mathbf{M} \cdot \hat{\mathbf{e}}) \, \exp\left(\beta \sum_i \mathbf{m}_i \cdot \mathbf{E}_0 \right) e^{-\beta U} \\
&\approx \frac{\beta \, E_0}{Z_0} \int d(1) \cdots \int d(N) (\mathbf{M} \cdot \hat{\mathbf{e}})(\mathbf{M} \cdot \hat{\mathbf{e}}_0) \, e^{-\beta U_0} \\
&\approx \beta \, E_0 \, \langle (\mathbf{M} \cdot \hat{\mathbf{e}})(\mathbf{M} \cdot \hat{\mathbf{e}}_0) \rangle_0 ,
\end{aligned} \tag{1.29}$$

where the subscript 0 in the last line and on the potential indicates that the field $\mathbf{E}_0 = 0$. Also, one must note that the constant term in the expansion of the exponential leads to

the average of the total dipole in the absence of the external field, which is zero due to the averaging over the orientations. Plugging Eq. (1.29) into Eq. (1.26), one finds

$$\frac{\epsilon-1}{4\pi}\frac{VE}{\beta E_0} = \langle(\mathbf{M}\cdot\hat{\mathbf{e}})(\mathbf{M}\cdot\hat{\mathbf{e}}_0)\rangle_0\,. \tag{1.30}$$

From Eq. (1.30), one can obtain a generalization to the Onsager equation, known as the *Onsager-Kirkwood* equation. Taking a sphere of volume V containing $\mathcal{N}$ molecules embedded in a continuum dielectric of the remaining $N-\mathcal{N}$ molecules with dielectric constant ϵ such that the average dielectric constant of the molecules in the sphere is also ϵ leads to an 'external' field acting on the cavity given by the cavity field in Eq. (1.18). Using this cavity field in Eq. (1.30), one finds

$$\begin{aligned}\frac{(\epsilon-1)(2\epsilon+1)}{12\pi\,\epsilon} &= \frac{\beta}{V}\langle(\mathbf{M}\cdot\hat{\mathbf{e}}_0)^2\rangle_0 \\ &= \frac{\beta}{3\,V}\,\langle\mathbf{M}^2\rangle_0\,,\end{aligned} \tag{1.31}$$

where we have used that the average of $\left\langle\cos^2\theta\right\rangle_0 = 1$. Thus, one may express the dielectric constant in terms of the dipolar density $y = 4\pi\rho\beta\mu^2/9$ as

$$\frac{(\epsilon-1)(2\epsilon+1)}{9\epsilon y} = \frac{\langle M^2\rangle_0}{N\mu^2}\,. \tag{1.32}$$

In finding the average of the total dipole moment squared, one must use the statistical average given in Eq. (1.27) with $A=\mathbf{M}^2$. In following the original derivation by Kirkwood [14], the average of the total dipole moment squared will be calculated by first averaging over all the configurations of the molecules leaving the i^{th} molecule fixed, then averaging over the positions and orientations of the i^{th} molecule separately. The average of the total moment after fixing the position and orientation of the i^{th} molecule results in the expression

$$\langle\mathbf{M}\rangle_i = \frac{\int d(1)\cdots\int d(\mathcal{N}-i)\,\mathbf{M}\,e^{-\beta U_0}}{\int d(1)\cdots\int d(\mathcal{N})\,e^{-\beta U_0}}\,, \tag{1.33}$$

where the integration $d(\mathcal{N}-i)$ denotes integration over all positions and orientations except those corresponding to the i^{th} molecule which only effects the numerator in the average. Thus, the resulting function will be dependent upon both the position and orientation of the i^{th} molecule. With Eq. (1.33), the weight factor

$$P(i) \;=\; \frac{\int d(1)\cdots\int d(\mathcal{N}-i)\, e^{-\beta U_0}}{\int d(1)\cdots\int d(\mathcal{N})\, e^{-\beta U_0}}\,, \tag{1.34}$$

and definition of the total dipole moment inside the sphere,

$$\mathbf{M} \;=\; \sum_{i=1}^{\mathcal{N}} \mathbf{m}_i\,, \tag{1.35}$$

one can write the average of the total dipole moment due to the $\mathcal{N}$ molecules in the sphere as

$$\begin{aligned}\langle \mathbf{M}^2\rangle_0 \;&=\; \sum_{i=1}^{\mathcal{N}} \int d(i)\, P(i)\, \mathbf{m}_i\cdot\langle\mathbf{M}\rangle_i \\ &=\; \mathcal{N}\int d(i)\, P(i)\, \mathbf{m}_i\cdot\langle\mathbf{M}\rangle_i\,.\end{aligned} \tag{1.36}$$

The sum in the last step of Eq. (1.36) has been done explicitly resulting in the factor of $\mathcal{N}$. The result is reasonable since, for a liquid, $\mathbf{m}_i\cdot\langle\mathbf{M}\rangle_i$ must be independent of the positions and orientations of the i^{th} molecule except in the local region surrounding the i^{th} molecule, which will be neglected here. Using Eqs. (1.33) and (1.35), one can write

$$\begin{aligned}\mathbf{m}_i\cdot\langle\mathbf{M}\rangle_i \;&=\; \sum_{j=1}^{\mathcal{N}} \frac{\int d(1)\cdots\int d(\mathcal{N}-i)\,(\mathbf{m}_i\cdot\mathbf{m}_j)\, e^{-\beta U_0}}{\int d(1)\cdots\int d(\mathcal{N})\, e^{-\beta U_0}} \\ &=\; \mu^2 \sum_{j=1}^{\mathcal{N}} \frac{\int d(1)\cdots\int d(\mathcal{N}-i)\,\cos\gamma_{ij}\, e^{-\beta U_0}}{\int d(1)\cdots\int d(\mathcal{N})\, e^{-\beta U_0}} \\ &\equiv\; \mu^2 \sum_{j=1}^{\mathcal{N}} \langle\cos\gamma_{ij}\rangle_i\,,\end{aligned} \tag{1.37}$$

where γ_{ij} is the angle between the i^{th} and j^{th} particle and the i subscript on the average again indicates that the integration is restricted to the positions and configurations of the

$\mathcal{N}-i$ particles. Plugging Eq. (1.37) into Eq. (1.36) results in the expression

$$\begin{aligned}\langle \mathbf{M}^2 \rangle_0 &= \mathcal{N} m^2 \sum_{j=1}^{\mathcal{N}} \int d(i)\, P(i)\, \langle \cos\gamma_{ij} \rangle_i \\ &= \mathcal{N} m^2 \sum_{j=1}^{\mathcal{N}} \langle \cos\gamma_{ij} \rangle_0 \,. \end{aligned} \tag{1.38}$$

Finally, putting this back into Eq. (1.30) and substituting in the dipolar density y, one finds

$$\frac{(\epsilon-1)(2\epsilon+1)}{9\,\epsilon} = y \sum_{j=1}^{\mathcal{N}} \langle \cos\gamma_{ij} \rangle_0 = y g_K \,, \tag{1.39}$$

where the number density $\rho = \mathcal{N}/V$ has been used. In examining Eq. (1.39), it is easy to see that by neglecting the average angular fluctuations $\langle \cos\gamma_{ij} \rangle$ the expression reduces to the Onsager equation. This average over the angles including the sum is known as the Kirkwood g-factor [14].

V. K-Space and Polarization

Following in part the notation and formalism in [24] and starting with the general equation for the polarization of a system of discrete individual dipoles with permanent dipole moment $\mathbf{m}$

$$\mathbf{P}(\mathbf{r}) = \sum_{i=1}^{\mathcal{N}} \delta(\mathbf{r}-\mathbf{r}_i)\, \mathbf{m}_i \,, \tag{1.40}$$

one can see that the three dimensional Fourier transform is given by

$$\begin{aligned}\tilde{\mathbf{P}}(\mathbf{k}) &= \int_V d^3r\, \mathbf{P}(\mathbf{r})\, e^{-i\mathbf{k}\cdot\mathbf{r}} \\ &= \sum_i \mathbf{m}_i\, e^{-i\mathbf{k}\cdot\mathbf{r}_i} \equiv \tilde{\mathbf{M}}(\mathbf{k}) \,. \end{aligned} \tag{1.41}$$

The energy of the system of dipoles is given by

$$-\beta\,\mathcal{E}_0 = \beta \sum_j \mathbf{m}_j \cdot \mathbf{E}_0(\mathbf{r}_j) = \beta \sum_j \mathbf{m}_j \cdot \mathbf{E}_0\, e^{i\mathbf{k}\cdot\mathbf{r}_j} \,, \tag{1.42}$$

where the static electric field has been expanded in terms of plane waves. Thus, in calculating the average of the Fourier transform of the polarization, one finds

$$\begin{aligned}\langle\tilde{\mathbf{P}}(\mathbf{k})\rangle_{E_0} &= \beta\left\langle\sum_i\sum_j \mathbf{m}_i\,(\mathbf{m}_j\cdot\mathbf{E}_0)\,e^{i\mathbf{k}\cdot(\mathbf{r}_j-\mathbf{r}_i)}\right\rangle_0 \\ &= \beta\left\langle\tilde{\mathbf{M}}(\mathbf{k})\,\tilde{\mathbf{M}}(-\mathbf{k})\right\rangle_0\cdot\mathbf{E}_0 \\ &= \frac{\beta}{V}\left\langle\tilde{\mathbf{M}}(\mathbf{k})\,\tilde{\mathbf{M}}(-\mathbf{k})\right\rangle_0\cdot\tilde{\mathbf{E}}_0(\mathbf{k})\,, \end{aligned} \tag{1.43}$$

where the Fourier transform of the external field is $\tilde{\mathbf{E}}(\mathbf{k}') = \mathbf{E}_0\,\delta_{\mathbf{k},\mathbf{k}'}$ and the Kronecker delta function $\delta_{\mathbf{k},\mathbf{k}'}$ is normalized to the volume V,

$$\delta_{\mathbf{k},\mathbf{k}'} = \begin{cases} V & \mathbf{k}=\mathbf{k}' \\ 0 & \mathbf{k}\neq\mathbf{k}' \end{cases}. \tag{1.44}$$

From Eq. (1.43), one can see that if the k-dependent external field was known, then the polarization could be found from the average of the bulk dipole moment. Thus, an independent expression relating the Maxwell field, the external field and the polarization would be very useful. This relationship does exist in a general macroscopic form given by

$$\mathbf{E}(\mathbf{r}_i) = \mathbf{E}_0(\mathbf{r}_i) + \int_V d^3r_j\,\mathbf{S}(\mathbf{r}_i-\mathbf{r}_j)\cdot\mathbf{P}(\mathbf{r}_j)\,, \tag{1.45}$$

where the tensor $\mathbf{S}$ is given by the modified dipolar tensor added with the polarization of a dipolar at $\mathbf{r}_i = \mathbf{r}_j$,

$$\mathbf{S}(\mathbf{r}_i-\mathbf{r}_j) = -\frac{4\pi}{3}\,\delta(\mathbf{r}_i-\mathbf{r}_j)\,\mathbf{I} + \mathbf{T}_{\rm mod}(\mathbf{r}_i-\mathbf{r}_j)\,. \tag{1.46}$$

The modified dipolar tensor can be written in general as

$$\mathbf{T}_{\rm mod}(\mathbf{r}) = a(r)\,(3\,\hat{\mathbf{r}}\hat{\mathbf{r}}-\mathbf{I}) + b(r)\,\mathbf{I}\,. \tag{1.47}$$

This generalization of the dipolar tensor serves to be useful since it allows one to consider a finite system in which the boundary conditions could not be easily eliminated. The Fourier

transform of Eq. (1.47) is a much more useful form when dealing with the microscopic theory of dielectrics and in forming it one must use the convolution theorem. The total result of this calculation is given by

$$\tilde{\mathbf{E}}(\mathbf{k}) \;=\; \tilde{\mathbf{E}}_0(\mathbf{k}) + \tilde{\mathbf{S}}(\mathbf{k}) \cdot \tilde{\mathbf{P}}(\mathbf{k})\,. \tag{1.48}$$

The final step is to eliminate the polarization completely. This task is done simply by using the Fourier transform of Eq. (1.15),

$$\tilde{\mathbf{P}}(\mathbf{k}) \;=\; \frac{\tilde{\boldsymbol{\epsilon}}(\mathbf{k}) - \mathbf{I}}{4\pi}\, \tilde{\mathbf{E}}(\mathbf{k})\,, \tag{1.49}$$

which in general depends on the second rank k-dependent dielectric tensor $\tilde{\boldsymbol{\epsilon}}(\mathbf{k})$. In putting Eq. (1.49) into Eq. (1.48) and solving for $\tilde{\mathbf{E}}_0(\mathbf{k})$, one finds

$$\tilde{\mathbf{E}}_0(\mathbf{k}) \;=\; \left\{ \mathbf{I} - \tilde{\mathbf{S}}(\mathbf{k}) \cdot \left(\frac{\tilde{\boldsymbol{\epsilon}}(\mathbf{k}) - \mathbf{I}}{4\pi} \right) \right\} \cdot \tilde{\mathbf{E}}(\mathbf{k})\,. \tag{1.50}$$

The dependence of Eq. (1.50) on the Fourier transform of the tensor $\mathbf{S}$ can be dealt with by first finding the Fourier transform of $\mathbf{T}_{\rm mod}$ defined in Eq. (1.47). This task can be done by expanding the tensor $(3\hat{\mathbf{r}}\hat{\mathbf{r}} - \mathbf{I})$ in terms of spherical harmonics dependent upon the orientation of $\mathbf{r}_{ij}$ and using the *Rayleigh* expansion for the exponential. In doing so, one finds

$$\begin{aligned} \tilde{\mathbf{T}}_{\rm mod}(\mathbf{k}) \;&=\; \frac{4\pi}{3} \left[f_1(k)(3\,\hat{\mathbf{k}}\hat{\mathbf{k}} - \mathbf{I}) + f_2(k)\mathbf{I} \right] \\ &=\; \frac{4\pi}{3} \left[\Lambda^L \boldsymbol{\mathcal{J}}^L + \Lambda^T \boldsymbol{\mathcal{J}}^T \right]\,, \end{aligned} \tag{1.51}$$

where the functions $f_1(k)$ and $f_2(k)$ are given by integrals over spherical Bessel functions defined in Appendix E, Eqs. (E3)-(E5) and $\boldsymbol{\mathcal{J}}^{L,T}$ are the longitudinal and transverse projections operators defined as $\hat{\mathbf{k}}\hat{\mathbf{k}}$ and $\mathbf{I} - \hat{\mathbf{k}}\hat{\mathbf{k}}$, respectively.

At this point, almost all the equations are in place to calculate the relationship between the Maxwell field and the external field with no ambiguity. The only job that

remains is the dielectric tensor which for finite wavelengths can be broken up into pieces parallel and perpendicular to the k-vector. Generally, a tensor that is dependent on both the direction and magnitude of the vector $\mathbf{k}$ can be split into components that are longitudinal and transverse to $\mathbf{k}$. For instance, the dielectric tensor $\tilde{\boldsymbol{\epsilon}}(\mathbf{k})$ can be split into

$$\tilde{\boldsymbol{\epsilon}}_L(\mathbf{k}) \;=\; \epsilon_L(k)\,\boldsymbol{\mathcal{J}}_L \tag{1.52}$$

and

$$\tilde{\boldsymbol{\epsilon}}_T(\mathbf{k}) \;=\; \epsilon_T(k)\,\boldsymbol{\mathcal{J}}_T\,, \tag{1.53}$$

Thus, the dielectric constant may be written as

$$\tilde{\boldsymbol{\epsilon}}(\mathbf{k}) \;=\; \tilde{\boldsymbol{\epsilon}}_L(\mathbf{k}) + \tilde{\boldsymbol{\epsilon}}_T(\mathbf{k}) \;=\; \epsilon_T(k)\,\mathbf{I} + \left[\epsilon_L(k) - \epsilon_T(k)\right]\,\hat{\mathbf{k}}\hat{\mathbf{k}}\,. \tag{1.54}$$

Finally, using the complete Fourier transform of the $\mathbf{S}$-tensor,

$$\tilde{\mathbf{S}}(\mathbf{k}) \;=\; -\frac{4\pi}{3}\,\mathbf{I} + \tilde{\mathbf{T}}_{\rm mod}(\mathbf{k})\,, \tag{1.55}$$

with Eqs. (1.51) and (1.54) in Eq. (1.50), one finds

$$\begin{aligned}\mathbf{E}_0(\mathbf{k}) \;&=\; \left[A_{\mathbf{I}}(k)\,\mathbf{I} + A_{\hat{\mathbf{k}}\hat{\mathbf{k}}}(k)\,\hat{\mathbf{k}}\hat{\mathbf{k}}\right]\cdot\mathbf{E}(\mathbf{k}) \\ &\equiv\; \boldsymbol{\Gamma}(\mathbf{k})\cdot\mathbf{E}(\mathbf{k})\,,\end{aligned} \tag{1.56}$$

where

$$A_{\mathbf{I}}(k) \;=\; \frac{1}{3}\,\left[\epsilon_T(k) - 1\right]\,\left[f_1(k) - f_2(k)\right] + \frac{1}{3}\,\left[\epsilon_T(k) + 2\right] \tag{1.57}$$

and

$$\begin{aligned}A_{\hat{\mathbf{k}}\hat{\mathbf{k}}}(k) \;&=\; -\frac{1}{3}\left[\left(\epsilon_T(k) - 1\right) + 2\left(\epsilon_L(k) - 1\right)\right]\,f_1(k) \\ &\quad + \frac{1}{3}\left[\epsilon_T(k) - \epsilon_L(k)\right]\,\left[f_2(k) - 1\right]\,.\end{aligned} \tag{1.58}$$

For some cases, it is important to have the inverse of the relationship given in Eq. (1.50), *i.e.* $\mathbf{E}(\mathbf{k})$ in terms of $\mathbf{E}_0(\mathbf{k})$. In considering the inverse of $\mathbf{\Gamma}(\mathbf{k})$, it is apparent that it can be expanded in terms of a linear combination of $\mathbf{I}$ and $\hat{\mathbf{k}}\hat{\mathbf{k}}$ since these tensors span the space. Therefore, with no loss in generality, one may write

$$[\mathbf{\Gamma}(\mathbf{k})]^{-1} \;=\; A'_{\mathbf{I}}(k)\,\mathbf{I} + A'_{\hat{\mathbf{k}}\hat{\mathbf{k}}}(k)\,\hat{\mathbf{k}}\hat{\mathbf{k}}\,, \tag{1.59}$$

where $A'_{\mathbf{I}}(k)$ and $A'_{\hat{\mathbf{k}}\hat{\mathbf{k}}}(k)$ are yet to be determined. Determining these unknowns is a simple task of computing $\mathbf{\Gamma}\cdot\mathbf{\Gamma}^{-1}=\mathbf{I}$. In doing so, one finds

$$\mathbf{I} \;=\; A_{\mathbf{I}}(k)\,A'_{\mathbf{I}}(k)\,\mathbf{I} + \Big[A_{\mathbf{I}}(k)\,A'_{\hat{\mathbf{k}}\hat{\mathbf{k}}}(k) + A'_{\mathbf{I}}(k)\,A_{\hat{\mathbf{k}}\hat{\mathbf{k}}}(k) + A_{\hat{\mathbf{k}}\hat{\mathbf{k}}}(k)A'_{\hat{\mathbf{k}}\hat{\mathbf{k}}}(k)\Big]\,\hat{\mathbf{k}}\hat{\mathbf{k}}\,, \tag{1.60}$$

which leads to

$$A'_{\mathbf{I}}(k) \;=\; [A_{\mathbf{I}}(k)]^{-1} \tag{1.61}$$

and

$$A'_{\hat{\mathbf{k}}\hat{\mathbf{k}}}(k) \;=\; -A_{\hat{\mathbf{k}}\hat{\mathbf{k}}}(k)\,\big[A_{\mathbf{I}}(k)\,\big(A_{\mathbf{I}}(k)+A_{\hat{\mathbf{k}}\hat{\mathbf{k}}}(k)\big)\big]^{-1}\,. \tag{1.62}$$

Projecting out the longitudinal and transverse components of the Maxwell field, one finds for the longitudinal component

$$\begin{aligned}
\tilde{\mathbf{E}}_L(\mathbf{k}) \;&=\; \boldsymbol{\mathcal{J}}_L\cdot\tilde{\mathbf{E}}(\mathbf{k}) \;=\; \boldsymbol{\mathcal{J}}_L\cdot\mathbf{\Gamma}^{-1}(\mathbf{k})\cdot\tilde{\mathbf{E}}_0(\mathbf{k}) \\
&=\; \frac{\boldsymbol{\mathcal{J}}_L}{A_{\mathbf{I}}(k)+A_{\hat{\mathbf{k}}\hat{\mathbf{k}}}(k)}\cdot\tilde{\mathbf{E}}_0(\mathbf{k}) \\
&=\; \frac{3}{\epsilon_L(k)-1}\left[\frac{\epsilon_L(k)+2}{\epsilon_L(k)-1}-2f_1(k)-f_2(k)\right]^{-1}\cdot\tilde{\mathbf{E}}_{0L}(\mathbf{k})\,.
\end{aligned} \tag{1.63}$$

while the transverse component takes the form

$$\begin{aligned}
\tilde{\mathbf{E}}_T(\mathbf{k}) \;&=\; \boldsymbol{\mathcal{J}}_T\cdot\mathbf{\Gamma}^{-1}(\mathbf{k})\cdot\tilde{\mathbf{E}}_0(\mathbf{k}) \;=\; \frac{\boldsymbol{\mathcal{J}}_T}{A_{\mathbf{I}}(k)}\cdot\tilde{\mathbf{E}}_0(\mathbf{k}) \\
&=\; \frac{3}{\epsilon_T(k)-1}\left[\frac{\epsilon_T(k)+2}{\epsilon_T(k)-1}+f_1(k)-f_2(k)\right]^{-1}\cdot\tilde{\mathbf{E}}_{0T}(\mathbf{k})
\end{aligned} \tag{1.64}$$

Finally, using Eqs. (1.49) and (1.50), the complete polarization is found to be

$$\begin{aligned}\tilde{\mathbf{P}}(\mathbf{k}) &= \left(\frac{\tilde{\boldsymbol{\epsilon}}(\mathbf{k})-\mathbf{I}}{4\pi}\right)\cdot\tilde{\mathbf{E}}(\mathbf{k}) \\ &= \frac{1}{4\pi}\left[\epsilon_L(k)\,\boldsymbol{\mathcal{J}}_L+\epsilon_T(k)\,\boldsymbol{\mathcal{J}}_T-\mathbf{I}\right]\cdot\left[\tilde{\mathbf{E}}_L(\mathbf{k})+\tilde{\mathbf{E}}_T(\mathbf{k})\right] \\ &= \left[\left(\frac{\epsilon_L(k)-1}{4\pi}\right)\tilde{\mathbf{E}}_L(\mathbf{k})+\left(\frac{\epsilon_T(k)-1}{4\pi}\right)\tilde{\mathbf{E}}_T(\mathbf{k})\right]. \qquad (1.65)\end{aligned}$$

In terms of the external field, one can define the longitudinal and transverse polarizations as

$$\tilde{\mathbf{P}}_L(\mathbf{k}) = \frac{3}{4\pi}\left[\frac{\epsilon_L(k)+2}{\epsilon_L(k)-1}-2f_1(k)-f_2(k)\right]^{-1}\cdot\tilde{\mathbf{E}}_{0L}(\mathbf{k}) \qquad (1.66)$$

and

$$\tilde{\mathbf{P}}_T(\mathbf{k}) = \frac{3}{4\pi}\left[\frac{\epsilon_T(k)+2}{\epsilon_T(k)-1}+f_1(k)-f_2(k)\right]^{-1}\cdot\tilde{\mathbf{E}}_{0T}(\mathbf{k})\,. \qquad (1.67)$$

As a last task, Eqs. (1.66) and (1.67) can be compared to the the longitudinal and transverse projections of the average polarization in Eq. (1.43), which can be found as

$$\begin{aligned}\tilde{\mathbf{P}}_L(\mathbf{k}) &= \frac{\beta\,\rho\,\mu^2}{3}\left\langle\frac{3}{N}\sum_i\sum_j(\hat{\mathbf{e}}_i\cdot\hat{\mathbf{k}})\,(\hat{\mathbf{k}}\cdot\hat{\mathbf{e}}_j)\,e^{i\mathbf{k}\cdot\mathbf{r}_{ji}}\right\rangle_0\tilde{\mathbf{E}}_{0L} \\ &= \frac{3\,y}{4\pi}\,S_L(k)\,\boldsymbol{\mathcal{J}}_L\cdot\tilde{\mathbf{E}}_0 \qquad (1.68)\end{aligned}$$

and

$$\begin{aligned}\tilde{\mathbf{P}}_T(\mathbf{k}) &= \frac{2\beta\,\rho\,\mu^2}{3}\left\langle\frac{3}{2N}\sum_i\sum_j\left[(\hat{\mathbf{e}}_i\cdot\hat{\mathbf{e}}_j)-(\hat{\mathbf{e}}_i\cdot\hat{\mathbf{k}})\,(\hat{\mathbf{k}}\cdot\hat{\mathbf{e}}_j)\,e^{i\mathbf{k}\cdot\mathbf{r}_{ji}}\right]\right\rangle_0\tilde{\mathbf{E}}_{0T} \\ &= \frac{3\,y}{4\pi}\,S_T(k)\,\boldsymbol{\mathcal{J}}_T\cdot\tilde{\mathbf{E}}_0\,, \qquad (1.69)\end{aligned}$$

where $S_L(k)$ and $S_T(k)$ are the longitudinal and transverse structure factors. These two function are plotted in Fig. (1). Comparing Eqs. (1.66) and (1.67) with Eqs. (1.68) and (1.69), one can relate the microscopic structure factors to the longitudinal and transverse components of the k-dependent macroscopic dielectric constant.

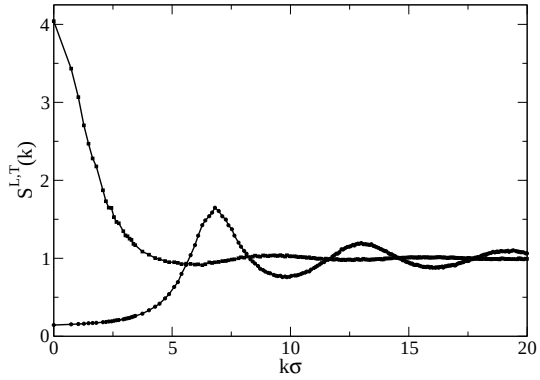

FIG. 1. The longitudinal and transverse structure factors $S^L(k)$ and $S^T(k)$ plotted as a function of the lattice points k directly from MC simulation data for $(m*)^2 = 2.0$ and $\rho* = 0.8$ and calculated directly from the relationships given in Eqs. (1.68) and (1.69).

This comparison leads to the expressions,

$$\begin{aligned} \tilde{\mathbf{P}}(\mathbf{k}) &= \tilde{\mathbf{P}}_L(\mathbf{k}) + \tilde{\mathbf{P}}_T(\mathbf{k}) \\ &= \frac{3\,y}{4\pi}\,[S_L(k)\,\boldsymbol{\mathcal{J}}_L + S_T(k)\,\boldsymbol{\mathcal{J}}_T]\cdot\tilde{\mathbf{E}}_0\,, \end{aligned} \tag{1.70}$$

where the structure factors are given by

$$S_L(k) = \left[\frac{\epsilon_L(k)+2}{\epsilon_L(k)-1} - 2f_1(k) - f_2(k)\right]^{-1} \tag{1.71}$$

and

$$S_T(k) = \left[\frac{\epsilon_T(k)+2}{\epsilon_T(k)-1} + f_1(k) - f_2(k)\right]^{-1}. \tag{1.72}$$

For an infinite system, it can be shown that $f_1(k) = -1$ and $f_2(k) = 0$, and therefore after taking the $k \to 0$ limit, the structure factors can be written as

$$S_L(0) = \frac{\epsilon_L(0)-1}{3y\,\epsilon_L(0)} \tag{1.73}$$

$$S_T(0) = \frac{\epsilon_T(0)-1}{3y}\,. \tag{1.74}$$

Taking a third of the sum of these and letting $\epsilon_L(0) = \epsilon_T(0) \equiv \epsilon$, one finds the Kirkwood factor

$$g_K \;=\; \frac{1}{3}\,[S_L(0) + 2\,S_T(0)] \;\;=\;\; \frac{(\epsilon-1)(2\epsilon+1)}{9y\,\epsilon}\,. \tag{1.75}$$

The structure factors given above can be related to the angular pair correlation functions $\tilde{h}_{110}(k)$ and $\tilde{h}_{112}(k)$ through the equations

$$\begin{aligned} S_L(k) =& 1 + \frac{\rho}{3}\left[\tilde{h}_{110}(k) - 2\tilde{h}_{112}(k)\right] = 1 + \chi'^{L}\,, \\ S_T(k) =& 1 + \frac{\rho}{3}\left[\tilde{h}_{110}(k) + \tilde{h}_{112}(k)\right] = 1 + \chi'^{T}\,. \end{aligned} \tag{1.76}$$

The response function $\chi'^{L,T}$ in Eqs. (1.76) are extremely useful in this form since one can directly use the data obtained from MC simulations for their calculation. As will be seen, they appear in calculations involving microscopic solvation theory when one excludes the volume of a cavity from the polarization field inside the dielectric. They also appear in direct calculations of electric fields inside of dielectrics. In all cases, they give a means to compare analytical calculations to that from the data generated in MC simulations.

CHAPTER 2

Fields Inside Dielectrics: A Modern Approach

I. Current Formalism

In order to set up the calculation of dielectric response in terms of microscopic properties of dielectrics, we will consider the Gaussian generating functional for the polarization field $\mathbf{P}$ in the dielectric [27, 28]:

$$G(\mathbf{A}) \;=\; \int e^{\mathbf{A}*\mathbf{P}-\beta H_{\mathrm{B}}[\delta\mathbf{P}]} \prod_{\Omega_0} \delta\left[\mathbf{P}(\mathbf{r})\right] \mathcal{D}\mathbf{P}. \tag{2.1}$$

The asterisk between the two vector fields in the exponent of Eq. (2.1) refer to both the spatial integration and tensorial contraction. When an asterisk connects fields with tildes, as in $\tilde{\mathbf{E}} * \tilde{\mathbf{P}}$, the k-space integration of the Fourier transforms $\tilde{\mathbf{E}}$ and $\tilde{\mathbf{P}}$ of the fields $\mathbf{E}$ and $\mathbf{P}$ is assumed. In Eq. (2.1), $H_{\mathrm{B}}[\delta\mathbf{P}]$ is the Hamiltonian of the polarization fluctuations $\delta\mathbf{P}$ characterized by the response function of the pure isotropic solvent $\boldsymbol{\chi}_s(\mathbf{k})$

$$H_{\mathrm{B}}[\delta\mathbf{P}] \;=\; \frac{1}{2}\left|\delta\tilde{\mathbf{P}}\right|^2 * \boldsymbol{\chi}_s^{-1}. \tag{2.2}$$

The product of δ-functions in Eq. (2.1) excludes the polarization field, over which the functional integral is taken, from some volume Ω_0 within the liquid [27]. This volume can specify the cavity in the dielectric for the cavity field calculations or the volume of a given target solute molecule within the liquid for the calculation of local fields in bulk dielectrics. To combine these two possibilities, we will generally call the volume Ω_0 the 'solute volume'. In some cases the solute volume can be represented by an effective volume for which an effective solute radius will be used. This effective radius can be calculated as in Ref. [29],

$$R_{\mathrm{eff}}^{-3}(r_{0s}, \rho^*) \;=\; 3\int_0^\infty \frac{dr}{r^4} g_{0s}(r)\,, \tag{2.3}$$

where $r_{0s} = R_0/\sigma + 0.5$ is defined as the radius of closest approach, $\rho^* = \rho\sigma^3$ is the reduced density, and $g_{0s}(r)$ is the hard-sphere distribution function evaluated a distance r from the solute center taken to be at the origin.

The constraint imposed on the polarization field to vanish from the solute volume modifies the response function from that of the pure solvent $\boldsymbol{\chi}_s(\mathbf{k}_1)$ to a non-local response function $\boldsymbol{\chi}(\mathbf{k}_1, \mathbf{k}_2)$ depending on two wavevectors [25]. This function is obtained by taking the second derivative of $\ln[G(\mathbf{A})]$ in Eq. (2.1) with respect to the auxiliary field $\mathbf{A}$ and then letting $\mathbf{A} = 0$. The result is found to be

$$\boldsymbol{\chi}(\mathbf{k}_1, \mathbf{k}_2) \quad = \quad \boldsymbol{\chi}_s(\mathbf{k}_1)\delta_{\mathbf{k}_1,\mathbf{k}_2} - \boldsymbol{\chi}^{\mathrm{corr}}(\mathbf{k}_1, \mathbf{k}_2), \tag{2.4}$$

where the correction response function $\boldsymbol{\chi}^{\mathrm{corr}}(\mathbf{k}_1, \mathbf{k}_2)$ accounts for the excluded polarization field due to the presence of the solute volume within the dielectric. This correction to the response function is given by the following equation:

$$\boldsymbol{\chi}^{\mathrm{corr}}(\mathbf{k}_1, \mathbf{k}_2) \quad = \quad \boldsymbol{\chi}''(\mathbf{k}_1)\theta_0(\mathbf{k}_1 - \mathbf{k}_2)\boldsymbol{\chi}_s(\mathbf{k}_2). \tag{2.5}$$

Here, θ_0 is the Fourier transform of the Heaviside step function accounting for the hard-sphere solute volume

$$\theta_0(\mathbf{k}) \quad = \quad \int_{\Omega_0} e^{i\mathbf{k}\cdot\mathbf{r}} d\mathbf{r}\,, \tag{2.6}$$

which becomes

$$\theta_0(k) \quad = \quad 4\pi R_0^3 \frac{j_1(kR_0)}{kR_0} \tag{2.7}$$

for a spherical solute of radius R_0. The response function $\boldsymbol{\chi}''(\mathbf{k}_1)$ is then given as a sum of projections on the longitudinal and transverse dyadic projection operators

$$\boldsymbol{\chi}'' \quad = \quad \boldsymbol{\mathcal{J}}^L \chi''^L + \boldsymbol{\mathcal{J}}^T \chi''^T. \tag{2.8}$$

In Eq. (2.8),

$$\chi''^{L,T} = \frac{S^{L,T}}{S^{L,T} - \chi'^{L,T}}\,, \tag{2.9}$$

$S^L(k)$ and $S^T(k)$ are the corresponding longitudinal and transverse structure factors, respectively, and $\chi'^{L,T}$ are given similar to Eq. (1.75), by

$$\chi'^L(k) = (\rho/3)\int_{\Omega'} d^3r \left[h^{110}(r)j_0(kr) - 2h^{112}(r)j_2(kr)\right], \tag{2.10}$$

$$\chi'^T(k) = (\rho/3)\int_{\Omega'} d^3r \left[h^{110}(r)j_0(kr) + h^{112}(r)j_2(kr)\right]. \tag{2.11}$$

Here, Ω' is the volume of a sphere with radius twice the distance of closest approach ($2r_{0s}$) for a spherical solute of radius R_0. The projections $\chi'^{L,T}$ in Eqs. (2.10) and (2.11) renormalize the dielectric response by excluding the dipolar polarization field from the volume of the solvent. These expressions are a convenient representation of the response functions since they are expressed through projections of the pair distribution function on rotational invariants [25] and can be readily calculated from simulation data. These functions enter the response function of the homogeneous dipolar liquid through their appearance in the structure factors and in the form of longitudinal and transverse projections [16] of these structure factors onto the k-vector as was seen in Eq. (1.69) and repeated here for convenience,

$$\boldsymbol{\chi}_s(\mathbf{k}) = \frac{3y}{4\pi}\left[S^L(k)\boldsymbol{\mathcal{J}}^L + S^T(k)\boldsymbol{\mathcal{J}}^T\right] \tag{2.12}$$

The $k = 0$ values of the structure factors have been derived in Chapter 1, Section V, Eqs. (1.72) and (1.73) leading to general relationships between them and the bulk dielectric constant.

The solute effects the correction term in the response function in Eqs. (2.4) and (2.5) by the appearance of $\chi'^{L,T}$ in the denominator of Eq. (2.9). In some cases, the asymptotic form of $h_{112}(r)$ can be used without any lose of generality when short-range correlations are neglected. In particular, when $r \gg \sigma$ the asymptote

$$h_{112}(r) \simeq \frac{(\epsilon-1)^2}{4\pi y\epsilon}\frac{1}{r^3} \tag{2.13}$$

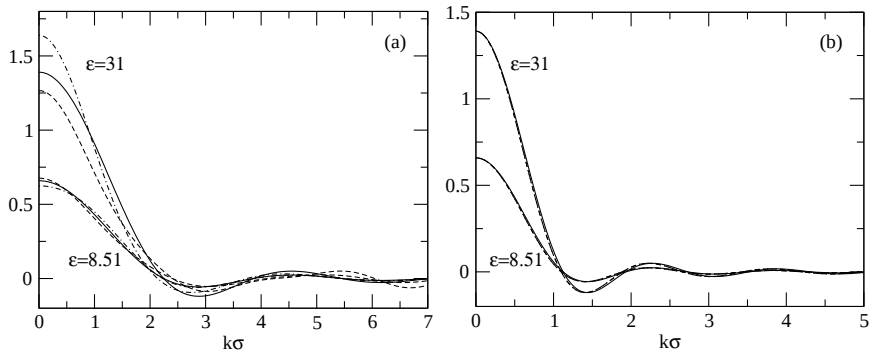

FIG. 2. Response functions $-\chi'^{L}(k)/2$ (dashed lines), $\chi'^{T}(k)$ (dash-doted line) calculated from Eqs. (2.10) and (2.11), and compared to $A(k)$ (solid line, see Eqs. (2.14) and (2.15)). The dielectric constant of the DHS liquid is indicated in the plot; $\rho^* = 0.8$. The $h^{110}(r)$ and $h^{112}(r)$ projections required for integration in Eq. (2.10) and (2.11) have been obtained from MC simulations. Panel (a), (b) corresponds to $R_0/\sigma = 0.5, 1.5$, respectively.

is sufficient in the integrals given in Eqs. (1.75), (2.10), and (2.11). This relationship will hold when integrating the response functions for large solutes such that $2r_{0s}/\sigma \gg 1$. If the short-range correlations are neglected and only the long-range form of $h_{112}(r)$ is used in the integration of Eqs. (2.10)and (2.11), one obtains a very simple form for $\chi'^{L,T}$,

$$\chi'^{L} = -2A(k) \tag{2.14}$$

$$\chi'^{T} = A(k)\,, \tag{2.15}$$

where

$$A(k) = \frac{(\epsilon-1)^2}{3\epsilon y}\frac{j_1(2kR_1)}{2kR_1}\,. \tag{2.16}$$

This approximation can be justified further simply by plotting $A(k)$, $-\chi'^{L}(k)/2$,

and $\chi^T(k)$ from simulation data and comparing them. Using the structure factors and distribution functions calculated from the simulation data, one can see in Figure 2 that the correspondence is good and the approximation can be used with some accuracy. Accordingly, as the solute volume grows, the approximation is supposed to become increasingly accurate which is apparent when one realizes the deviations for small values of k are effectively eliminated by the fact that $j_1^2(kR_1) \propto k^2$ for $k \ll 1$ appearing in the k-space integrations relevant in calculations of fields, energies, dielectric constants, polarizations, *etc.* This approximation is very accurate as is seen in comparing the two panels in Figure 2 for increasing solute radius.

The main concern of this manuscript is the calculation of electric fields and some quantities related to microscopic solvation. In all cases, an extremely important quantity that needs to be considered is

$$\int_\Omega \mathbf{T}(\mathbf{r}-\mathbf{r}')\cdot\mathbf{P}(\mathbf{r}')d^3r' \quad \rightarrow \quad \tilde{\mathbf{T}}(\mathbf{k}) * \tilde{\mathbf{P}}(\mathbf{k})\,, \tag{2.17}$$

where $\mathbf{T}$ is the usual dipole tensor, $\mathbf{P}$ is the polarization, and the tildes represent the Fourier transforms of the corresponding vectors and tensors. The Fourier transform of the dipolar tensor for an infinite system with a spherical solute with radius R_0 is given by

$$\begin{aligned} \tilde{\mathbf{T}} &= -4\pi \boldsymbol{D}_{\mathbf{k}} \frac{j_1(kR_0)}{kR_0} \\ &= -4\pi \left(2\boldsymbol{\mathcal{J}}^L - \boldsymbol{\mathcal{J}}^T\right) \frac{j_1(kR_0)}{kR_0}\,. \end{aligned} \tag{2.18}$$

It has been shown that within the realm of linear dielectrics a relationship holds between the Maxwell field and the polarization, namely $\tilde{\mathbf{P}} = \tilde{\boldsymbol{\chi}} * \tilde{\mathbf{E}}$, which is just the Fourier transform and convolution of Eq. (1.13) with the susceptibility taken in its general tensorial form. In all cases, the quantities that will be dealt with most often will be of the form of Eq. (2.17)

with the generalized polarization relation used. In particular,

$$\tilde{\mathbf{T}}(\mathbf{k}_1) * \tilde{\boldsymbol{\chi}}(\mathbf{k}_1, \mathbf{k}_2) * \tilde{\mathbf{E}}(\mathbf{k}_2) \quad = \quad -4\pi \frac{j_1(k_1 R_0)}{k_1 R_0} \mathbf{D}_{\mathbf{k}_1} * \tilde{\boldsymbol{\chi}}(\mathbf{k}_1, \mathbf{k}_2) * \tilde{\mathbf{E}}(\mathbf{k}_2)\,. \tag{2.19}$$

This quantity appears in some form in all calculations of fields inside of polar fluids considered as microscopic materials rather than the bulk materials discussed in detail in Chapter 1. Thus, to be as thorough as possible, the local, reaction, and cavity fields will be derived and discussed in detail in the following section.

II. Reaction, Cavity, and Local Fields Inside Dielectrics

Maxwell's initial idea to use cavities carved in continuum material to define the electric field **E** inside dielectrics [30] is possibly one of the most useful tools for beginning to understand what is physically happening within microscopic polarization. Lorentz, instead, used averages of microscopic fields over 'physically infinitesimal' volumes to derive material Maxwell's equations [31] which actually give a different perspective of the same ideas. Consequently, both approaches are different facets of the same question: How are microscopic fields within dielectrics related to the macroscopic (Maxwell) field? This question, which has many ramifications in condensed-matter physics [32], is certainly relevant to theories of dielectrics since any mean-field theory of dielectric response has to address the relationship between the local field acting on a liquid permanent or induced dipole and the field due to the bulk polarization. Debye's approach to this question [4] was to calculate the local field as the sum of the macroscopic field **E** and the field of the liquid dipoles proportional, on average, to the dipolar polarization **P**, realized as

$$\mathbf{E}_{\text{loc}} \quad = \quad \mathbf{E} + f\mathbf{P}\,, \tag{2.20}$$

where the coefficient f, which we will call the 'polarization coefficient', needs to be determined from dielectric theories.

It has already been seen how the polarization field $\mathbf{P}$ in Eq. (2.20) is related to the dielectric constant in Eq. (1.15), but it is also related to the density of dipoles induced in the liquid through local field in the relationship

$$\mathbf{P} \;=\; \frac{\epsilon-1}{4\pi}\mathbf{E} \;=\; \rho\alpha\mathbf{E}_{\rm loc}\,. \tag{2.21}$$

Here, ρ is the number density and α is the molecular polarizability which is equal to the dipolar polarizability for induced dipoles and to $\beta m^2/3$ for permanent dipoles m (see Appendix B); β is the inverse temperature.

The equation for the local field follows from Eqs. (2.20) and (2.21)

$$\mathbf{E}_{\rm loc} \;=\; (1-f\rho\alpha)^{-1}\mathbf{E}\,, \tag{2.22}$$

as well as the dielectric constant

$$\epsilon \;=\; 1+\frac{4\pi\rho\alpha}{1-f\rho\alpha}\,. \tag{2.23}$$

The relationship given in Eq. (2.23) anticipates the possibility of polarization catastrophe at $f\rho\alpha = 1$ which manifests itself in the Debye equation for the dielectric constant as a function of the dipolar density. When $f\rho\alpha > 1$, the system becomes globally unstable, $\epsilon < 0$, and transition to ferroelectric phase is expected. A relationship similar to Eq. (2.23) can be written for k-dependent response. If $\epsilon(k)$ becomes negative for any values of k [33], the systems is globally stable, but becomes unstable to some excitations, polarization waves [34] and Cooper pairs [32] are specific examples.

The choice of $f = 4\pi/3$ corresponds to the Lorentz local field [4] given in Eq. (1.19)

$$\mathbf{E}_L = \frac{\epsilon+2}{3}\mathbf{E}. \tag{2.24}$$

While this choice of f is generally accepted in the theory of ferromagnetism (Weiss theory) explaining the ferromagnetic transition, its electric/dipolar counterpart which, as stated,

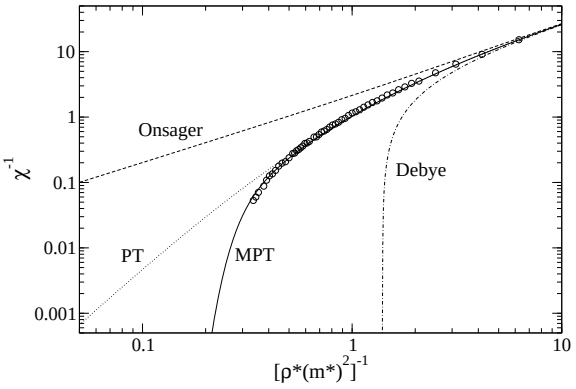

FIG. 3. The inverse of the dielectric susceptibility χ as a function of the inverse of the reduced dipole moment times the reduced density ($[(m*)^2\rho*]^{-1}$). The points represent direct calculation from simulation data. The solid line is that obtained from Eq. (2.29), the dotted line from Eq. (2.28). The remaining two lines are the continuum results obtained from the Debye and Onsager equations, Eq. (2.26) and Eq. (2.27), respectively.

leads to the Debye equation [4], predicting a ferroelectric transition at a dipolar density $y = (4\pi/9)\beta\rho m^2 = 1$, is still questionable. Since many polar liquids are paraelectric at $y > 1$, an alternative definition of polarization coefficient in Eq. (2.20) is required.

Onsager suggested [12] that the polarization coefficient should decrease with increasing dielectric constant according to the relationship

$$f = \frac{4\pi}{2\epsilon + 1}\,. \tag{2.25}$$

This value of f here, which coincides with the Lorentz approach only at $\epsilon = 1$, eliminates the polarization catastrophe and leads to the local field equal to the field inside a real physical spherical cavity seen in Eq. (1.18). Even though local correlations that are apparent in the formulation of the Kirkwood factor g_K [19] were missing from Onsager's formulation, the theory was successful since molecular quadrupoles have a destructive effect on local dipolar order making the Kirkwood factor close to one for most molecular liquids [4, 19].

The ferroelectric transition that appears in Debye's equation for the dielectric con-

stant in terms of the dipolar density has been highly scrutinized over for some time. Since the Onsager formulation had eliminated the ferroelectric transition from the theory there was a definite concern over the physical existence of such a transition. This result has been recently challenged by computer simulations which had produced ferroelectric phase in model dipolar fluids [35, 36]. It was also found that the result is sensitive to the boundary conditions employed in the simulation protocol, *i.e.* to the magnitude of the depolarization field, a result known since calculations of Luttinger and Tisza of dipolar crystals [37]. More recently, a systematic consideration of the effect of depolarization field of crystal ferroelectrics has shown that the ferroelectric state is unstable to increasing depolarization field transforming into the curling state with non-zero toroidal moment [38].

The simulations performed here have also shown definite signs of a ferroelectric transition. Figure 3 shows the inverse of the susceptibility verses the inverse of the reduced dipole moment squared for five different scenarios, the Debye picture

$$y = \frac{\epsilon - 1}{\epsilon + 2}, \tag{2.26}$$

the Onsager picture

$$y = \frac{(\epsilon - 1)(2\epsilon + 1)}{9\epsilon}, \tag{2.27}$$

the result of a perturbative expansion of the dielectric constant in terms of the dipolar density given by Tani *et al* [39]

$$\epsilon - 1 = 3y + 3y^2 + 3y^3 p, \tag{2.28}$$

the result of Matyushov *et al* [40]

$$\epsilon - 1 = 3y + 3y^2 + \frac{2}{p^2}\left(e^{3p^3y^3/2} - 1\right), \tag{2.29}$$

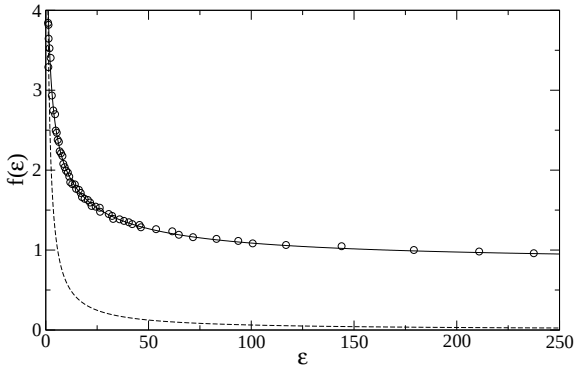

FIG. 4. The polarization coefficient $f(\epsilon)$ as a function of the dielectric constant ϵ for a DHS fluid at $\rho* = 0.8$. The solid line is the fit to the simulation data given by the points. The dashed line refers to the Onsager result given by Eq. (2.25).

and finally the data taken from the MC simulations. In Eqs. (2.28) and (2.29), p is related to the 3-particle perturbation integral $I_{0s}^{(3)}$ tabulated in Ref. [39] and given by

$$p = \frac{9I_{0s}^{(3)}}{16\pi^2} - 1\,. \tag{2.30}$$

From Figure 3, it is completely obvious that both the Debye theory and the Onsager theory fail to predict the results of simulations and the perturbation theory (PT) and modified perturbation theory (MPT) do very well for smaller values of ϵ while it seems that the MPT results holds for the data obtained in the simulation provided here although the data is still limited to $\epsilon \leq 300$. The value of y for the ferroelectric transition is of course different for all four theories and is in the Debye case equal to unity and for the Onsager theory does not even exist. Turning to the MPT and using $I_{0s}^{(3)}$ as a fitting parameter, one finds the ferroelectric transition occurring at $p = 0.3551$ from Eq. (2.30) which corresponds to $I_{0s}^{(3)} = 23.78$. The value of the dipolar density for the ferroelectric transition is difficult to obtain from Eq. (2.29) since for $\chi^{-1} \to 0$ the exponent softens the functional approach to zero and is therefore not convergent in any precise sense. However, using the data from

simulations one can fit the polarization coefficient $f(\epsilon)$ in Eq. (2.23) as a function of the dielectric constant to a Padé form given by

$$f(\epsilon) \quad = \quad A\frac{1+a_1\epsilon+b_1\epsilon^2}{1+a_2\epsilon+b_2\epsilon^2}\,. \tag{2.31}$$

With $A = 6.1768$, $a_1 = 0.2613$, $b_1 = 0.004178$, $a_2 = 0.8254$, and $b_2 = 0.03068$ the ferroelectric transition point is found to be at $y* = (4\pi/3)p'$ with $p' = 1.18$. This value for p' is slightly lower in comparison to the value of $p' = 1.28$ obtain by Camp and Patey and $p' = 1.25$ by Weis and Levesque, but does show that a ferroelectric transition in simulations for dipolar fluids is predicted. This behavior is quite apparent when considering the Onsager theory given by the dashed curve in Figure 4 which predicts no transition and the Debye theory which would be a flat line at $f(\epsilon \to \infty) = 4\pi/3$ in the plot given in the aforementioned figure.

An important question lingering behind many of these developments, which has remained mostly unanswered, is to what extent continuum electrostatics can be applied to the calculation of the microscopic fields within dielectrics, with particular respect to the local field $\mathbf{E}_{\rm loc}$, the cavity field $\mathbf{E}_c$, and the reaction field $\mathbf{R}$, which is central for the Onsager picture and its applications to spectroscopy and solvation. Studying the dependence of the cavity, reaction, and local fields on the parameters of dielectric liquids will be the remaining goal of this chapter.

A. Reaction Field. The reaction field, created at the center of a molecule from the polarization in the liquid due to the dipole moment of that molecule, can be calculated directly from the chemical potential derived in Appendix E leading up to Eq. (E39) and in Ref. [25]. Since the response function of the polar liquid follows directly from the generating functional in Eq. (2.1), the reaction field is also obtained from the formalism outlined above

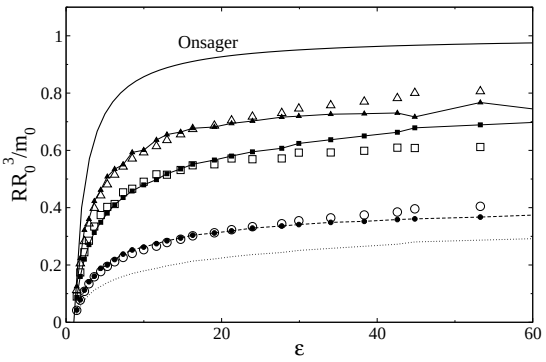

FIG. 5. The reduced reaction field plotted $R(\epsilon)\sigma^3/8m_0$ vs. ϵ. The dotted line represents Eq. (2.33) verbatim, while the solid circles, squares, and triangles with connected lines represent Eq. (2.33) with the perturbation theory effective radius of Eq. (2.3) with $R_0 = 0.5$, 1.0, and 1.5, respectively. The open points correspond to the MC simulation data for the same R_0's as the closed points. The solid line represents the Onsager reaction field given in Eq. (2.34).

after replacing the uniform external field in Eq. (2.19) with the field of a point dipole:

$$\tilde{\mathbf{E}}_0 \;=\; -4\pi \frac{j_1(kR_0)}{kR_0} \mathbf{D}_{\mathbf{k}} \cdot \mathbf{m}_0 \,, \tag{2.32}$$

where $\mathbf{m}_0$ is the dipole moment of a target particle or a solute dipole at the center of the cavity with the radius R_0. The result of this calculation for the reaction field R (see Eq. (E38)) is given by

$$R \;=\; \frac{12ym_0}{\pi R_0^2(2\epsilon+1)} \int_0^\infty j_1^2(kR_0) \left[2\epsilon S^L(k) + S^T(k)\right] dk \,. \tag{2.33}$$

The simulation results for the reaction field inside a homogeneous liquid ($R_0/\sigma = r_{0s} = 0.5$) are shown in Figure 5 along with the cases for a larger solute with $R_0/\sigma = 1.5$. The simulated points for the reaction field fall significantly below the continuum result [12] given in Eq. (1.20), repeated here for convenience,

$$R^{\rm cont} \;=\; \frac{2m_0}{R_0^3} \frac{\epsilon - 1}{2\epsilon + 1} \,. \tag{2.34}$$

Clearly, the simulated data does correspond with Eq. (2.33). In addition, the microscopic reaction field for the pure liquid does not saturate at $\epsilon \gg 1$, but instead keeps increasing approximately linearly with ϵ [41]. The direct calculation by using Eq. (2.33) yields the reaction field qualitatively reproducing the results of the simulations, but quantitatively too low. The reason for the deviation is well understood [42]: cutting out the polarization field from the solute volume in Eq. (2.33) does not incorporate the fact that other liquid fields, e.g. density, must also be zero inside the cavity. In particular, the interaction of the local density field around the solute with the polarization field accounts for a stronger reaction field. This deficiency of our formalism can be remedied in the mean-field fashion by using the effective solute radius given in Eq. (2.3) and appearing in perturbation solvation theories [40]. If the corresponding function for hard spheres is used in Eq. (2.3), the effective radius can be approximated by a simple polynomial function of the density and powers of $1/r_{0s}$ [40]. Using R_{eff} instead of R_0 in Eq. (2.33) in fact gives results very close to the simulations for all three solute sizes in Figure 5. Since the structure factors in such calculations are well approximated by the parametrized MSA solution [25], the problem of calculating the reaction field in dipolar fluids from Eq. (2.33) reduces to a simple quadrature.

B. Cavity Field. The cavity field can be formulated in a similar fashion to that used to derive the microscopic expression for the reaction field. Using the technology from Appendix E, the microscopic expression for the electric field inside a real physical spherical cavity sitting within a dielectric material is found by computing

$$\frac{E_c}{E_0} \quad = \quad 1 + \hat{\mathbf{e}}_0 \cdot \tilde{\mathbf{T}} * \boldsymbol{\chi} * \tilde{\mathbf{E}}_0 \cdot \hat{\mathbf{e}}_0 \,, \tag{2.35}$$

as seen in Eq. (E8). This calculation leads to an expression for the cavity field in terms of longitudinal and transverse structure factors along with the response functions given in

Eqs. (2.10) and (2.11):

$$\frac{E_c}{E_0} = \frac{\epsilon+2}{3\epsilon} - \frac{4R_0}{3\pi}\frac{\epsilon-1}{\epsilon} \times \int_0^\infty j_1^2(kR_0)\left(\chi''^T(k) - \chi''^L(k)\right) dk\,, \tag{2.36}$$

where $\chi''^{L,T}$ are the renormalized response functions given in Eqs. (1.73) and (1.74).

The continuum limit of a macroscopically large cavity is now obtained by assuming that the functions $\chi''^{L,T}(k)$ do not change on the range of k-values, $k \simeq 2\pi/R_0$, on which $j_1^2(kR_0)$ decays and, therefore, by replacing $\chi''^{L,T}(k)$ with their $k=0$ values, $\chi''^{L,T}(0)$. This immediately leads to the result of continuum electrostatics:

$$\frac{E_c^{\rm cont}}{E_0} = \frac{3}{2\epsilon+1}. \tag{2.37}$$

Our formulation therefore contains two well-established limits for the cavity field corresponding to small cavities, much smaller that the length-scale of dipolar correlations (Lorentz field), and the macroscopic cavities for which macroscopic electrostatics apply [Eq. (1.18)]. However, it is easy to realize that there are problems with the derivation of Eq. (1.18) for cavities of finite size. First, it is not clear if the $k=0$ limit can be applied to both $S^{L,T}(k)$ and $\chi'^{L,T}(k)$ in Eq. (2.36) since $\chi'^{L,T}(k)$ decay on about the same scale of k as does $j_1^2(kR_0)$ in Eqs. (2.14)-(2.16). Second, whereas the longitudinal structure factor is reasonably flat at small k-values, the transverse structure factor decays very sharply from its $k=0$ value approaching delta function at the ferroelectric transition. The application of the continuum limit to the transverse part of the response is therefore not well justified. This problem is clearly seen in the fact that $\chi''^T(k) - \chi''^L(k)$ can be rewritten as

$$\chi''^T(k) - \chi''^L(k) = \frac{\chi'^T}{S^T - \chi'^T} - \frac{\chi'^L}{S^L - \chi'^L}\,. \tag{2.38}$$

When Eqs. (2.14) and (2.15) ($\chi'^L(k) = -2A(k)$ and $\chi'^T = A(k)$) are used in Eq.(2.38), the oscillatory function $A(k)$ [Eq. (2.16)] becomes a part of the integral. If the continuum

$k = 0$ substitute is used only for the denominators in Eq. (2.38), one obtains an alternative 'continuum limit' for the cavity field:

$$\frac{E_c^{\rm cont}}{E_0} \;=\; \frac{7(\epsilon+1)^2+8\epsilon}{12\epsilon(2\epsilon+1)}\,. \tag{2.39}$$

This cavity field does not decay to zero with increasing ϵ, but, instead, saturates at 7/24 implying that the ability of a polar liquid to screen the external field is not unlimited as Eq. (2.37) would suggest. An alternative explanation for using the expression for $A(k)$ rather than $A(k \to 0)$ in the integral given in Eq. (2.36) is simply that since $A(k)$ decays on the same length scale as $j_1^2(kR_0)$, by neglecting $A(k)$ one is essentially ignoring the correlations that it produces. Thus, the expression given in Eq. (2.39) is justifiably a more general form of the continuum, at least at mesoscopic length scales.

The most obvious difference in the continuum results and the result given from direct integration of Eq. (2.36) is the appearance of k-poles along the real axis. These real-axis singularities can be used to interpret the result in Figure 6. Since the poles do not appear on the real axis at low values of ϵ, they can be interpreted as giving rise to non-decaying polarization waves at some finite ϵ that are responsible for the appearance of surface charges on the boundaries of the dielectric. These surface charges are what is needed to explain Maxwell's equations in macroscopic dielectric theory. Thus, without these singularities, the behavior of real macroscopic dielectrics is not realized and the results of the 'mesoscopic' world apply. In the range of ϵ after the appearance of these singularities, the integrals are performed as the sum of poles which corresponds to the usual continuum limit for the cavity field given by Eq. (2.37). If the integral in Eq. (2.38) is replaced by a sum over k-points, as is done in the usual way,

$$\int \frac{d^3k}{(2\pi)^3} \;\;\rightarrow\;\; \frac{1}{V}\sum_{\ell,m,n}\,, \tag{2.40}$$

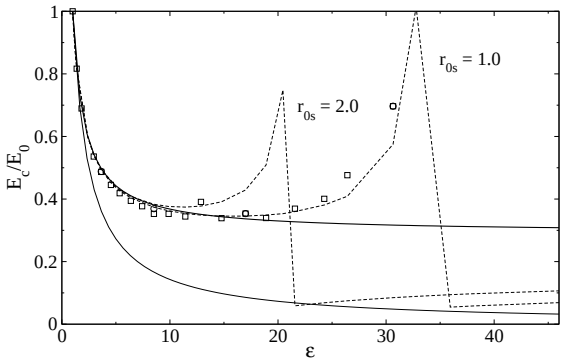

FIG. 6. The cavity field calculated from Eq. (2.36) for two sizes indicated by the distance of closest approach $r_{0s} = R_0/\sigma + 0.5$. The points in the plot were obtained by numerically integrating Eq. (2.36) with $\chi'^{L,T}$ and $S^{L,T}(k)$ directly from MC simulations. The dashed lines correspond to using Eqs. (2.14) and (2.15) for $\chi^{L,T}$ and $S^{L,T}(k)$ from the parametrized MSA [25] along with Eq. (2.9) in Eq. (2.36). The upper and lower solid lines refer to the two continuum limits in Eqs. (2.39) and (2.37), respectively.

one sees the 'mesoscopic' result of Eq. (2.39) as the more viable solution. This idea becomes more transparent when one realizes that the poles established by the continuity of the integration vanish in the discrete sum over k-points ($\mathbf{k} = (2\pi/L)\{\ell, m, n\}$) since it is improbable that the spectrum of lattice vectors will coincide with the singularity needed to establish the polarization wave. A more detailed explanation of this behavior can be found in Ref. [43].

The simulation results for the cavity field also provide access to some new insight into the 'mesoscopic' world since the cavity field can be calculated directly from a system of dipolar hard spheres (DHS) in the density range of real liquids. Of course, as is in all cases of fields, a correction term must be subtracted from the simulation result due to the nature of finite simulation boxes and the use of boundary conditions. This correction is calculated

in Appendix E and is given by

$$E_{\rm corr} = \frac{2\epsilon_{\rm RF}(\epsilon-1)}{\epsilon(2\epsilon_{\rm RF}+1)} + \frac{2(\epsilon-1)}{3\epsilon}\left(\frac{R_0}{r_c}\right)^3\left[\frac{\epsilon-1}{2\epsilon+1}-\frac{\epsilon_{\rm RF}-1}{2\epsilon_{\rm RF}+1}\right], \quad (2.41)$$

where $\epsilon_{\rm RF}$ is the dielectric constant outside of the simulation sphere of radius r_c. A simplification occurs for this correction term when $\epsilon_{\rm RF} = \epsilon$ in which case the dependence of the cut-off radius disappears leaving just the first term in Eq. (2.41). Calculations of the cavity field using perturbation techniques were used in Ref. [44], but the linear response techniques used here give more precise results. The linear response result for the electric field inside an empty cavity is found to be

$$\frac{E_{\rm cav}}{E_0} = 1 + \frac{\beta}{3}\langle\delta\mathbf{E}\cdot\delta\mathbf{M}\rangle_0 - E_{\rm corr}\,, \quad (2.42)$$

where $\mathbf{E} = -\sum \mathbf{T}_{0i}\cdot\mathbf{m}_i$ and $\mathbf{M}$ is the total dipole moment of the entire system. The results of MC simulations for the cavity field are given in Figure 7 for different polarities and cavity sizes. One clearly sees that for all the cavity sizes studied, the Maxwell continuum (dashed line) is never established and it appears that the mesoscopic result is approached for increasing cavity size, shown by the solid line in Figure 7. There is, however, an indication that the Maxwell result may be obtained for specific ranges of $\{R_0, \epsilon\}$ [43]. This observation can been seen in the insert in Figure 8 which shows a slight decrease in the cavity field for the $R_0 \geq 6$ for larger values of ϵ. For smaller values of the dielectric constant, this decrease in the cavity field is never seen as seen in Figure 8.

There does appear some dependence on the number particles used in the simulation when calculating the cavity field. Thus, separate simulations were used, increasing the number of particles each time and extrapolating to the $N \to \infty$ value. These extrapolated

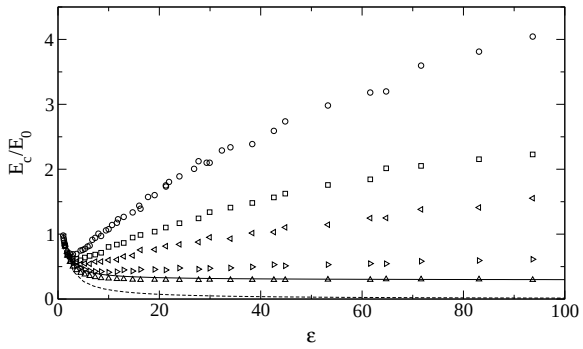

FIG. 7. The cavity field in Eq. (2.42) calculated directly from MC simulations with circles, squares, left triangles, right triangles, and up triangles corresponding $r_1 = 1.0$ ($N = 108$), 1.5 ($N = 108$), 2.0 ($N = 256$), 3.0 ($N = 256$), and 5.5 ($N = 500$), respectively. The solid line corresponds to the continuum expression given in Eq. (2.39) while the dashed line corresponds to Eq. (2.37).

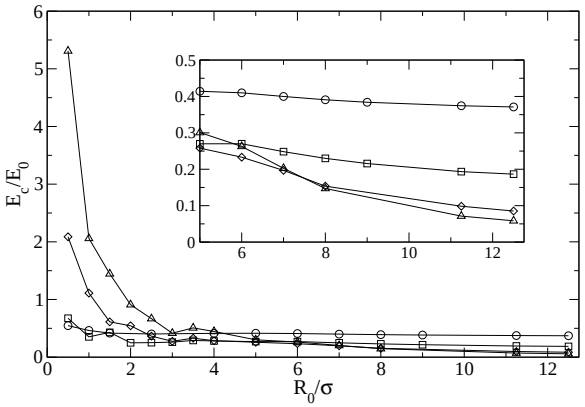

FIG. 8. The cavity field in Eq. (2.42) calculated directly from simulations as a function of the radius R_0/σ. The insert is an expanded section show in the drop in the cavity field. The circles represent $(m^*)^2 = 0.5$, squares 1.0, diamonds 2.0, up-triangles 3.0.

TABLE I. Average cavity field. The averages were performed on system sizes indicated in the footnotes.

	$(m^*)^2$						
R_0/σ	0.1	0.5	1.0	1.5	2.0	2.5	3.0
0.5[a]	0.807±0.003	0.58±0.08	0.65±0.08	1.1±0.2	2.1±0.2	3.0±0.3	3.8±0.9
1.0[b]	0.813±0.004	0.46±0.03	0.44±0.06	0.66±0.07	1.02±0.09	1.6±0.2	2.2±0.2
1.5[c]	0.805±0.002	0.43±0.01	0.39±0.03	0.46±0.07	0.51±0.06	0.89±0.04	1.40±0.08
2.0[c]	–	–	0.32±0.05	–	0.66±0.04	–	–
2.5[c]	0.8053±0.0001	0.41±0.01	0.28±0.02	0.27±0.03	0.35±0.04	0.34±0.02	0.6±0.1
3.0[d]	–	–	0.29±0.03	–	0.34±0.05	–	0.54±0.09
3.5[d]	–	–	0.291±0.003	–	0.321±0.007	–	0.45±0.04
4.0[e]	0.8042±0.0002	0.417±0.004	0.27±0.02	–	0.29±0.01	–	0.40±0.06
5.0[f]	0.805±0.001	0.40±0.01	0.27±0.02	0.24±0.02	0.25±0.02	0.27±0.04	0.29±0.05
6.0[g]	–	0.407±0.004	0.265±0.005	–	0.238±0.005	0.26±0.02	0.28±0.02
7.0[g]	–	0.405±0.004	0.257±0.006	–	0.22±0.01	0.21±0.02	0.23±0.02
8.0[g]	–	0.400±0.005	0.25±0.01	–	0.17±0.02	0.17±0.02	0.17±0.02
9.0[g]	–	0.395±0.007	0.24±0.01	–	–	–	–
10.0	–	–	0.24	–	0.18	–	0.19
11.25	–	0.37	0.19	–	0.098	–	0.071
12.5	–	0.37	0.19	–	0.09	–	0.058

[a] 108, 256, 500, 1372, 2048
[b] 108, 256, 500, 864, 1372
[c] 256, 500, 864, 1372
[d] 500, 864, 1372
[e] 864, 1372, 2048
[f] 500, 864, 1372, 2048, 2916, 4000
[g] 1372, 2048, 2916, 4000

values for the electric field are given in Table I with the corresponding number of particles used in each simulation given in the footnotes.

The curves for smaller cavities do not resemble any predicted analytical result, but all share the same basic dependence on the polarity. The initial drop in the cavity field is qualitatively similar in behavior to that predicted by the analytical theory. However, there is no discontinuity as in Figure 6 for the polarization waves. Thus, one needs to characterize the origins of the increase in the field with increasing dielectric constant. The unexpected dependence of the cavity field on the dielectric constant can be traced back to a local liquid structure formed on the cavity surface which is different than what is used to produce Maxwell's result. Figure 9 shows the distance dependence of the orientational order parameter based on the projection of the unit dipole vector, $\hat{\mathbf{e}}_j$, on the unit radius-vector,

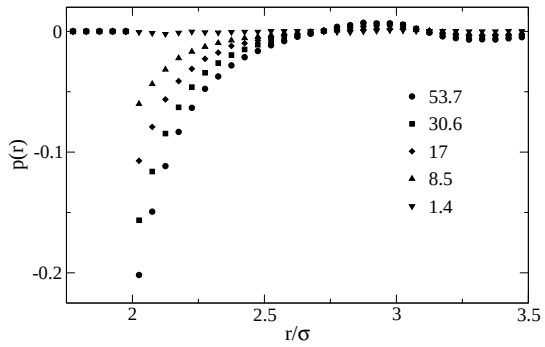

FIG. 9. The orientational order parameter given in Eq. (2.43) plotted verses the radial distance from the center of the cavity r/σ for different values of the polarity indicated on the graph.

$\hat{\mathbf{r}} = \mathbf{r}/r$:

$$p(r) \quad = \quad \left\langle \sum_j P_2(\hat{\mathbf{r}} \cdot \hat{\mathbf{e}}_j) \delta\left(\mathbf{r}_j - \mathbf{r}\right) \right\rangle , \tag{2.43}$$

where $P_2(x) = (1/2)(3x^2 - 1)$ is the second order Legendre polynomial. It is seen that, with increasing polarity, the surface dipoles tend to orient orthogonal to the surface normal (indicated by the negative peak at r_{0s} in Figure 9), a behavior well documented for 2D dipolar fluids [46]. The orientational pattern seen here results in over-screening of the external field which leads to the electric field from the first solvation shell directed opposite to the external field seen in Figure 10. This over-screening is compensated by a positive field from the second solvation shell. The compensation is far from complete for small cavities indicating that the formation of a cavity field is a non-local event involving several solvation shells also seen in Figure 10. For larger cavities (not shown here), the fields of the two first solvation shells make almost the entire cavity field such that the solvent response is more local and continuum-like. However, even for large cavities, over-screening still exists and it takes at least two solvation shells to produce the overall field inside the cavity along

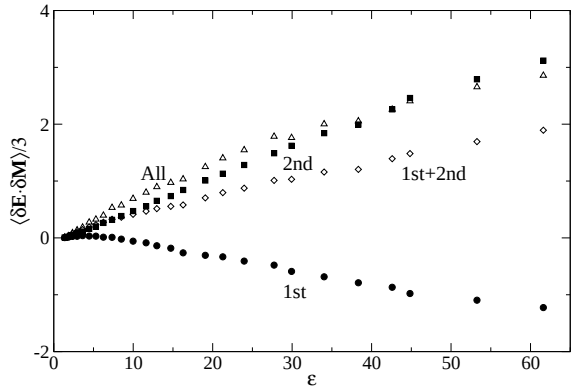

FIG. 10. The correlator $< \delta\mathbf{E} \cdot \delta\mathbf{M} >_0 /3$ given in Eq. (2.42) as a function of ϵ calculated from MC simulations for different contributions to solvation shells. The closed circles represent contributions to this correlator from only the first solvation shell while the closed squares correspond to the second solvation shell only. The first and second solvation shell contributions are added together (open diamonds) and the total contribution is given (open triangles) as well. The cavity radius corresponding to this plot is $R_0/\sigma = 1.0$.

the direction of the external field. The orientation of the surface dipoles perpendicular the surface normal does however dissipate as the cavity radius increases. This behavior is apparent in Figure 9 from the next chapter. This figure shows the contact value of the orientational order parameter given in Eq. (2.43).

III. Linear Response and Continuum Local Field

The electric field acting on a dipole sitting in a uniform electric field can be generally written as

$$\begin{aligned} \mathbf{E}_i &= \mathbf{E}_0 + \sum_{j \neq i} \mathbf{T}_{ij} \cdot \mathbf{m}_j \\ &= \mathbf{E}_0 + \mathbf{F}_i \,. \end{aligned} \tag{2.44}$$

The statistical average of Eq. (2.44) can be readily found as

$$\begin{aligned}\langle \mathbf{F}_i \rangle &= \frac{\int \mathbf{F}_i e^{-\beta(H_0 - \mathbf{E}_0 \cdot \mathbf{M})}}{\int e^{-\beta(H_0 - \mathbf{E}_0 \cdot \mathbf{M})}} = \frac{1}{Z_0} \frac{\int \mathbf{F}_i e^{-\beta H_0} \left(1 + \mathbf{E}_0 \cdot \mathbf{M}\right)}{1 + \langle \mathbf{E}_0 \cdot \mathbf{M} \rangle_0} \\ &= \langle \mathbf{F}_i \rangle_0 + \beta \left[\langle (\mathbf{E}_0 \cdot \mathbf{M}) \, \mathbf{F}_i \rangle_0 - \langle (\mathbf{E}_0 \cdot \mathbf{M}) \rangle_0 \langle \mathbf{F}_i \rangle_0 \right] + \mathcal{O}(\beta^2 E_0^2) \\ &= \langle \mathbf{F}_i \rangle_0 + \beta \mathbf{E}_0 \cdot \langle \delta \mathbf{M} \delta \mathbf{F}_i \rangle_0 \, , \end{aligned} \tag{2.45}$$

where we have only included the terms linear in the field (linear response). Thus one finds

$$\mathbf{E}_i = \mathbf{E}_0 + \langle \mathbf{F}_i \rangle_0 + \beta \mathbf{E}_0 \cdot \langle \delta \mathbf{M} \delta \mathbf{F}_i \rangle_0 \, . \tag{2.46}$$

This relationship is used, after the inclusion of the correction terms, for computing the local field acting on a dipole given from simulation data.

Using the general expression for the electric field at the position of a dipole similar to that in Eq. (2.18),

$$\begin{aligned}\mathbf{E}_i(\mathbf{r}) &= \mathbf{E}_0(\mathbf{r}) + \int_\Omega \mathbf{T}(\mathbf{r} - \mathbf{r}') \cdot \mathbf{P}(\mathbf{r}') d^3 r' \\ \tilde{\mathbf{E}}_i(\mathbf{k}) &= \tilde{\mathbf{E}}_0(\mathbf{k}) + \tilde{\mathbf{T}}(\mathbf{k}) * \tilde{\mathbf{P}}(\mathbf{k}) \, . \end{aligned} \tag{2.47}$$

The dipolar polarization that occurs here is due to both the external field and the local field caused by the interaction of the dipole i and the rest of the molecules in the fluid. Therefore, since

$$\tilde{\mathbf{P}} = \tilde{\boldsymbol{\chi}} \left(\tilde{\mathbf{E}}_0 + \tilde{\mathbf{E}}_i \right) , \tag{2.48}$$

one finds

$$\tilde{\mathbf{E}}_i = \tilde{\mathbf{E}}_0 + \tilde{\mathbf{T}} * \tilde{\boldsymbol{\chi}} * \tilde{\mathbf{E}}_0 + \tilde{\mathbf{T}} * \tilde{\boldsymbol{\chi}} * \tilde{\mathbf{E}}_i \, . \tag{2.49}$$

The first two terms above are exactly the cavity field calculated earlier, while the third term is due to the interaction of the field produced by a dipole and the rest of the dipoles in

the system, *i.e.* the 'reaction field'. Since we have recognized this as being proportional to the reaction field, then we know that it is equal to the dipole moment multiplied by some factor. Particularly,

$$\begin{aligned} E_{loc} &= E_c + \langle \hat{\mathbf{e}}_0 \cdot \mathbf{R} \rangle \\ &= E_c + f \langle \hat{\mathbf{e}}_0 \cdot \mathbf{m}_i \rangle \\ &\approx E_c + \beta f \langle (\hat{\mathbf{e}}_0 \cdot \mathbf{m}_i)(\mathbf{m}_i \cdot \mathbf{E}_0) \rangle_0 \\ &= E_c + f \frac{\beta m_i^2}{3} E_0 \,. \end{aligned} \tag{2.50}$$

In continuum electrostatics,

$$E_c = \frac{3}{2\epsilon + 1} E_0 \,, \tag{2.51}$$

and

$$f = \frac{2(\epsilon - 1)}{2\epsilon + 1} \frac{1}{a_0^3} \,. \tag{2.52}$$

Plugging these into the equation for the field acting on the dipole, and using the definition of the dipolar density, $y = 4\pi\beta\rho m^2/9$, one finds

$$\frac{E_{loc}}{E_0} = \frac{3}{2\epsilon + 1} \left[1 + \frac{2(\epsilon - 1)}{3} \left(\frac{y g_K}{\eta} \right) \right] , \tag{2.53}$$

where $\eta \equiv (\pi/6)\rho\sigma^3$ is the liquid packing fraction. The Onsager-Kirkwood expression for the dipolar density in terms of the bulk dielectric constant is given by

$$y g_K = \frac{(\epsilon - 1)(2\epsilon + 1)}{9\epsilon} \,, \tag{2.54}$$

which when substituted into Eq. (2.53) leads directly to

$$\frac{E_{loc}}{E_0} = \frac{3}{2\epsilon + 1} + \frac{2(\epsilon - 1)^2}{9\epsilon\eta} \,. \tag{2.55}$$

The full result for field acting on a single dipole of radius R_0 can be obtained by first realizing that the reaction field is on average directed along the dipole $\mathbf{m}_0$. Using this information one can obtain the expression

$$E_{loc} = E_c + f\left(\frac{\beta m_0^2}{3}\right) g_K^{(0)} E_0 \,, \tag{2.56}$$

where the solute-solvent Kirkwood factor $g_K^{(0)}$ is defined as

$$g_K^{(0)} = 1 + \frac{m_0}{m} \sum_{i\neq 0}^{N} \langle \hat{\mathbf{m}}_0 \cdot \hat{\mathbf{m}}_i \rangle_0 \,. \tag{2.57}$$

Now, by using the Maxwell cavity field and the Onsager reaction field, one finds the continuum prediction for the micrscopic field acting on a single dipole to be given by

$$\frac{E_{loc}}{E_0} = \frac{3}{2\epsilon+1} + \frac{2(\epsilon-1)}{2\epsilon+1}\left(\frac{m_0}{m}\right)^2 \left(\frac{\sigma}{2R_0}\right)^3 \frac{y g_K^{(0)}}{\eta} \,. \tag{2.58}$$

For the case of large cavities, $g_K^{(0)} \to 1$, and one obtains the result

$$\frac{E_{loc}}{E_0} = \frac{3}{2\epsilon+1} + \frac{2(\epsilon-1)^2}{9\eta\epsilon g_K}\left(\frac{m_0}{m}\right)^2 \left(\frac{\sigma}{2R_0}\right)^3 \,. \tag{2.59}$$

For large ϵ, the second term in Eq. (2.59) dominates and the local field becomes a linear function of ϵ with slope equal to $2/(9\eta)$.

It is clear that in simulations both the terms $\langle F_i \rangle_0$ and $\langle \delta M \delta F_i \rangle_0$ must be corrected since the simulations represent finite systems and only corresponds to the continuum limit through these correction terms. In a similar fashion to the cavity field, the local field can be calculated from linear response, correcting for the boundary conditions resulting in the expression given

$$\frac{E_{loc}}{E_0} = 1 + \left(\frac{\beta m_0^2}{3}\right) g_K^{(0)} \left(\frac{\langle \mathbf{E}_s \cdot \hat{\mathbf{m}}_0 \rangle}{m_0} - f_{corr}\right) + \frac{\beta}{3} \langle \delta\mathbf{M} \cdot \delta\mathbf{E}_s \rangle - E_{corr} \,, \tag{2.60}$$

where E_{corr} and f_{corr} are given by Eqs. (E27) and (E45).

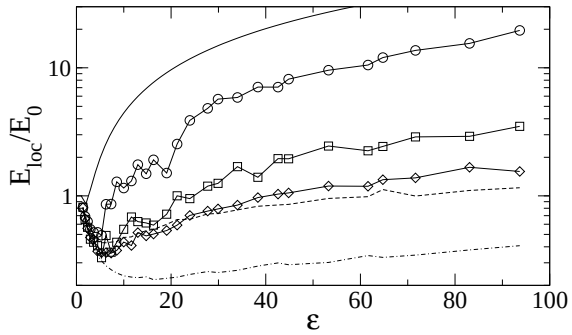

FIG. 11. Local field plotted verses the dielectric constant ϵ. Circles, squares, and triangles represent the calculation from simulation data using Eq. (2.60) for $R_0/\sigma = 0.5$, 1.0, and 1.5, respectively. The solid, dashed, and dashed-dotted lines are the continuum results of Eq. (2.55) and Eq. (2.59), respectively.

The results from simulation and continuum are plotted in Figure 11. One can see that for the pure liquid the results from continuum and simulations correspond very well together, where the continuum expression Eq. (2.55). For larger solutes, $R_0/\sigma = 1.0$ and 1.5, however, the continuum result does not predict that from simulations. We have already seen that there are discrepancies between the local properties on the surface of the solute and that which has been assumed by continuum electrostatics. The continuum results for the local field for $R_0/\sigma > 0.5$ are quite different than that calculated from MC simulation data. The MC data shows that as the solute size is increased the local field for small ϵ does not really change from the pure liquid, but as the solvent dipolar strength increases, the solvent does screen the external field as it should just not to the full extent expected from the continuum result. Another interesting aspect of the local field for the larger solute sizes in Figure 11 is that there is not much difference between the results for $R_0/\sigma = 1.0$ and

TABLE II. Average local field calculated from Eq. (2.60), function f from Eq. (2.23), and g_K calculated according to [40]. All data was calculated with $N = 500$, $\epsilon_{RF} = \epsilon$, and $m_0 = m$. Solute size is indicated in the table.

	$R_0/\sigma = 0.5$				1.0			1.5		
$(m*)^2$	g_K	f	E_{loc}/E_0	$R\,R_0^3/m_0$	$g_K^{(0)}$	E_{loc}/E_0	$R\,R_0^3/m_0$	$g_K^{(0)}$	E_{loc}/E_0	$R\,R_0^3/m_0$
0.1	0.99	3.65	0.81	0.043	1.06	0.81	0.090	0.99	0.81	0.12
0.2	1.04	3.53	0.69	0.078	1.02	0.66	0.17	0.99	0.66	0.22
0.3	1.09	3.41	0.63	0.11	1.12	0.57	0.24	1.10	0.56	0.32
0.4	1.14	2.93	0.55	0.14	1.22	0.46	0.29	0.89	0.47	0.36
0.5	1.33	2.75	0.52	0.16	0.96	0.43	0.33	0.99	0.46	0.42
0.6	1.23	2.67	0.52	0.19	1.07	0.41	0.37	0.88	0.37	0.46
0.7	1.37	2.47	0.49	0.20	0.97	0.33	0.40	1.07	0.36	0.51
0.8	1.43	2.35	0.86	0.22	1.28	0.49	0.41	1.14	0.36	0.53
0.9	1.45	2.21	0.86	0.24	1.01	0.36	0.45	1.29	0.36	0.55
1.0	1.58	2.08	1.29	0.25	1.25	0.43	0.47	1.18	0.38	0.59
1.1	1.64	1.99	1.15	0.26	1.42	0.55	0.49	1.00	0.44	0.60
1.2	1.83	1.92	1.31	0.27	1.56	0.68	0.52	1.33	0.41	0.64
1.3	1.87	1.83	1.75	0.28	1.28	0.63	0.52	1.22	0.52	0.66
1.4	2.03	1.77	1.49	0.29	1.37	0.61	0.53	1.26	0.49	0.66
1.5	2.04	1.71	1.91	0.30	1.40	0.59	0.55	1.31	0.50	0.68
1.6	2.19	1.64	1.51	0.31	1.54	0.72	0.55	1.41	0.54	0.68
1.7	2.30	1.60	2.54	0.32	1.70	1.00	0.57	1.55	0.59	0.69
1.8	2.38	1.54	3.88	0.33	1.45	0.95	0.57	1.68	0.70	0.70
1.9	2.65	1.48	4.82	0.34	1.88	1.19	0.57	1.59	0.76	0.72
2.0	2.74	1.45	5.69	0.34	1.92	1.25	0.59	1.89	0.79	0.72
2.1	2.96	1.39	5.86	0.35	2.14	1.69	0.59	1.71	0.85	0.73
2.2	3.14	1.37	7.07	0.35	1.83	1.40	0.60	1.74	0.97	0.73
2.3	3.19	1.33	7.06	0.36	2.25	1.95	0.61	1.72	1.03	0.73
2.4	3.53	1.31	8.15	0.36	2.36	1.95	0.61	1.59	1.05	0.72
2.5	3.64	1.26	9.58	0.37	2.76	2.45	0.62	2.26	1.19	0.77
2.6	3.96	1.24	10.5	0.38	2.40	2.25	0.62	1.84	1.19	0.74
2.7	4.09	1.19	12.0	0.38	2.55	2.43	0.62	2.20	1.34	0.74
2.8	4.99	1.16	13.7	0.38	2.98	2.89	0.62	2.07	1.38	0.76
2.9	4.99	1.14	15.5	0.39	2.63	2.92	0.63	2.37	1.67	0.75
3.0	5.42	1.11	19.6	0.39	3.00	3.49	0.63	2.16	1.55	0.76

1.5. It is as if the size of the solute, to some extent, does not effect the overall screening of the external field, preventing the local field to decrease to zero for increasing dielectric constant. This observation is quite similar to that seen for the cavity field.

IV. Discussion and Conclusions for Fields Inside Dielectrics

We have seen that the simple understanding of the ideas presented by Maxwell, Debye, Onsager, and some of the other originators of modern electrostatic and dielectric theory can be challenged in a modern perspective. Although this treatment of electric fields inside of dielectrics from the modern point of view still gives rise to many unanswered questions, there has been many interesting facets of the problem that have been presented. For instance, we have seen that the continuum solutions arising from the microscopic theory arise

from k-space singularities in the response function producing a non-decaying longitudinal polarization wave. The appearance of this singularity does not effect the electrostatic free energy for polarizing the dielectric since the total dipole moment of the cavity does not depend on which form of the cavity field is used. Thus, the decrease in the total electrostatic energy by the lower cavity field, is released into the polarization wave.

The cavity size reached in our simulations, $2R_0 \simeq 5$ nm, is of the order of that commonly realized for small nanoparticles, given the typical length-scale of molecular liquids $\sigma \simeq 4-5$ Å. Our results thus suggest that the electrostatics of nanocavities is not consistent with material Maxwell's equations. The discussion so far has been limited to a hollow cavity with the dielectric constant of vacuum, $\epsilon_0 = 1$. However, the results of continuum electrostatics depend only on the ratio of two dielectric constants at the interface [3], ϵ/ϵ_0. Therefore, both the continuum results and the microscopic formalism developed here can be applied to situations with $\epsilon_0 > 1$ by simple replacement $\epsilon \to \epsilon/\epsilon_0$. In this way, our approach is generally applicable to all problems related to inserting impurities into polar liquids given the condition $\epsilon > \epsilon_0$ is satisfied. We also want to notice that no direct measurements of fields within microscopic cavities in polar liquids have been, to our knowledge, reported in the literature. Experimental evidence may arrive from measurements of dielectric relaxation of photoexcited dipolar impurities [45]. If a polar liquid is placed in an external electric field, the torque imposed on a dipole instantaneously created by photoexcitation will be determined by the cavity field.

CHAPTER 3

Electrostatic Fluctuations in Cavities within Polar Liquids and Thermodynamics of Polar Solvation

I. Introduction to Solvation in Polar Liquids

In studying the ionic properties of infinite dilution one encounters the difficulty in treating the long-range forces since the simulation box is not electroneutral and Ewald sums diverge. This trouble, in some sense, can be overcome by using the reaction field geometry, but a deeper understanding of solvation in terms of treating the solute as a cavity can provide much insight into the nature of the continuum electrostatics and solvation. As was seen in the treatment of electric fields in microscopic systems, the standard approach may be problematic since continuum expression are typically used. Thus, understanding the details of microscopic solvation both from a qualitative and quantitative perspective may provide the details needed to completely understand the solvation of mesoscopic systems such as medium to large sized biomolecules. This treatment is difficult in most cases since to do calculations and simulations on molecules with many thousands of atoms is time consuming at the least. There is, however, an approach that can provide such insight into the mesoscopic world by using the idea of cavities and large solutes thus far developed. This chapter is therefore dedicated to such a task. That is, by splitting the solvent-solute interactions into a non-polar interaction and the interaction of a multipole sitting at the center of a cavity, one finds that the continuum theory of electrostatic solvation does not predict the results from direct simulations.

Generally, the solvation energy is the free energy change of a system when an object is inserted. Typically the object is some sort of molecule and the system is some condensed phase. The study of polar liquids invites the notion of simplicity while still provided a great deal of insight into more complex systems and since most of 'life' involves solvation in water (which is polar) it provides some key concepts for understanding the solvation

of biomolecules. The contributions to the free energy almost fully compensate each other since there is a positive free energy associated with creating a cavity for the solute to reside and a negative stabilization free energy from van der Waals and electrostatic interactions [47]. This competitive compensation is what leads to the solvation free energy and is very analogous to that which arise in normal liquids that are in equilibrium [20].

Electrostatic solvation plays in an important role in 'normal' interactions, such as biomolecules solvated in water. Thus, we will be concerned here with electrostatic interactions between charge distributions of the solute and the liquid solvent. In doing so, one sees that treating the solvent as multipoles is well-established in classical electrostatics [3] and dielectric theory [4, 5]. Also, the treatment of such a system in computer simulations is completely known and therefore very easily accessible [26].

Electrostatic solvation has always been thought of as well understood in terms of continuum electrostatics *a la* Born [48] and Onsager [12]. A cavity is constructed within a dielectric in which the solute charge or dipole is placed. This method has been thoroughly tested against the experimental database of the solvation of small molecules in polar liquids [49].

This approach to electrostatic solvation is essentially a boundary value problem in which solving the Poison equation and applying the proper boundary conditions at the dielectric surface essentially leads to that presented by Born and Onsager. As stated in Chapter 1, at the boundary of a macroscopic dielectric interface surface charges are used in order to find the proper potential according to Maxwell's original ideas. What we have seen thus far in the development of electric fields inside real cavities is that the initial assumptions about the boundary interfaces in the mesoscopic region are questionable in that there is a particular alignment of the dipole moments not parallel to the surface normal,

but perpendicular to this surface normal [43].

A new additional piece of evidence comes from studies of hydrophobic solvation essential for colloid stability, biopolymer folding, and formation of biological supramolecular structures [50, 51]. It was found that solvation of non-polar solutes changes dramatically in character at the length of about 1 nm, which is about three molecular diameters for aqueous solvation [52]. Solvation of solutes larger than this characteristic length was found to be dominated by surface effects, i.e. the structure of water at the hydrophobic interface. Weak dewetting [53, 54], i.e. a substantial decrease of the water density at the interface compared to the bulk water, was found to be a central part of solvation of large hydrophobic solutes.

Given the current interest in solvation at mesoscale [55, 56], to a large extent driven by biological applications [57], we address here the problem of electrostatic solvation of solutes significantly larger than those that have been mostly studied. Our interest is thus driven by the question whether the change in the solvation character established for hydrophobic solutes [50] is reflected in an equally dramatic change in the character of electrostatic solvation. The fact that the properties of a polar liquid interface are inconsistent with the assumptions of Maxwell's electrostatics [43] points to the possibility of a new solution once the size of the solute exceeds some critical dimension. This is indeed the result that is seen here.

We have found from numerical simulations that the scaling of the fluctuations of the electrostatic potential and electric field with the cavity radius is consistent with the expectations of electrostatics (qualitatively) and molecular solvation models (quantitatively) for small solutes, but changes dramatically at approximately the same solute/solvent size ratio as observed for hydrophobic solvation. It turns out that the core of the solute becomes non-polar with its growing size much faster than is normally anticipated. We will start with

formulating the general results of the Gaussian solvation thermodynamics and discuss the outcome of computer simulations next.

II. Thermodynamics of Electrostatic Solvation

The chemical potential of electrostatic solvation is defined by the ratio of two partition functions: the one which includes the electrostatic solute-solvent potential V_{0s} and the one which is based on the non-electrostatic solute-solvent interactions and the interactions between the solvent particles. If one considers that all the solute-solvent interactions to be incorporated in the Hamiltonian H_0, one can write down the relationship for the chemical potential μ_{0s} as

$$e^{-\beta\mu_{0s}(\beta)} = Z(\beta)^{-1} \int e^{-\beta V_{0s} - \beta H_0} d\Gamma \,, \tag{3.1}$$

where

$$Z(\beta) = \int e^{-\beta H_0} d\Gamma \,. \tag{3.2}$$

Here, we use the subscript '0' for the solute and the subscript 's' for the solvent, $d\Gamma$ denotes integration over the system phase space including the position, orientations, and momentum (even though the momentum part will drop out when considering electrostatic interactions only), and β is the normal inverse temperature Boltzmann factor. Equation (3.1) can be conveniently re-written in terms of the product of the Boltzmann distribution of finding the solute-solvent energy $\epsilon = V_{0s}$ and the probability density $P(\epsilon, \beta)$

$$e^{-\beta\mu_{0s}(\beta)} = \int P(\epsilon, \beta) e^{-\beta\epsilon} d\epsilon \,, \tag{3.3}$$

where

$$P(\epsilon, \beta) = Q(\beta)^{-1} \int \delta(\epsilon - V_{0s}) e^{-\beta H_0} d\Gamma. \tag{3.4}$$

Equation (3.3) is exact and states that all the thermodynamic information required to understand electrostatic solvation is contained in the distribution of fluctuations of the interaction energy $\epsilon = V_{0s}$ produced by the solvent which is actually not polarized by this potential.

The approximation that we will adopt in our formalism, which is supported by our present simulations and data from other groups [58, 59, 60], is to assume that the distribution function $P(\epsilon, \beta)$ is a Gaussian function with zero average

$$P(\epsilon, \beta) \quad \propto \quad \exp\left[-\frac{\epsilon^2}{2\sigma^2(\beta)}\right]. \tag{3.5}$$

The approximation of zero average is a reflection of the fact that no specific orientation of the solvent dipoles is created around a non-polar solute which we have already seen is not always the case for a cavity constructed inside a dielectric. This approximation is not necessarily correct [61, 62, 63], but is insignificant for most of our development sine a non-zero average, if it exists, can always be incorporated in a linear shift of ϵ. What is the most significant property for our analysis is the magnitude and temperature dependence of the Gaussian width $\sigma^2(\beta)$ since this is directly related to the chemical potential through the fluctuations of the electrostatic energy.

Within the Gaussian approximation for the electrostatic fluctuation around a non-polar solute the thermodynamics of solvation gains a simple and physically transparent form. The chemical potential of solvation is

$$\mu_{0s} \quad = \quad -(\beta/2)\sigma^2(\beta). \tag{3.6}$$

In addition, one can determine the energy e and entropy s of electrostatic solvation

$$\begin{aligned} e &= \langle V_{0s} \rangle + \Delta e_{ss}\,, \\ Ts &= \frac{\langle V_{0s} \rangle}{2} + \Delta e_{ss}\,. \end{aligned} \tag{3.7}$$

In this equation, $\langle V_{0s} \rangle$ is the average solute-solvent electrostatic interaction energy when full solute-solvent interaction is in consideration. From Eqs. (3.6) and (3.7),

$$\langle V_{0s} \rangle \quad = \quad -\beta\sigma^2(\beta). \tag{3.8}$$

The term Δe_{ss} in Eq. (3.7) determines the change in the interaction energy between the solvent molecules induced by electrostatic solute-solvent interaction. This energy term is identically equal to the corresponding contribution to the solvation entropy, $T\Delta s_{ss} = \Delta e_{ss}$, so that Δe_{ss} cancels out in the solvation chemical potential which is determined by solute-solvent interaction thermodynamics only [64, 65]. The term Δe_{ss} can be calculated by either taking the derivative of the Gaussian width $\sigma^2(\beta)$ or from a third-order correlation function

$$\Delta e_{ss} \quad = \quad -\frac{\beta^2}{2}\frac{\partial \sigma^2}{\partial \beta} \quad = \quad (\beta^2/2)\langle \delta V_{0s}^2 \delta H_0 \rangle_0 \tag{3.9}$$

In Eq. (3.9), the average $\langle \ldots \rangle_0$ is over the ensemble of the non-polar solute in equilibrium with the solvent, collectively described by the Hamiltonian H_0. In addition, $\delta V_{0s} = V_{0s} - \langle V_{0s} \rangle_0$ and $\delta H_0 = H_0 - \langle H_0 \rangle_0$ are deviations from the average values determined on the same unpolarized ensemble.

III. Simulations and Data Analysis

While the equations presented in Sec. II are generally applicable to an arbitrary solute, we will use numerical Monte Carlo (MC) simulations to determine the statistics of fluctuations produced in real spherical cavities in a liquid of dipolar hard spheres (see Appendix F for the description of the simulation protocol). The fluid of dipolar hard spheres leaves out many important properties of real liquids, most notably the van der Waals forces and higher order multipoles such as qudrupoles, *etc.* However, it allows a

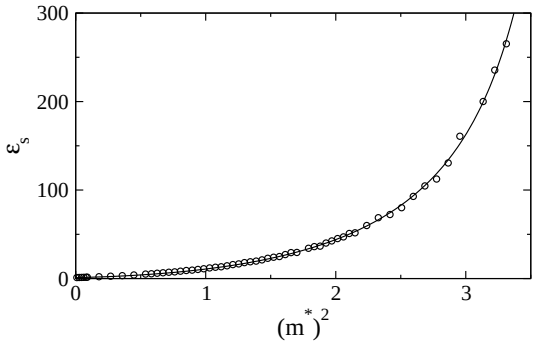

FIG. 12. Dielectric constant ϵ of the liquid of dipolar hard spheres vs the dipolar parameter $(m^*)^2 = \beta m^2/\sigma^3$; $\rho^* = 0.8$. The solid line represents the Padé approximation of the simulation data: $\epsilon_s(x) = (1 + a_1 x + a_2 x^2)/(1 + b_1 x + b_2 x^2)$ with $a_1 = 2.506$, $a_2 = 3.057$, $b_1 = -0.180$, $b_2 = -0.00865$ and $x = (m^*)^2$.

significant simplification of the solvation thermodynamics since all physical properties of the solvent are expressed in terms of the the reduced density $\rho^* = \rho\sigma^3$ and the reduced dipole moment $(m^*)^2 = \beta m^2/\sigma^3$, where m is the dipole moment and σ is the diameter of the solvent dipolar particles. Since the reduced density is fixed to $\rho^* = 0.8$ in our simulations will represent our result in terms of the cavity radius R_0 and the polarity parameter $(m^*)^2$ (or ϵ_s). Figure. 12 shows the relationship between $(m^*)^2$ and ϵ_s calculated from our MC simulations using the formalism from Neumann [24] as described in detail in Ref. [40].

The two type of interaction we will be considering here will be the electrostatic multipoles most commonly studied in theories and applications of solvation, spherical ion and spherical dipole. In both cases, the corresponding charge or dipole is placed at the center of a spherical cavity. The solute-solvent interaction potential is then given by $V_{0s} = q_0\phi_s$ in the case of the ion and $V_{0s} = -\mathbf{m}_0 \cdot \mathbf{E}_s$ for the dipole. In these relations, q_0 and m_0 are the charge and dipole moment of the solute and ϕ_s and $\mathbf{E}_s$ are the respective potential and electric field produced by the solvent at the cavity center taken to be the origin.

The main parameter entering the Gaussian model of solvation that we want to

monitor is the Gaussian width $\sigma^2(\beta)$ since it is related to the potential fluctuations which in turn is related to the solvation free energy. Dimensionless quantities are always nice when treating complex behavior, therefore we will be calculating the temperature reduced parameter

$$\Gamma \;=\; \beta^2\sigma^2(\beta) \;=\; \beta^2\langle(\delta V_{0s})^2\rangle_0\,. \tag{3.10}$$

Since this parameter depends on the electrostatic nature of the solute, it is convenient to reduce it even further by considering the parameter Δ such that the temperature-reduced electrostatic energy factor of the solute is taken out:

$$\Gamma = w\Delta\,, \tag{3.11}$$

where the electric field of the charge or dipole E_0 is used to define the electrostatic energy in the standard way, *i.e.*

$$w \;=\; (\beta/8\pi)\int_\Omega E_0(\mathbf{r})^2 d\mathbf{r}, \tag{3.12}$$

The integral here is taken over the solvent volume outside the spherical cavity of radius R_0.

The parameter w is found easily by performing the integral in Eq. (3.12) with the corresponding electric field used and is found to be equal to $\beta q_0^2/(2R_0)$ for an ion and $\beta m_0^2/(3R_0^3)$ for a dipole. Therefore, one can calculate the parameter Δ according to the following relationships for either an ionic (subscript "i") or a dipolar (subscript "d") solute

$$\Delta_i \;=\; 2\beta R_0\langle(\delta\phi_s)^2\rangle_0, \tag{3.13}$$

$$\Delta_d \;=\; \beta R_0^3\langle(\delta\mathbf{E}_s)^2\rangle_0\,. \tag{3.14}$$

Similarly, we can introduce the reduced parameter Δ_{ss} for the component of the internal

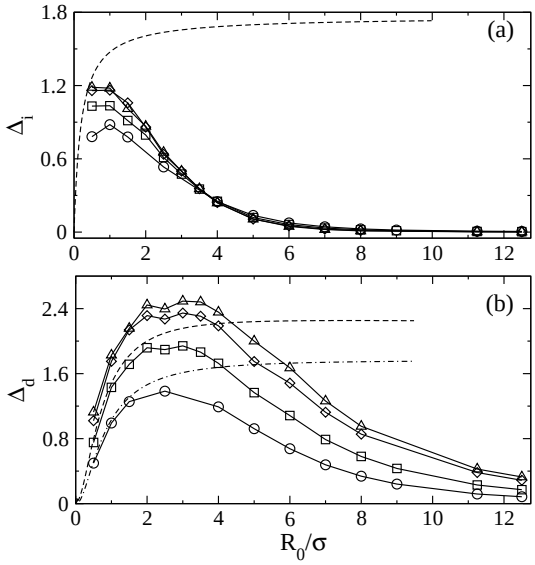

FIG. 13. Δ_i (a) and Δ_d (b) vs the cavity radius R_0 for $(m^*)^2 = 0.5$ (circles), 1.0 (squares), 2.0 (diamonds), and 3.0 (up-triangles). The dashed line in (a) gives the result of Eq. (3.19) for $m^* = 1.0$. The dash-dotted and dashed lines in (b) shows the application of Eq. (3.20) at $(m^*)^2 = 0.5$ and 1.0, respectively.

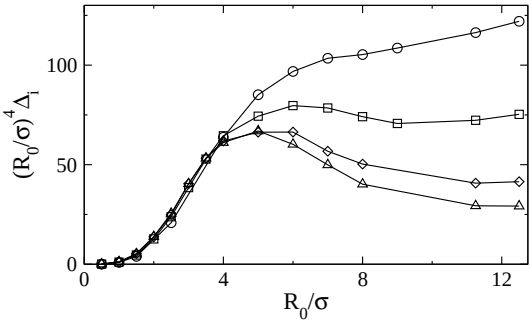

FIG. 14. $(R_0/\sigma)^4\Delta_i$ vs the cavity radius R_0 for $(m^*)^2 = 0.5$ (circles), 1.0 (squares), 2.0 (diamonds), and 3.0 (up-triangles).

energy and entropy that arises from the the solvent-solvent interactions, $\beta\Delta\epsilon_{ss} = w\Delta_{ss}$:

$$\Delta^i_{ss} = \beta^2 R_0 \langle \delta\phi_s^2 \delta H_0 \rangle_0, \tag{3.15}$$

$$\Delta^d_{ss} = (\beta^2 R_0^3/2) \langle \delta E_s^2 \delta H_0 \rangle_0 \,. \tag{3.16}$$

A few analytical results exist in the literature and can be used as benchmarks in calculating Δ_i and Δ_d. The continuum electrostatics of Born [48] and Onsager [12] equations

gives the functions depending only on the dielectric constant ϵ_s of the dipolar liquid:

$$\Delta_i^{\text{cont.}} = 2\left(1 - \frac{1}{\epsilon_s}\right) \tag{3.17}$$

and

$$\Delta_d^{\text{cont.}} = \frac{6(\epsilon_s - 1)}{2\epsilon_s + 1}\,. \tag{3.18}$$

In addition, several microscopic relations have been derived based on different formulations of the liquid-state theory. A closed-form equation for ion solvation is provided by the Ornstein-Zernike integral equations for the ion-dipole mixture solved in the mean-spherical approximation (MSA) [66]:

$$\Delta_i = \frac{2R_0}{R_0 + \Lambda_L}\left(1 - \frac{1}{\epsilon_s}\right) \tag{3.19}$$

In this equation, $\Lambda_L = 3\sigma\xi/(1 + 4\xi)$ is the correlation length of longitudinal polarization fluctuations of a dipolar liquid; ξ is the MSA polarity parameter [18].

An analogous MSA solution exists for the mixture of dipolar particles of different size [67] which gives the parameter Δ_d. Truncated perturbation expansions [68] are however known to work better in this case with the result [40, 25]

$$\Delta_d = 6\left(\frac{R_0}{R_{\text{eff}}}\right)^3 \frac{y}{1 + \kappa(y, r_{0s})y\sigma^3 I_{0s}^{(3)}/R_{\text{eff}}^3}\,. \tag{3.20}$$

$I_{0s}^{(3)}(r_{0s}, \rho^*)$ is the three-particle perturbation integral mentioned in Chapter 1 which is a function of the liquid density, r_{0s}, and the effective radius $R_{\text{eff}}(r_{0s}, \rho^*)$ given in Eq. (2.3). In this equation $g_{0s}^{(0)}(r)$ is, as usual, the hard-sphere distribution function of the liquid particles as a function of the distance r to the cavity center. All functions $R_{\text{eff}}(r_{0s}, \rho^*)$, $I_{0s}^{(3)}(r_{0s}, \rho^*)$, and $\kappa(y, r_{0s})$ are given by analytical expressions in Ref. [25].

IV. Results

The results from our simulations are unexpected in that the scaling of the electrostatic fluctuations at the cavity center and the corresponding chemical potentials do not correspond to either that predicted by continuum electrostatics or microscopic solvation models for large cavities. The plots seen in Fig. 13 show these discrepancies. As is seen, the parameter Δ_i decays much faster than the expected $1/R_0$ scaling for all cavities greater than the size of the solvent particle. The large cavity scaling does not follow any universal law, but instead depends on the polarity (m^*) of the liquid (Fig. 14). For the various liquid polarities studied here, the scaling of Δ_i is approximately $1/R_0^{4-6}$ at large cavities which is substantially different from that which was expected. Fluctuations of the electric field at the cavity center, representing dipole solvation, do not deviate that dramatically from the traditional expectations, but the parameter Δ_d still decays to zero instead of leveling off as suggested by Eqs. (3.17) and (3.20). In fact, Δ_d follows Eq. (3.20) quite well up to the cavity size about four times larger than the pure liquid size, but then starts to drop following qualitatively the trend seen for the potential fluctuations. Continuum electrostatics [Eq. (3.17)] fails both qualitatively and quantitatively for electrostatic fluctuations of both the potential and the electric field.

The first question that arises with such dramatic differences between the continuum electrostatics and the simulation results is whether or not the Gaussian approximation for the distribution of the electrostatic interaction energies for large cavities is justified. We have tested this question by looking at the non-gaussianity parameter for both the potential and electric field fluctuations:

$$\delta_G = \frac{\langle (\delta V_{0s})^4 \rangle}{\langle (\delta V_{0s})^2 \rangle^2} - 3. \tag{3.21}$$

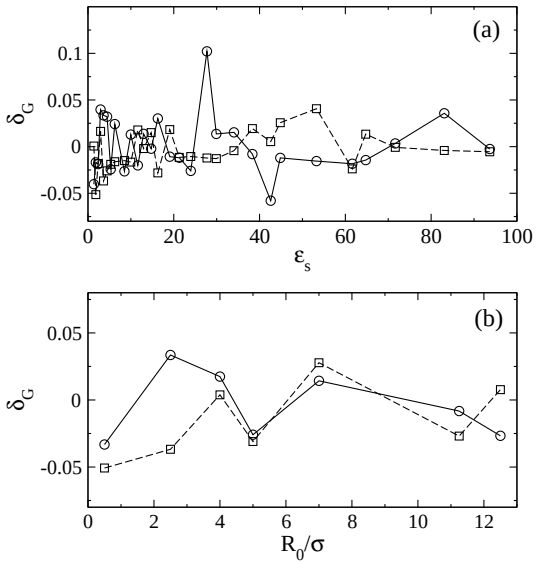

FIG. 15. Non-gaussianity parameter δ_G [Eq. (3.21)] vs ϵ (a) and R_0 (b). Points represent Δ_i (circles) and Δ_d (squares) for $R_0/\sigma = 2.5$ (a) and $(m^*)^2 = 0.5$ (b).

This parameter was found to be around very close to zero, as expected for Gaussian noise, within about 5% of the simulation uncertainties (Fig. 15). The Gaussian approximation therefore seems to be fairly reliable for the parameter database studied here.

Knowing from Chapter 2 that the local properties at the cavity surface are quite different from what was expected for electric fields inside of cavities, we have calculated two local parameters related to the orientational and density structure of the liquid/cavity interface. Figure 16a shows the orientational order parameter of the permanent dipoles in the first solvation shell at the cavity surface according to Eq. (2.43). The orientational order parameter shown in Figure 16a is calculated by limiting the distance r to liquid particles residing in the cavity's first solvation shell where it indicates the existence of a preferential orientational order. This property has already been seen in Figure (9) for a cavity of size three times that of the solvent liquid.

As the cavity gets larger the solvent dipoles find it more energetically favorable to

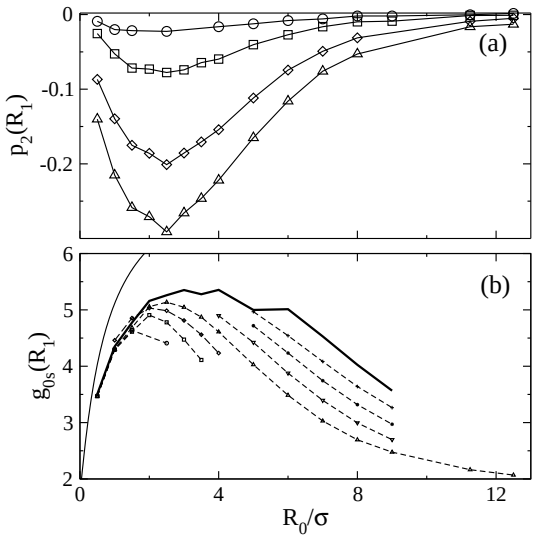

FIG. 16. Upper panel: the orientational order parameter vs the cavity size for different polarities of the solvent, $(m^*)^2 = 0.5$ (circles), 1.0 (squares), 2.0 (diamonds), and 3.0 (up-triangles). Lower panel: contact value of the radial distribution function at $R_1 = R_0+\sigma/2$ vs the cavity radius. Shown are the results for different number of particles in the simulation box $N = 256$ (circles), 500 (squares), 864 (diamonds), 1372 (up-triangles), 2048 (down-triangles), 2916 (stars), 4000 (pluses). Extrapolation to $N \to \infty$ is shown by bold solid line. The dashed lines connect the points. The thin solid line gives the contact value of the distribution function in the hard-spheres mixture from Ref. [70].

orient parallel to the interface, as was also observed for 2D dipolar liquids [46] and for water at cavity surfaces [69]. However, this preferential orientational order starts to drop with the further increase of the cavity size, after gaining maximum for the cavity about five times larger than the solvent particle. The decay of this parameter with increasing cavity size is related to the onset of softening of the first solvation shell indicated by the contact value of the pair cavity-solvent distribution function shown in Figure 16b.

The contact value of the pair distribution function first rises as expected for a hard-sphere impurity in densely packed hard spheres [70] (solid line in Figure 16b), but then starts to drop. This drop appears at approximately the same value $R_0/\sigma \simeq 2 - 2.5$ as both the downward turn of the orientational order parameter and the onset of deviation

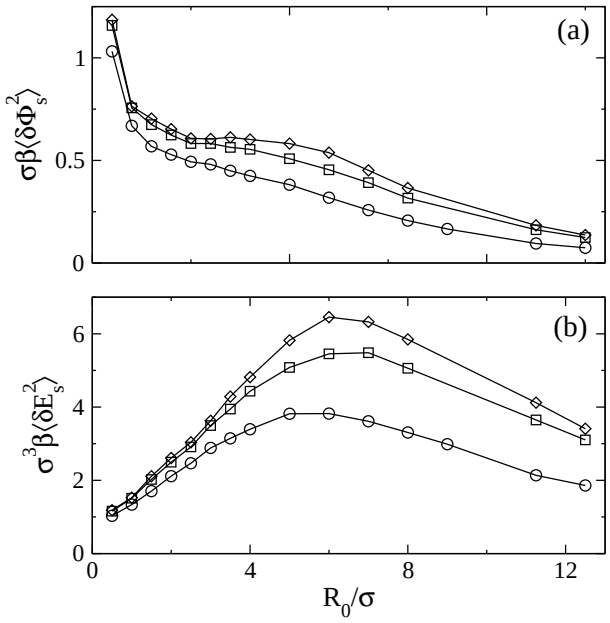

FIG. 17. $\sigma\beta\langle(\delta\phi_s)^2\rangle$ (a) and $\sigma^3\beta\langle(\delta\mathbf{E}_s)^2\rangle$ (b) vs the cavity size for probe charge and dipole located the distance $\sigma/2$ from the cavity surface. The points refer to $(m^*)^2 = 1.0$ (circles), 2.0 (squares), and 3.0 (diamonds); $N = 1372$.

of the electric field fluctuations from the traditional predictions [Figure 13]. We therefore can conclude that the observed change in the character of the electrostatic fluctuations is related to softening of the liquid/cavity interface, which also loosens the energetic push for a specific dipolar order. We note, however, that the peak of the distribution function stays at the closest-approach value $r_{0s} = R_0 + \sigma/2$ and thus no dewetting of the cavity interface occurs.

That the decay of the solvation energies is related to the softening of the interface is also seen from probing the fluctuations of the potential and the field close to the cavity interface. Figure 17 shows the corresponding quantities for a point within the cavity kept one solvent radius $\sigma/2$ away from the interface once the cavity size is increased. Again, simple electrostatic arguments suggest that the solvation energetics should approach that for a probe charge of dipole next to an infinite dielectric wall. Depending on how the

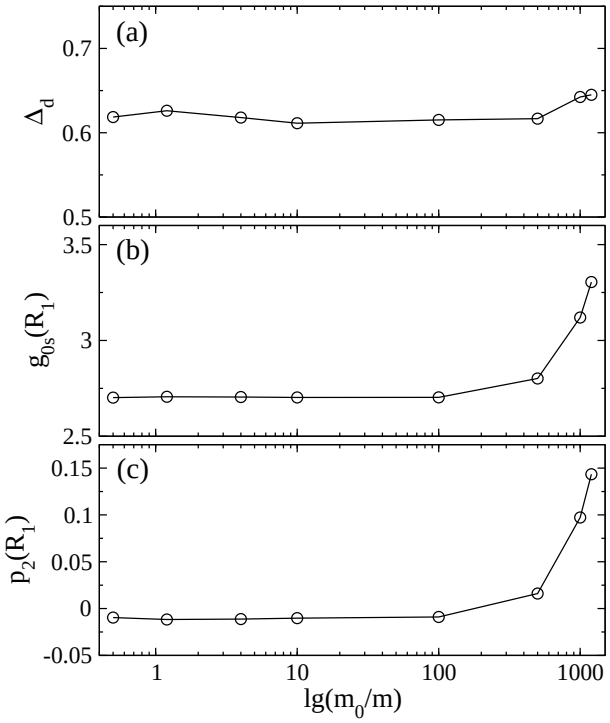

FIG. 18. Δ_i (a) and Δ_d (b) as functions of $(m^*)^2$ for $R_0/\sigma = 0.5$ (circles), 1.0 (squares), 1.5 (diamonds), and 6.0 (up-triangles). The solid line in (a) shows the result of using Eq. (3.19) at $R_0/\sigma = 1.0$. The solid lines in (b) show the result of Eq. (3.20) for $R_0/\sigma = 0.5$, 1.0, and 6.0 (from down up); the dashed lines in (a) and (b) connect the points.

dielectric interface is defined, by the cavity boundary or by the distance of the closest approach, continuum electrostatics predicts [3] for $\sigma\beta\langle(\delta\Phi_s)^2\rangle$ either $(\epsilon_s - 1)/(\epsilon_s + 1)$ or $0.5(\epsilon_s - 1)/(\epsilon_s + 1)$. The observed dependence does seem to inflect to a plateau at the level consistent with this prediction at intermediate cavity sizes, but then starts to decay. This decay is however much more gentle than in Figure 13 indicating that the area next to the interface is effectively stronger solvating than the part of the hollow space closer to the cavity center.

Figure 18a shows the dependence of Δ_i on the solvent dipole moment. For a small cavity size, when the standard scaling with the cavity size is expected to apply, the dependence of Δ_i on the polarity does not show a saturation predicted by continuum electrostatics

[Eq. (3.17)]. This saturation appears for a slightly larger cavities, but, as seen for a still larger cavity, it is simply en route to become a decreasing function of the polarity for the largest cavities studied here. We can therefore conclude that there is no range of parameters where both the size scaling and the dependence on polarity predicted by the continuum electrostatics for the potential fluctuations are satisfied even at the qualitative level, not to mention the fact that the predicted values are significantly off.

The saturation predicted by the Onsager equation for dipole solvation [Eq. (3.18)] is never reached. In contrast to the potential fluctuations, the variance of the field is a uniformly increasing function with increasing solvent dipole for all cavity sizes studied here. A similar trend for a narrower range of parameters was observed previously by us [41] and it manifests itself in the solvation dynamics uniformly slower than continuum predictions [71]. The results for Δ_d from Eq. (3.20) are shown by solid lines in Fig. 18b. As expected, there is a good agreement with the simulations for small cavities, but then the theory fails when the regime of solvation changes and Δ_d turns downward (Fig. 13).

In Figure 21 we show the results of calculations of the solvent-solvent component of the solvation entropy [Eq. (3.7)]. Within the Gaussian approximation, the ratio of the solvent-solvent component of the solvation entropy, $Ts_{ss} = \Delta e_{ss}$, and the solute-solvent component, $Ts_{0s} = -\beta\sigma^2(\beta)/2$, is given as the ratio of the corresponding reduced response functions

$$\chi_s \;=\; -\frac{s_{ss}^{i,d}}{s_{0s}^{i,d}} \;=\; \frac{\Delta_{ss}^{i,d}}{\Delta^{i,d}}\,. \tag{3.22}$$

As is seen, for both the ionic and dipolar solvations, there is a compensation between the ordering of the solvent by the solute, expressed the the fact that $s_{0s} < 0$, and the disordering of the solute-solvent structure, expressed by $s_{ss} > 0$. This compensation, however, is far

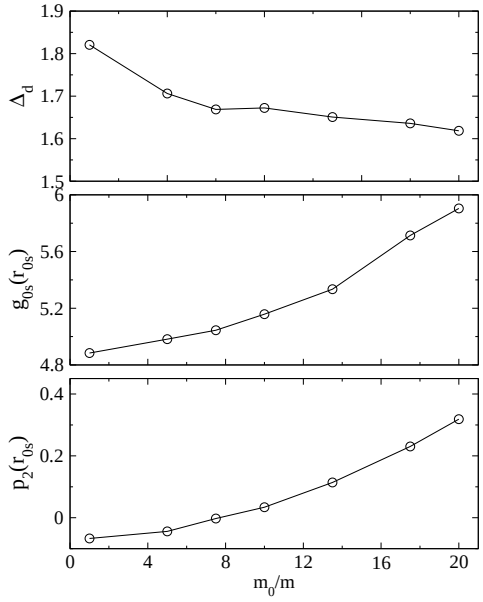

FIG. 19. Response function Δ_d (a), contact value of the cavity-solvent pair distribution $g_{0s}(r_{0s})$ (b), and the orientational order parameter of the dipoles in the first solvation shell $p_2(r_{0s})$ (c) verses the magnitude of the solute dipole at the cavity center m_0. Points are the results of MC simulations with $R_0/\sigma = 9.0$, $(m^*)^2 = 1.0$, and $N = 2048$. The lines connect the simulation points.

from complete, in contrast to a much stronger compensation found for aqueous solvation [72]. The overall entropy of electrostatic solvation is therefore negative. Since the parameter χ_s in Eq. (3.22) depends weakly on the cavity size, the dramatic change in the characterization of solvation found here for $\sigma^2(\beta)$ will be reflected in both the enthalpy and entropy of electrostatic solvation which are often more accessible experimentally than solvation free energies.

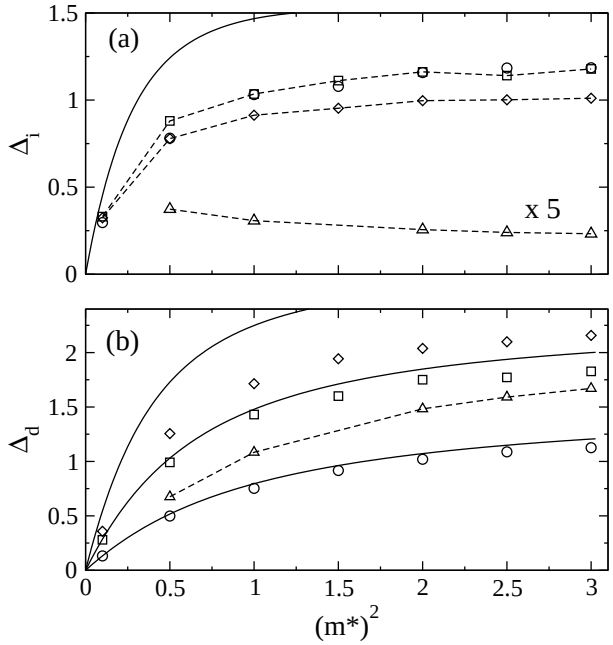

FIG. 20. Δ_i (a) and Δ_d (b) as functions of $(m^*)^2$ for $R_0/\sigma = 0.5$ (circles), 1.0 (squares), 1.5 (diamonds), and 6.0 (up-triangles). The solid line in (a) shows the result of using Eq. (3.19) at $R_0\sigma = 1.0$. The solid lines in (b) show the result of Eq.(3.20) for $R_0/\sigma = 0.5$, 1.0 and 6.0 (from down to up); the dashed lines in (a) and (b) connect the points. The data for Δ_i at $R_0 = 6.0$ (up-triangles) in (a) have been multiplied by a factor of five to bring them to the same scale of the plot. The simulation points were obtained at $N = 1372$ dipolar hard spheres in the simulation box.

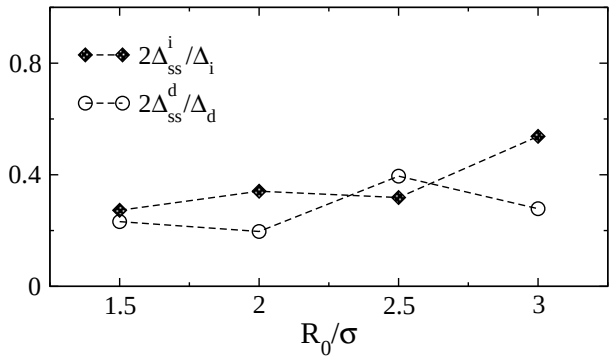

FIG. 21. The ration of the solute-solvent and solvent-solvent components of the solvation entropy [Eq. (3.22)] verses the cavity radius calculated for charge (diamonds) and dipolar (circles) probe multipoles.

V. Discussion of Cavity and Non-Polar Solute Solvation

In this paper we have suggested to study polar solvation by using Eq. (3.3) which states that all the information required to calculate the solvation thermodynamics is contained in the distribution of electrostatic interaction energies around a fictitious solute in which the solute-solvent electrostatic coupling has been switched off. This equation is exact and the approximation adopted here is that the distribution function $P(\epsilon)$ can be approximated by a Gaussian. The distribution $P(\epsilon)$ can generally be written as

$$P(\epsilon) \quad \propto \quad \exp\left[\beta\omega(\epsilon)\right] \tag{3.23}$$

and then the integral over ϵ in Eq. (3.3) can be taken by the steepest descent around the stationary point ϵ_0 defined by the condition $\omega'(\epsilon_0) = 1$. The Gaussian approximation is then equivalent to assuming all the terms except the linear one can be dropped from the series expansion of $\omega'(\epsilon)$ in powers of $(\epsilon - \epsilon_0)$.

Our simulations have not identified any significant deviations from non-gaussianity. Extensive simulations done with ionic and dipolar solutes over the last decades have also resulted in the conclusion that the Gaussian picture is an accurate one implying that $P(\epsilon)$ is globally a Gaussian function. However, one can argue that we could not sample sufficiently around ϵ_0 and thus cannot assess the deviations from Gaussianity. While that might be true for strong solute-solvent interactions, for which a significant data-base pointing otherwise exists, energy ϵ_0 is expected to decrease with increasing the cavity size and the Gaussian approximation is expected to become increasingly accurate. However, it is in this range of large cavities, almost completely neglected in previous studies of electrostatic solvation, that we found the most dramatic deviations from the traditional expectations.

Our simulations have not identified any significant deviations from non-gaussianity.

Extensive simulations done with ionic and dipolar solutes over the last decades [41, 59, 58, 60] have also resulted in the conclusion that the Gaussian picture is an accurate one implying that $P(\epsilon)$ is globally a Gaussian function. However, one can argue that we could not sample sufficiently around ϵ_0 and thus cannot assess the deviations from Gaussianity. While that might be true for strong solute-solvent interactions, for which a significant database pointing otherwise exists [41], energy ϵ_0 is expected to decrease with increasing the cavity size and the Gaussian approximation is expected to become increasingly accurate (as indeed seen from comparing Figures 18 and 19). However, it is in this range of large cavities, almost completely neglected in previous studies of electrostatic solvation, that we found the most dramatic deviations from the traditional expectations.

The main finding of this study is that electrostatic solvation by polar liquids changes its regime at the size of the cavity about 4-5 times larger than the size of the solvent particle. The regime of small cavities can be reasonably understood with molecular solvation models and in particular the results for the electric field fluctuations (probe dipole) are in a very good quantitative agreement with the results of perturbation solvation models. The regime of large cavities is dramatically different and cannot be described by the present models traditionally used for solvation problems.

What we have observed here is a dramatic decay of the solvation strength in the middle of the cavity, much faster than expected from both the continuum electrostatics and microscopic solvation models. For instance, the variance of the electrostatic potential decays as $1/R_0^{4-6}$ instead of the expected $1/R_0$ scaling. The core of a hollow cavity thus becomes non-polar much faster than previously anticipated. What it practically means is that there is very little solvation stabilization for charges inside a large mesoscale object. This might be a reason why natural systems requiring hydration of large molecular assemblies (proteins,

TABLE III. Values of Δ_i and Δ_d for $(m^*)^2 = 0.5, 1.0, 2.0, 3.0$, $\epsilon = 3.63, 8.51, 29.9, 93.7$, respectively. Extrapolations (ext.) were done with $N = 108$, 256, 500, 864, 1372, 2048, 2916, 4000 data when available, linearly fitting $\Delta_{i,d}$ vs. $1/N$ and taking the intercept. The system sizes used for the extrapolations are given in the footnotes.

		$(m^*)^2$							
		0.5		1.0		2.0		3.0	
R_0/σ	N	Δ_i	Δ_d	Δ_i	Δ_d	Δ_i	Δ_d	Δ_i	Δ_d
0.5	1372	0.781	0.498	1.031	0.753	1.158	1.020	1.185	1.126
	ext.[a]	0.814	0.572	1.052	0.761	1.210	1.030	1.265	1.153
1.0	1372	0.892	1.001	1.035	1.431	1.184	1.801	1.240	1.939
	ext.[b]	0.863	1.009	1.050	1.449	1.171	1.768	1.198	1.854
1.5	1372	0.778	1.256	0.936	1.760	1.058	2.137	1.073	2.286
	ext.[c]	0.834	1.292	1.011	1.772	1.084	2.112	1.103	2.238
2.0	1372	–	–	0.795	1.918	0.859	2.314	0.866	2.444
	ext.[c]	–	–	0.862	1.965	0.844	2.300	0.859	2.394
2.5	1372	0.533	1.384	0.632	1.955	0.670	2.365	0.666	2.513
	ext.[c]	0.619	1.491	0.692	2.079	0.695	2.470	0.710	2.627
3.0	1372	–	–	0.475	1.941	0.499	2.345	0.499	2.492
	ext.[d]	–	–	0.612	2.122	0.550	2.468	0.556	2.587
3.5	1372	–	–	0.352	1.864	0.355	2.307	0.355	2.482
	ext.[d]	–	–	0.459	2.129	0.376	2.539	0.375	2.578
4.0	1372	0.249	1.191	0.252	1.723	0.242	2.188	0.239	2.356
	ext.[e]	–	–	0.495	2.186	0.528	2.597	0.533	2.699
5.0	1372	0.136	0.927	0.124	1.431	0.112	1.830	0.107	2.000
	ext.[f]	0.299	1.393	0.310	2.004	0.251	2.388	0.246	2.556
6.0	1372	0.075	0.675	0.061	1.084	0.051	1.483	0.046	1.670
	ext.[g]	0.298	1.449	0.296	2.061	0.236	2.484	0.233	2.553
7.0	1372	0.043	0.478	0.033	0.789	0.024	1.124	0.021	1.263
	ext.[g]	0.192	1.233	0.183	1.834	0.133	2.203	0.125	2.373
8.0	1372	0.026	0.338	0.018	0.581	0.012	0.855	0.010	0.952
	ext.[g]	0.128	1.003	0.114	1.540	0.054	1.790	0.048	2.004
9.0	1372	0.017	0.241	0.011	0.433	–	–	–	–
	ext.[g]	0.087	0.803	0.071	1.258	–	–	–	–
10.0	4000	–	–	0.036	0.830	0.029	1.176	0.025	1.304
11.25	1372	0.0073	0.119	0.0045	0.230	0.0025	0.383	0.0018	0.426
12.5	1372	0.0050	0.085	0.0031	0.172	0.0017	0.287	0.0012	0.329

[a] 108, 256, 500, 1372, 2048
[b] 108, 256, 500, 864, 1372
[c] 256, 500, 864, 1372
[d] 500, 864, 1372
[e] 864, 1372, 2048
[f] 500, 864, 1372, 2048, 2916, 4000
[g] 1372, 2048, 2916, 4000

etc.) rely on solvation of surface charges for which much slower decay of solvating power due to softening of the interface was found here.

REFERENCES

[1] D. J. Griffiths, *Introduction to Electrodynamics, 2nd Ed.* (Prentice Hall, New Jersey, 1989).

[2] J. D. Jackson, *Classical Electrodynamics, 3rd Ed.* (John Wiley & Sons, Inc., New York, 1998).

[3] L. D. Landau, *Electrodynamics of Continuous Media* (Addison-Wesley, Massachusetts, 1960).

[4] C. J. F. Böttcher, *Theory of Electric Polarization* vol. 1 (Elsevier Scientific, New York, 1973).

[5] H. Fröhlich, *Theory of Dielectrics* (Oxford Press, Clarendon, 1949).

[6] H. A. Lorentz, *The Theory of Electrons, 2nd Ed.* (Dover, New York, 1952).

[7] H. A. Lorentz, Ann. Phys., **9**, 641 (1880).

[8] L. V. Lorenz, Ann. Phys., **11**, 70 (1880).

[9] O. F. Mossotti, Bibl. Univ. Modena, **6**, 193 (1847); Mem. di mathem. e fisica Modena, **24** II, 49 (1850)

[10] R. Claussius, *Die mechanische Wärmetheorie Vol. II*, (Braunschweig, 1879).

[11] P. Debye, Physik. Z., **13**, 97 (1912).

[12] L. Onsager, J. Am. Chem. Soc., **58**, 1486 (1936).

[13] G. Nienhuist, J. M. Deutch, J. Chem. Phys., **55**, 4213 (1971).

[14] J. G. Kirkwood, J. Chem. Phys., **4**, 592 (1936); J. Chem. Phys., **7**, 911 (1939).

[15] J. M. Deutch, Ann. Rev. Phys. Chem., **24**, 301 (1973).

[16] P. Madden, D. Kivelson, Adv. Chem. Phys., **56**, 467 (1984).

[17] M. S. Wertheim, Ann. Rev. Phys. Chem., **30**, 471 (1979).

[18] M. S. Wertheim, J. Chem. Phys., **55**, 4291 (1971).

[19] G. Stell, G. N. Patey, J. S. Høye, Adv. Chem. Phys., **18**, 183 (1981).

[20] J. P.Hansen and I. R. McDonald, *Theory of Simple Liquids* (Academic Press, Amsterdam, 2003).

[21] S. A. Rice, P. Gray, *The Statistical Mechanics of Simple Liquids*, (Wiley & Sons, Inc., New York, 1965).

[22] H. N. V. Temperley, J. S. Rowlinson, G. S. Rushbrooke, *Physics of Simple Liquids*, (Wiley & Sons, Inc., New York,1968).

[23] C. G. Gray, K. E. Gubbins, *Theory of Molecular Liquids*, (Clarendon, Oxford, 1984).

[24] M. Neumann, Mol. Phys., **57**, 97 (1986).

[25] D. V. Matyushov, J. Chem. Phys., **120**, 1375 (2004).

[26] M. P. Allen and D. J. Tildesley, *Computer Simulation of Liquids* (Oxford; Clarendon Press, 1989).

[27] H. Li and M. Kardar, Phys. Rev. A **46**, 6490 (1992).

[28] D. Chandler, Phys. Rev. E **48**, 2898 (1993).

[29] S. Gupta and D. V. Matyushov, J. Phys. Chem. A **108**, 2087 (2004).

[30] J. C. Maxwell, *A Treatise on Electricity and Magnetism*, vol. 2 (Dover Publications, New York 1954).

[31] P. Mazur, Adv. Chem. Phys. **1**, 309 (1958).

[32] V. L. Ginsburg, Phys. Usp. **44**, 1037 (2001).

[33] O. V. Dolgov, D. A. Kirzhnits and E. G. Maksimov, Rev. Mod. Phys. **53**, 81 (1981).

[34] F. O. Raineri and H. L. Friedman, Adv. Phy. Chem. **107**, 81 (1999).

[35] D. Wei and G. N. Patey, Phys. Rev. Lett. **68**, 2043 (1992).

[36] B. Huke and M. Lüke, Rep. Prog. Phys. **67**, 1731 (2004).

[37] J. M. Luttinger and L. Tisza, Phys. Rev. **70**, 954 (1946).

[38] I. Ponomareva, I. I. Naumov, I. Kornev, H. Fu, and L. Bellaiche, Phys. Rev. B **72**, 140102(R) (2005).

[39] A. Tani, D. Henderson, and J. A. Barker, Mol. Phys. **48**, 863 (1983).

[40] D. V. Matyushov and B. M. Ladanyi, J. Chem. Phys. **110**, 994 (1999).

[41] A. Milischuk and D. V. Matyushov, J. Phys. Chem. **106**, 2146 (2002).

[42] A. Milischuk and D. V. Matyushov, J. Chem. Phys. **124**, 204502 (2006).

[43] D. Martin and D. V. Matyushov, Euro. Phys. Lett. **82**, 16003 (2008).

[44] Z. Wang, C. Holman, and H. W. Müller, Phys. Rev. E **66**, 021405 (2002).

[45] S. N. Smirnov and C. L. Braun, J. Phys. Chem. **98**, 1953 (1994).

[46] J. J. Weis, Mol. Phys. **100**, 579 (2002).

[47] T. L. Beck, M. E. Paulaitis, and L. R. Pratt, *The Potential Distribution Theorem and Models of Molecular Solutions* (Cambridge University Press, Cambridge, 2006).

[48] M. Born, Z. Phys. **1**, 45 (1920).

[49] A. V. Marenich, C. J. Cramer, and D. G. Truhlar, J. Chem. Theory Computat. **4**, 877 (2008).

[50] D. Chandler, Nature **437**, 640 (2005).

[51] A. A. Rashin, Prog. Biophys. Molec. Biol. **60**, 73 (1993).

[52] K. Lum, D. Chandler, and J. Weeks, J. Phys. Chem. B **103**, 4570 (1999).

[53] G. Hummer and S. Garde, Phys. Rev. Lett. **80**, 4193 (1998).

[54] D. M. Huang and D. Chandler, Phys. Rev. E **61**, 1501 (2000).

[55] A. C. Maggs and R. Everaers, Phys. Rev. Lett. **96**, 230603 (2006).

[56] H. S. Ashbaugh and L. R. Pratt, Rev. Mod. Phys. **78**, 159 (2006).

[57] T. Rudas, C. Schröder, and O. Steinhauser, J. Chem. Phys. **124**, 234908 (2006).

[58] R. A. Kuharski, J. S. Bader, D. Chandler, M. L. Klein, M. Sprik, and R. W. Impey, J. Chem. Phys. **89**, 3248 (1988).

[59] J. Blumberger and M. Sprik, J. Phys. Chem. B **109**, 6793 (2005).

[60] J. Aqvist and T. Hansson, J. Phys. Chem. **100**, 9512 (1996).

[61] V. P. Sokhan and D. J. Tildesley, Mol. Phys. **92**, 625 (1997).

[62] H. S. Ashbaugh, J. Phys. Chem. B **104**, 7235 (2000).

[63] D. S. Cerutti, N. A. Baker, and J. A. McCammon, J. Chem. Phys. **127**, 155101 (2007).

[64] H. A. Yu and M. Karplus, J. Chem. Phys. **89**, 2366 (1988).

[65] D. Ben-Amotz, F. O. Raineri, and G. Stell, J. Phys. Chem. B **109**, 6866 (2005).

[66] D. Y. C. Chan, D. J. Mitchell, and B. W. Ninham, J. Chem. Phys. **70**, 2946 (1979).

[67] B. C. Freasier and D. J. Isbister, Mol. Phys. **38**, 81 (1979).

[68] B. Larsen, J. C. Rasaiah, and G. Stell, Mol. Phys. **33**, 987 (1977).

[69] S. Rajamani, T. Ghosh, and S. Garde, J. Chem. Phys. **120**, 4457 (2004).

[70] D. V. Matyushov and B. M. Ladanyi, J. Chem. Phys. **107**, 5815 (1997).

[71] D. V. Matyushov, J. Chem. Phys. **122**, 044502 (2005).

[72] P. K. Ghorai and D. V. Matyushov, J. Phys. Chem. A **110**, 8857 (2006).

APPENDIX A

DERIVATION OF THE FIELD DUE TO THE POLARIZATION

1. Method 1: Integral Method

Using Eq. (1.5) for the potential and taking the polarization vector constant and along the $\hat{z}$ direction, one finds the second term vanishes and the potential is given by

$$V(\mathbf{r}) \;=\; P \oint_{\partial\Omega'} \frac{\cos\theta'}{|\mathbf{r}-\mathbf{r}'|}\, d^2r' \,. \tag{A1}$$

Taking the volume to be a sphere, the differential surface element is given by $d^2r' = R^2 \sin\theta'\, d\theta'\, d\phi'$ and the potential is simply

$$V(\mathbf{r}) \;=\; 2\pi R^2 P \int_0^\pi \frac{1}{|\mathbf{r}-\mathbf{r}'|} \cos\theta' \,\sin\theta'\, d\theta' \,, \tag{A2}$$

noting, of course, that the vector $\mathbf{r}'$ is on the surface of the sphere and has magnitude R. Now, the electric field is negative the gradient of the potential. Thus, the electric field is

$$\begin{aligned} \mathbf{E}(\mathbf{r}) \,=\, -\boldsymbol{\nabla} V(\mathbf{r}) \;&=\; -2\pi R^2 P \int_0^\pi \boldsymbol{\nabla} \frac{1}{|\mathbf{r}-\mathbf{r}'|} \cos\theta' \,\sin\theta'\, d\theta' \\ &=\; 2\pi R^2 P \int_0^\pi \frac{\mathbf{r}-\mathbf{r}'}{|\mathbf{r}-\mathbf{r}'|^3} \cos\theta' \,\sin\theta'\, d\theta' \,. \end{aligned} \tag{A3}$$

Finally, taking the electric field along the z-axis and evaluating at $\mathbf{r} = 0$ (in the center of the sphere), one finds

$$\begin{aligned} \mathbf{E}(0) \;&=\; -2\pi R^2 P \int_0^\pi \frac{R\,\cos\theta'\,\hat{z}}{R^3} \cos\theta' \,\sin\theta'\, d\theta' \\ &=\; -2\pi P\hat{z} \int_0^\pi \cos^2\theta' \,\sin\theta'\, d\theta' \\ &=\; -2\pi \mathbf{P} \int_{-1}^1 x^2\, dx \\ &=\; -\frac{4\pi}{3}\,\mathbf{P} \,. \end{aligned} \tag{A4}$$

Note: the derivative of the object

$$\frac{1}{|\mathbf{r}-\mathbf{r}'|}$$

carries different signs depending upon the coordinates with which the derivative is taken respect to, *i.e.*

$$\boldsymbol{\nabla}\left(\frac{1}{|\mathbf{r}-\mathbf{r}'|}\right) = -\frac{(\mathbf{r}-\mathbf{r}')}{|\mathbf{r}-\mathbf{r}'|^3}\,,$$

while

$$\boldsymbol{\nabla}'\left(\frac{1}{|\mathbf{r}-\mathbf{r}'|}\right) = \frac{(\mathbf{r}-\mathbf{r}')}{|\mathbf{r}-\mathbf{r}'|^3}\,.$$

2. Method 2: Boundary Value Problem

Choosing $\mathbf{P}$ constant in the $\hat{z}$ direction as is for the geometry of the problem, one can define the surface charge density by Eq. (1.6)

$$\begin{aligned}\sigma &= = \mathbf{P}\cdot\hat{\boldsymbol{n}} \\ &= P\,\cos\theta\,. \end{aligned} \tag{A5}$$

Due to the symmetry of the problem, one may expand the potential in terms of Legendre polynomials and radial functions as is typically done. Thus, the general potential may be written as

$$V(r,\theta) = \sum_{\ell=0}^{\infty}\left(A_\ell\, r^\ell + B_\ell\, r^{-(\ell+1)}\right) P_\ell(\cos\theta)\,. \tag{A6}$$

Due to the finite value the potential has at the origin, $B_\ell = 0$ inside the sphere. Similarly, the coefficient $A_\ell = 0$ outside the sphere since the potential must go to zero as $r \to \infty$. The application of the boundary condition that the potential must be zero at the sphere boundary requires that $B_\ell = A_\ell\, R^{2\ell+1}$. This is easily seen from evaluating the potential on either side of the sphere at $r = R$ and equating them, *i.e.*

$$\sum_{\ell=0}^{\infty} A_\ell\, R^\ell P_\ell(\cos\theta) = \sum_{\ell=0}^{\infty} B_\ell\, R^{-(\ell+1)} P_\ell(\cos\theta)\,, \tag{A7}$$

multiplying both sides by $P_m(\cos\theta)\,\sin\theta$, and integrating θ from 0 to π. The second boundary condition states that the discontinuity in the electric displacement normal to the surface

across the boundary is equal to the surface charge density, explicitly written as

$$(\mathbf{D}_2 - \mathbf{D}_1) \cdot \hat{\boldsymbol{n}}_{21} \;=\; 4\pi\,\sigma(\mathbf{r})\,, \tag{A8}$$

where the unit vector $\hat{\boldsymbol{n}}_{21}$ is the unit normal to the surface of the boundary and directed from region 1 to region 2. Since the electric displacement is related to the potential through the relation $\varepsilon\,\mathbf{E}(\mathbf{r}) = -\boldsymbol{\nabla} V(\mathbf{r})$. Specifically,

$$\left(\frac{\partial V_2}{\partial r} - \frac{\partial V_1}{\partial r}\right)\bigg|_{r=R} \;=\; -4\pi\,\sigma(\mathbf{r})\,, \tag{A9}$$

where the dielectric constant has been taken to equal 1 since the potential is due only to the surface charge density in this macroscopic point of view. This boundary condition along with the result of solving Eq. (A7) for B_ℓ, leads to the set of equations

$$\sum_{\ell=0}^{\infty} (2\,\ell + 1)\, A_\ell\, R^{\ell-1}\, P_\ell(\cos\theta) \;=\; 4\pi\,\sigma(\theta) \tag{A10}$$

Using the orthogonality of Legendre polynomials

$$\int_0^\pi P_\ell(\cos\theta)\, P_m(\cos\theta)\, \sin\theta\, d\theta \;=\; \frac{2\,\delta_{\ell,m}}{2\ell + 1}\,, \tag{A11}$$

it straight forward to show

$$\begin{aligned} A_\ell &= \frac{4\pi}{2\,R^{\ell-1}} \int_0^\pi \sigma(\theta) P_\ell(\cos\theta)\, \sin\theta\, d\theta \\ &= \frac{4\pi\,P}{2\,R^{\ell-1}} \int_0^\pi \cos\theta\, P_\ell(\cos\theta)\, \sin\theta\, d\theta\,, \end{aligned} \tag{A12}$$

where Eq. (A5) has been used for the charge density. Again, due to the orthogonality of Legendre polynomials, ℓ must equal one and only one. Thus,

$$A_1 \;=\; \frac{4\pi}{3} P\,, \tag{A13}$$

and the potential inside and outside the sphere is simply given by

$$V(\mathbf{r}) \;=\; \frac{4\pi}{3}\,P \begin{cases} r\,\cos\theta & r \le R \\ \frac{R^3}{r^2}\cos\theta & r \ge R \end{cases}\,. \tag{A14}$$

Finally, using the fact that $z = r\cos\theta$ and $\mathbf{E}(\mathbf{r}) = -\boldsymbol{\nabla} V(\mathbf{r})$, one obtains the same results as given in Eq. (A4) for the electric field inside the cavity.

$$\begin{aligned} \mathbf{E}(\mathbf{r}) &= -\frac{4\pi}{3} P\,\hat{z} \\ &= -\frac{4\pi}{3}\,\mathbf{P} \end{aligned} \tag{A15}$$

APPENDIX B

LANGEVIN FUNCTION AND THE AVERAGE OF COSINE

The importance of understanding the statistical average of the cosine function when dipoles are in the presence of an electric field becomes recognized when deriving the dielectric constant. If the electric field acting on a dipole is split into the part that is responsible for spacial orientational and translational deviations, respectively, then one can right the energy corresponding to the orientational degrees of freedom as

$$W = -\boldsymbol{\mu} \cdot \mathbf{E} = -\mu E \cos\theta \,. \tag{B1}$$

Therefore, the average of cosine becomes an important quantity to consider when deriving an expression for the average energy corresponding to the directing of the dipoles. Explicitly, one may write

$$\langle \cos\theta \rangle = \frac{\int \cos\theta \, e^{-\beta\mu E_d \cos\theta} \, d\Omega}{\int e^{-\beta\mu E_d \cos\theta} \, d\Omega} \,, \tag{B2}$$

where $d\Omega = 2\pi \, \sin\theta \, d\theta$ is the solid angle between θ and $\theta + d\theta$. The numerator in Eq. (B2) can be cast into the simpler form

$$\begin{aligned} \int_{-1}^{1} x \, e^{-\eta \, x} \, dx &= -\frac{\partial}{\partial \eta} \int_{-1}^{1} e^{-\eta \, x} \, dx \\ &= -\frac{\partial}{\partial \eta} \left[\frac{1}{\eta} \left(e^{-\eta} - e^{\eta} \right) \right] \\ &= -\frac{1}{\eta^2} \left(e^{\eta} - e^{-\eta} \right) + \frac{1}{\eta} \left(e^{\eta} + e^{-\eta} \right) \,, \end{aligned} \tag{B3}$$

where $\eta = \beta\mu E_d$ and $\beta = (k_B T)^{-1}$. The denominator is very simple to compute and results in

$$\int_{-1}^{1} e^{-\eta \, x} \, dx = \frac{1}{\eta} \left(e^{\eta} - e^{-\eta} \right) \,. \tag{B4}$$

Thus, the result of Eq. (B2) is given by

$$\langle \cos\theta \rangle = \coth\eta - \frac{1}{\eta} \,. \tag{B5}$$

Eq. (B5) is referred to as the *Langevin* function (1905). One can expand $\coth\eta$ for small η corresponding to $\mu E_d \ll k_B T$ resulting in the expression

$$\langle\cos\theta\rangle \;=\; \left(\frac{1}{\eta}+\frac{\eta}{3}-\frac{\eta^3}{45}+\frac{2\eta^5}{945}-\frac{2\eta^7}{4725}+\mathcal{O}(\eta^9)\right)-\frac{1}{\eta}\,. \tag{B6}$$

Therefore, to first order in η the statistical average of the cosine function in terms of the permanent dipole moments and the electric field responsible for orienting the dipoles is given by

$$\langle\cos\theta\rangle \;\simeq\; \frac{\mu E_d}{3k_B T}+\mathcal{O}(E_d^3)\,. \tag{B7}$$

Using Eq. (B7) and the energy defined in Eq. (B1), it is seen that

$$\begin{aligned}\langle\boldsymbol{\mu}\cdot\mathbf{E}_d\rangle &= \mu E_d\,\langle\cos\theta\rangle \\ &\simeq \frac{\mu^2 E_d^2}{3k_B T}+\mathcal{O}(E_d^4)\,,\end{aligned} \tag{B8}$$

and therefore for the permanent electric dipole moment one obtains

$$\boldsymbol{\mu} \;\simeq\; \frac{\mu^2}{3k_B T}\,\mathbf{E}_d\,. \tag{B9}$$

APPENDIX C

GENERAL BOUNDARY VALUE PROBLEM FOR A DIELECTRIC SPHERE

Consider a point dipole $\boldsymbol{\mu} = \mu\,\hat{\mathbf{r}}'$ within a cavity of radius a in a dielectric sphere with dielectric constant ϵ_2 and radius R. Now, place this dielectric sphere with spherical cavity into a dielectric with dielectric constant ϵ_3 and then apply an external electric field $\mathbf{E}_0 = E_0\hat{\mathbf{z}}$. One could deal with the fact that the point dipole in the center of the sphere is offset from the $\hat{z}$ direction by expanding the potential in spherical harmonics and solving from there, but in light of the averaging technique given in Appendix B, one can take the average of the dipole moment in the $\hat{z}$ direction along the direction of the applied field. Although this does seem reasonable for the purposes presented here, it must be noted that the 'real' directing field is only partially due to the applied field and does include a part from the dielectric material, especially that in region 2 for $a \ll R$.

The average dipole in region 1 can be found by first writing the potential due to this dipole as

$$V_{dip} \;=\; \frac{\boldsymbol{\mu}\cdot\mathbf{r}}{r^3} \;=\; \frac{\mu}{r^2}\,\hat{\mathbf{r}}'\cdot\hat{\mathbf{r}} \;=\; \frac{\mu}{r^2}\cos\gamma\,, \tag{C1}$$

where γ is the angle between the dipole and the point at which the potential is being evaluated. The unit vectors given in Eq. (C1) may be written in terms of Cartesian coordinates as $\hat{\mathbf{r}} = \cos\phi\sin\theta\,\hat{x} + \sin\phi\sin\theta\,\hat{y} + \cos\theta\,\hat{z}$ and similarly for $\hat{\mathbf{r}}'$ with the angles replaced by primes on the angles. With these definitions for the unit vectors, it is easy to show that $\cos\gamma = \cos\theta\cos\theta' + \sin\theta\sin\theta'\cos(\phi-\phi')$. At this point one can easily see that in finding the average potential due to the fluctuations of the point dipole at the center of the cavity, one must average over the primed angles. In doing so using the method of Appendix B, one finds the potential introduced in Eq. (C1) can be taken as

$$\langle V_{dip}\rangle_{(\theta',\,\phi')} \;=\; \frac{\mu'\,\cos\theta}{r^2}\,, \tag{C2}$$

where $\mu' = \mu\,\eta/3$, $\eta = \beta\mu E_d$, and $\beta = (k_B T)^{-1}$. In this case, the directing field is taken

as E_d just as a reminder of the approximation being made, but $E_d = E_0$ will be used throughout this derivation.

The potential is generally given by Eq. (A6) for all three regions. The corresponding boundary conditions are given as follows:

1. The potentials are continuous across the boundaries,

$$\begin{aligned} V_1(r=a) &= V_2(r=a) \\ V_2(r=R) &= V_3(r=R)\,. \end{aligned}$$

2. The derivatives of the potentials across the boundary are given by

$$\left(\frac{\partial V_1}{\partial r}\right)_{r=a} = \epsilon_2 \left(\frac{\partial V_2}{\partial r}\right)_{r=a}$$

$$\epsilon_2 \left(\frac{\partial V_2}{\partial r}\right)_{r=R} = \epsilon_3 \left(\frac{\partial V_3}{\partial r}\right)_{r=R}\,.$$

3. The potential at $r = \infty$ is only due to the electric field,

$$V_3(r \to \infty) = -E_0 r\,\cos\theta\,.$$

4. The potential at $r = 0$ is only due to the dipole at the origin,

$$V_1(r=0) = V_{dip}\,.$$

Applying boundary conditions 3 and 4, give the potentials for the regions 1, 2, and 3 as

$$V_1(r \le a, \theta) = A_1\, r\,\cos\theta + \frac{\mu'\,\cos\theta}{r^2} \tag{C3}$$

$$V_2(a \le r \le R, \theta) = A_2\, r\,\cos\theta + B_2\, r^{-2}\,\cos\theta \tag{C4}$$

$$V_3(r \ge R, \theta) = B_3\, r^{-2}\,\cos\theta - E_0\, r\,\cos\theta\,. \tag{C5}$$

In applying the remaining boundary conditions (1 and 2), one finds the unknown coefficients

$$A_1 = \frac{2\mu'\rho\epsilon_{23}(\epsilon_2+2) - 2\mu'(\epsilon_2-1)(\epsilon_2+2\epsilon_3) - 9\epsilon_2\epsilon_3 E_0 a^3}{a^3\left[\,(2\epsilon_2+1)(\epsilon_2+2\epsilon_3) - 2\rho\epsilon_{23}(\epsilon_2-1)\,\right]} \tag{C6}$$

$$A_2 = \frac{3\left[\,2\mu'\epsilon_{23} - E_0 R^3\epsilon_3(2\epsilon_2+1)\,\right]}{R^3\left[\,(2\epsilon_2+1)(\epsilon_2+2\epsilon_3) - 2\rho\epsilon_{23}(\epsilon_2-1)\,\right]} \tag{C7}$$

$$B_2 = \frac{3\left[\,\mu'(\epsilon_2+2\epsilon_3) - E_0 a^3\epsilon_3(\epsilon_2-1)\,\right]}{(2\epsilon_2+1)(\epsilon_2+2\epsilon_3) - 2\rho\epsilon_{23}(\epsilon_2-1)} \tag{C8}$$

$$B_3 = \frac{9\epsilon_2\mu' - E_0 a^3(\epsilon_2-1)(2\epsilon_2+\epsilon_3) + E_0 R^3\epsilon_{23}(2\epsilon_2+1)}{(2\epsilon_2+1)(\epsilon_2+2\epsilon_3) - 2\rho\epsilon_{23}(\epsilon_2-1)}\,, \tag{C9}$$

where $\epsilon_{23} = \epsilon_2 - \epsilon_3$ and $\rho = (a/R)^3$.

The purpose of using the more complicated boundary value problem given rather than the typical ones that are treated in the context of dielectrics is that one can obtain all the pertinent fields as limiting case of the potentials given in Eqs. (C3)–(C9). For instance, one can find the potential in a spherical cavity submerged in a dielectric with dielectric constant ϵ containing a dipole by taking $E_0 = 0$, $\epsilon_2 = \epsilon$, and taking the limit as $R \to \infty$ with the potential given by V_1. The result of this calculation is

$$V_{in}(r \le a) = \frac{\mu'\,\cos\theta}{r^2} - \frac{2(\epsilon-1)}{(2\epsilon+1)}\,\frac{\mu'}{a^3}\,r\cos\theta\,. \tag{C10}$$

One can now subtract off the potential due to the dipole and take the negative gradient to find the field the dipole causes in the cavity from the reaction with the dielectric, *i.e.* the reaction field. Thus, this reaction field is given by

$$\mathbf{R} = \frac{1}{a^3}\,\frac{2(\epsilon-1)}{(2\epsilon+1}\,\boldsymbol{\mu}'\,. \tag{C11}$$

Another significant result that can derived as a limiting case of Eqs. (C3)–(C9) is found by taking $\epsilon_3 = \epsilon$, $\mu' = 0$, and setting $R = a$. By doing so, one finds for the field inside the

cavity (with no dipole) due to the dielectric outside and the applied field, *i.e.* the cavity field, is given by

$$\mathbf{E}_c \;=\; \frac{3\epsilon}{2\epsilon+1}\,\mathbf{E}_0\,. \tag{C12}$$

As a final case, one can examine the Onsager internal field. This constitutes the 'condition for equilibrium *in the environment of the molecule*'. This case can be obtained by setting $\epsilon_3 = \epsilon$, $R = a$, and subtracting off the point dipole field. The resulting electric field inside the cavity is given by the sum of Eqs. (C11) and (C12),

$$\mathbf{E}_{Onsager} \;=\; \mathbf{R} + \mathbf{E}_{cav} \;=\; \frac{1}{a^3}\,\frac{2(\epsilon-1)}{(2\epsilon+1}\,\boldsymbol{\mu}' + \frac{3\epsilon}{2\epsilon+1}\,\mathbf{E}_0\,. \tag{C13}$$

APPENDIX D

PROOF OF THE CONVOLUTION THEOREM

There are two ways of expressing the convolution theorem. The first simply states that the Fourier transform of a convolution is the product of the Fourier transforms. The second states that the Fourier transform of a product is the convolution of the Fourier transforms. In considering the convolution theorem, one must first specify what is meant by a convolution and Fourier transform explicitly. Generally, the one dimensional convolution of two functions $f(x)$ and $g(x)$ is given by

$$(f * g)(x) \;=\; \int_{-\infty}^{\infty} f(x)\, g(u-x)\, dx\,, \tag{D1}$$

while the one dimensional Fourier transform of a function $f(x)$ is given by

$$\mathcal{F}\,[f(x)] \;=\; \tilde{f}(k) \;=\; \int f(x)\, e^{ikx}\, dx\,. \tag{D2}$$

The first statement of the convolution theorem can therefore be expressed mathematically as

$$\mathcal{F}\,[(f * g)(x)] \;=\; \tilde{f}(k)\, \tilde{g}(k)\,. \tag{D3}$$

It is to be assumed that the notation used on the left hand side of Eq. (D3) indicates that the Fourier transform $\mathcal{F}$ is to be taken after the convolution. The left hand side of Eq. (D3) can be expanded by explicitly computing the convolution and the Fourier transform. Doing this, one finds

$$\begin{aligned}
\mathcal{F}\,[(f * g)(x)] &= \mathcal{F}\left[\int_{-\infty}^{\infty} f(x)\, g(u-x)\, dx\right] \\
&= \int_{-\infty}^{\infty}\int_{-\infty}^{\infty} f(x)\, g(u-x)\, e^{iku}\, dx\, du \\
&= \int_{-\infty}^{\infty}\int_{-\infty}^{\infty} f(x)\, g(w)\, e^{ik(x+w)}\, dx\, dw \\
&= \left[\int_{-\infty}^{\infty} f(x)\, e^{ikx}\, dx\right]\left[\int_{-\infty}^{\infty} g(w)\, e^{ikw}\, dw\right] \\
&= \tilde{f}(k)\, \tilde{g}(k)\,.
\end{aligned} \tag{D4}$$

The second statement of the convolution theorem can be expressed as

$$\mathcal{F}\left[f(x)\,g(x)\right] \;=\; \tilde{f}(k) * \tilde{g}(k)\,, \tag{D5}$$

of which the left hand side is easily written as

$$\mathcal{F}\left[f(x)\,g(x)\right] \;=\; \int_{-\infty}^{\infty} f(x)\,g(x)\,e^{ikx}\,dx\,. \tag{D6}$$

The right hand side of Eq. (D5) can be written as

$$\begin{aligned}
\tilde{f}(k) * \tilde{g}(k) &= \int_{-\infty}^{\infty} \tilde{f}(k')\,\tilde{g}(k-k')\,dk' \\
&= \int_{-\infty}^{\infty} \left[\int_{-\infty}^{\infty} e^{ik'x}\,f(x)\,dx\right]\left[\int_{-\infty}^{\infty} e^{i(k-k')x'}\,g(x')\,dx'\right]\,dk' \\
&= \int_{-\infty}^{\infty} dx \int_{-\infty}^{\infty} dx'\,e^{ikx'}\,f(x)\,g(x') \int_{-\infty}^{\infty} dk' e^{ik'(x-x')} \\
&= \int_{-\infty}^{\infty} dx \int_{-\infty}^{\infty} dx'\,e^{ikx'}\,f(x)\,g(x')\,\delta(x-x') \\
&= \int_{-\infty}^{\infty} e^{ikx}\,f(x)\,g(x)\,dx\,.
\end{aligned} \tag{D7}$$

Thus, Eq. (D5) holds.

APPENDIX E

DERIVATION OF THE CORRECTION TERMS

1. Modified Dipolar Tensor

It can be shown [24], any interaction of the type given by the modified dipolar interaction tensor

$$\begin{aligned} \mathbf{T}_{\rm mod}(\mathbf{r}) &= a(r)\,(3\hat{\mathbf{r}}\hat{\mathbf{r}} - \mathbf{I}) + b(r)\mathbf{I} \\ &\equiv a(r)\mathbf{D}_{\mathbf{r}} + b(r)\mathbf{I} \end{aligned} \tag{E1}$$

has a Fourier transform given by

$$\tilde{\mathbf{T}}_{\rm mod}(\mathbf{k}) = \frac{4\pi}{3}\left[f_1(k)\tilde{\mathbf{D}}_{\mathbf{k}} + f_2(k)\mathbf{I}\right], \tag{E2}$$

where

$$\begin{aligned} f_1(k) &= -3\int_0^\infty dr\, r^2 j_2(kr)\, a(r) \\ f_2(k) &= 3\int_0^\infty dr\, r^2 j_0(kr)\, b(r)\,. \end{aligned} \tag{E3}$$

In terms of the longitudinal and transverse projection operators $\boldsymbol{\mathcal{J}}^L = \hat{\mathbf{k}}\hat{\mathbf{k}}$ and $\boldsymbol{\mathcal{J}}^T = \mathbf{I} - \boldsymbol{\mathcal{J}}^L$ Eq. (E2) can be written as

$$\tilde{\mathbf{T}}_{\rm mod}(\mathbf{k}) = \frac{4\pi}{3}\left\{\Lambda^L(k)\boldsymbol{\mathcal{J}}^L + \Lambda^T(k)\boldsymbol{\mathcal{J}}^T\right\}, \tag{E4}$$

where

$$\Lambda^L(k) = [2f_1(k) + f_2(k)] \tag{E5}$$

and

$$\Lambda^T(k) = [-f_1(k) + f_2(k)]\,. \tag{E6}$$

The electric field inside a dielectric medium can be written as in [24] as

$$\mathbf{E}(\mathbf{r}) = \mathbf{E}_0(\mathbf{r}) - \frac{4\pi}{3}\mathbf{P} + \int_V d^3r'\mathbf{T}(\mathbf{r}-\mathbf{r}')\cdot\mathbf{P}(\mathbf{r}')\,, \tag{E7}$$

where the volume V referred to on the integral corresponds to the entire volume excluding an infinitesimal spherical region surrounding the position $\mathbf{r}$. This region is accounted for by the polarization term in the equation. For a cavity carved into the dielectric, the polarization term vanishes and after taking the Fourier transform and using the convolution theorem the field inside a cavity can be written as

$$\frac{E_c}{E_0} = 1 + \hat{\mathbf{e}}_0 \cdot \tilde{\mathbf{T}}_{\mathrm{mod}} \cdot \tilde{\boldsymbol{\chi}}(\mathbf{k}, 0) * \hat{\mathbf{e}}_0 \,. \tag{E8}$$

Now, to derive an expression for the cavity field one simply needs to use the appropriate expressions for the dipolar tensor and generalized response function in Eq. (E8). At this point the rest is pretty much mathematics, but the expression given in Eq. (E8) can be simplified substantially by using the results from [25]. As has been shown, the response function can be written as

$$\tilde{\boldsymbol{\chi}}(\mathbf{k}_1, \mathbf{k}_2) = \delta_{\mathbf{k}_1,\mathbf{k}_2}\, \tilde{\boldsymbol{\chi}}_s(\mathbf{k}_1) - \tilde{\boldsymbol{\chi}}(\mathbf{k}_1)'' \Theta(\mathbf{k}_1 - \mathbf{k}_2) \tilde{\boldsymbol{\chi}}_s(\mathbf{k}_2) \tag{E9}$$

where

$$\tilde{\boldsymbol{\chi}}_s = \left(\frac{3y}{4\pi}\right) \left[S^L \boldsymbol{\mathcal{J}}^L + S^T \boldsymbol{\mathcal{J}}^T\right] \tag{E10}$$

and

$$\tilde{\boldsymbol{\chi}}'' = \frac{S^L}{S^L + 2A}\, \boldsymbol{\mathcal{J}}^L + \frac{S^T}{S^T - A}\, \boldsymbol{\mathcal{J}}^T \,, \tag{E11}$$

Thus, one needs in general two terms $E_s^{(0)}$, the so-called solvent-solvent term, and $E_s^{(1)}$, the solvent-solute term. These two terms lead to general expressions for the electric field and will provide a means of calculating a correction term for the field found from simulation data. The solvent-solvent term can be simplified by using the dipolar tensor and the solvent

response function,

$$\begin{aligned} E_s^{(0)} &= \hat{\mathbf{e}}_0 \cdot \tilde{\mathbf{T}}_{\rm mod} \cdot \tilde{\boldsymbol{\chi}}_s(0) \cdot \hat{\mathbf{e}}_0 \\ &= y\hat{\mathbf{e}}_0 \cdot \left[\Lambda^L(0) S^L(0) \boldsymbol{\mathcal{J}}^L + \Lambda^T(0) S^T(0) \boldsymbol{\mathcal{J}}^T\right] \cdot \hat{\mathbf{e}}_0 \\ &= y S^L(0) \Lambda^L(0) \\ &= \frac{(\epsilon - 1)}{3\epsilon} \Lambda^L(0)\,, \end{aligned} \tag{E12}$$

since for $\hat{\mathbf{e}}_0$ parallel to $\hat{\mathbf{k}}$, $\hat{\mathbf{e}}_0 \cdot \boldsymbol{\mathcal{J}}^L \cdot \hat{\mathbf{e}}_0 = 1$ and $\hat{\mathbf{e}}_0 \cdot \boldsymbol{\mathcal{J}}^T \cdot \hat{\mathbf{e}}_0 = 0$.

The solvent-solute term is a little more involved since there is a k-space integration that has to be taken into consideration. Generally,

$$\begin{aligned} E_s^{(1)} &= -\int \frac{d\omega_k\, d^3k}{(2\pi)^3} \hat{\mathbf{e}}_0 \cdot \left\{\tilde{\mathbf{T}}_{\rm mod}(\mathbf{k}) \cdot \tilde{\boldsymbol{\chi}}''(\mathbf{k}) \Theta(\mathbf{k}) \tilde{\boldsymbol{\chi}}_s(0)\right\} \cdot \hat{\mathbf{e}}_0 \\ &= -\frac{4\pi(\epsilon - 1) R_0^2}{9\epsilon} \int \frac{d^3k}{(2\pi)^3} \frac{j_1(kR_0)}{k} \left\{\frac{\Lambda^L S^L}{S^L + 2A} + \frac{2\Lambda^T S^T}{S^T - A}\right\}, \end{aligned} \tag{E13}$$

where we have used that $\Theta(\mathbf{k}) = 4\pi R_0^3 j_1(kR_0)/(kR_0)$ for a spherical solute of radius R_0 and that $\left\langle \hat{\mathbf{e}}_0 \cdot \boldsymbol{\mathcal{J}}^L \cdot \hat{\mathbf{e}}_0 \right\rangle_{\omega_k} = \frac{1}{3}$ and $\left\langle \hat{\mathbf{e}}_0 \cdot \boldsymbol{\mathcal{J}}^T \cdot \hat{\mathbf{e}}_0 \right\rangle_{\omega_k} = \frac{2}{3}$. The nice thing about the expressions given in Eqs. (E12) and (E13) is that once the expressions for Λ^L and Λ^T are known one can derive an expression for the field. For instance, for a cavity inside of an infinite dielectric one finds the modified dipolar tensor to be

$$\tilde{\mathbf{T}}^{\infty}_{\rm mod}(\mathbf{k}) = -4\pi \tilde{\mathbf{D}}_{\mathbf{k}} \frac{j_1(kR_0)}{kR_0}\,, \tag{E14}$$

and therefore $\Lambda^L(k) = -6j_1(kR_0)/(kR_0)$ and $\Lambda^T(k) = 3j_1(kR_0)/(kR_0)$ and therefore since $\int j_1^2(kR_0)dk = \pi(6R_0)^{-1}$ we have

$$\begin{aligned} \frac{E_c^{\rm cont.}}{E_0} &= 1 - \frac{2(\epsilon - 1)}{3\epsilon} - \frac{2(\epsilon - 1)^2}{3\epsilon(2\epsilon + 1)} \\ &= \frac{\epsilon + 2}{3\epsilon} - \frac{2(\epsilon - 1)^2}{3\epsilon(2\epsilon + 1)} \\ &= \frac{3}{2\epsilon + 1}\,, \end{aligned} \tag{E15}$$

where the $k \to 0$ expressions for S^L and S^T have been used.

For the case of the reaction field method the dipole-dipole interaction is truncated at some cutoff distance r_c and the neglected long-ranged interactions are approximated by the Onsager reaction field which is due to the interaction of a dipole with some continuum dielectric beyond the cutoff. In this case, the modified dipolar tensor is of the form

$$\mathbf{T}_{RF}(\mathbf{r}) = \left[\mathbf{T}_{\rm dip}(\mathbf{r}) + \frac{R_{RF}}{r_c^3}\right]\Theta(r_c - r)\Theta(r - R_0)\,, \tag{E16}$$

where $\Theta(r)$ is the Heaviside step function, the functional form of R_{RF} is

$$R_{RF} = \frac{2(\epsilon_{RF} - 1)}{2\epsilon_{RF} + 1}\,. \tag{E17}$$

Now, if we include a hard sphere type interaction, then the functions $a(r)$ and $b(r)$ can be replaced by

$$a(r) = r^{-3}\,\Theta(r_c - r)\,\Theta(r - R_0) \tag{E18}$$

$$b(r) = r_c^{-3} R_{RF}\,\Theta(r_c - r)\,\Theta(r - R_0)\,, \tag{E19}$$

where R_0 is the radius of the spherical shell in the hard sphere (HS) interaction potential. Integration of these functions according to Eqs. (E3) leads to expressions for $A(k)$ and $B(k)$ which are given by

$$\begin{aligned} f_1(k) &= 3\left[\frac{j_1(kr_c)}{kr_c} - \frac{j_1(kR_0)}{kR_0}\right] \\ f_2(k) &= \frac{3R_{RF}}{r_c^3}\int_{R_0}^{r_c} dr r^2\, j_0(kr) \\ &= 3\,R_{RF}\left[\frac{j_1(kr_c)}{kr_c} - \left(\frac{R_0}{r_c}\right)^3\frac{j_1(kR_0)}{kR_0}\right]. \end{aligned} \tag{E20}$$

Now, that we have $f_1(k)$ and $f_2(k)$ at hand we can calculate Λ^L and Λ^T and in turn calculate the modified dipolar tensor and the field inside the cavity. First, from Eqs. (E5)

and (E6), we see that

$$\Lambda^L_{RF}(k) \;=\; [2+R_{RF}]\,\frac{3j_1(kr_c)}{kr_c} - \left[2+R_{RF}\left(\frac{R_0}{r_c}\right)^3\right]\frac{3j_1(kR_0)}{kR_0}\,. \tag{E21}$$

and

$$\Lambda^T_{RF}(k) \;=\; -\,[1-R_{RF}]\,\frac{3j_1(kr_c)}{kr_c} + \left[1-R_{RF}\left(\frac{R_0}{r_c}\right)^3\right]\frac{3j_1(kR_0)}{kR_0}\,, \tag{E22}$$

so that the modified T-tensor is given by

$$\tilde{\mathbf{T}}_{RF}(\mathbf{k}) \;=\; \frac{4\pi}{3}\left[\Lambda^L_{RF}(k)\boldsymbol{\mathcal{J}}^L + \Lambda^T_{RF}(k)\boldsymbol{\mathcal{J}}^T\right]\,. \tag{E23}$$

2. Cavity Field Correction

In both the cases of a solute or a cavity, the expressions derived thus far can be used to calculate the electric fields inside of these objects. The only remaining task is to correct for the specific boundary conditions. In the cases presented here, we are typically concerned with the reaction field boundary conditions, but all the technology derived here can be directly used to find similar expression for the case of lattice sums. Using the expression given in Eq. (E12), we find the electric field due to the solvent is given by

$$E^{(0)}_s \;=\; \frac{(\epsilon-1)}{3\epsilon}\left[1-\left(\frac{R_0}{r_c}\right)^3\right]R_{RF} \tag{E24}$$

The expression for the solvent-solute part of the field given in Eq. (E13) leads to the equation

$$E^{(1)}_s \;=\; -\frac{2(\epsilon-1)^2}{3\epsilon(2\epsilon+1)}\left[1-\left(\frac{R_0}{r_c}\right)^3\right] \tag{E25}$$

where the integral $\int j_1(kR_0)j_1(kr_c)dk = \pi R_0(6r_c^2)^{-1}$ has been used. Now, the cavity field inside of an infinite dielectric and the field accessible in simulations are related through a correction term given by

$$\frac{E^{\rm sim}_c}{E_0} \;=\; \frac{E^{\infty}_c}{E_0} + E^{\rm corr}\,. \tag{E26}$$

Finally, after some simplification and subtracting off the cavity field inside of the dielectric (since we have basically included it from the beginning), the correction field used in the simulations is found to be

$$\begin{aligned} E^{\rm corr} &= 1 + E_s^{(0)} + E_s^{(1)} - \frac{E_c^\infty}{E_0} \\ &= \frac{2\epsilon_{RF}(\epsilon-1)}{\epsilon(2\epsilon_{RF}+1)} + \frac{2(\epsilon-1)}{3\epsilon}\left(\frac{R_0}{r_c}\right)^3\left[\frac{\epsilon-1}{2\epsilon+1} - \frac{\epsilon_{RF}-1}{2\epsilon_{RF}+1}\right], \end{aligned} \tag{E27}$$

If we set the dielectric constant in the reaction field equal to that of the simulation region, *i.e.* $\epsilon_{RF} = \epsilon$, then this equation reduces to only the first term

$$E^{\rm corr}(\epsilon_{RF}=\epsilon) = \frac{2(\epsilon-1)}{2\epsilon+1}. \tag{E28}$$

3. Local Field Correction

Starting with the expression for the f–factor, $f = 2\mu_{0s}/m_0^2$, in terms of the chemical potential μ_{0s} and the solute dipole moment m_0, we see that to calculate the the reaction field term in the total electric field acting on a dipole the formalism derived in [25] can be employed. In terms of the longitudinal and transverse components, the chemical potential is given by

$$\mu_{0s} = \frac{3}{2\epsilon+1}\left[\epsilon\mu_{0s}^L + \mu_{0s}^T\right], \tag{E29}$$

where

$$-\mu_{0s}^{L,T} = \frac{3y}{4\pi}\int\frac{d^3k}{(2\pi)^3}|\tilde{\boldsymbol{E}}_0^{L,T}(\mathbf{k})|^2 S^{L,T}(k) \tag{E30}$$

and

$$\begin{aligned} \tilde{\boldsymbol{E}}_0(\mathbf{k}) &= \tilde{\mathbf{T}}(\mathbf{k})\cdot\mathbf{m}_0 \\ &= \frac{4\pi}{3}\left[\Lambda^L(k)\boldsymbol{\mathcal{J}}^L + \Lambda^T(k)\boldsymbol{\mathcal{J}}^T\right]\cdot\mathbf{m}_0 \\ &= \tilde{\boldsymbol{E}}_0^L(\mathbf{k}) + \tilde{\boldsymbol{E}}_0^T(\mathbf{k}). \end{aligned} \tag{E31}$$

Thus, one can identify the longitudinal and transverse components of the k–space electric field as

$$\tilde{\boldsymbol{E}}_0^L(\mathbf{k}) = \frac{4\pi}{3}\Lambda^L(k)\boldsymbol{\mathcal{J}}^L\cdot\mathbf{m}_0 \tag{E32}$$

and

$$\tilde{\boldsymbol{E}}_0^T(\mathbf{k}) = \frac{4\pi}{3}\Lambda^T(k)\boldsymbol{\mathcal{J}}^T\cdot\mathbf{m}_0\,. \tag{E33}$$

For a hard sphere solute in an infinite system with the dipolar tensor given by Eq. (E14), one finds

$$\Lambda^L(k) = -\frac{6j_1(kR_0)}{kR_0} \tag{E34}$$

$$\Lambda^T(k) = \frac{3j_1(kR_0)}{kR_0}\,. \tag{E35}$$

These expressions lead to the components of the chemical potential given by

$$-\mu_{0s}^L = \frac{4ym_0^2}{\pi R_0^2}\int_0^\infty j_1^2(kR_0)S^L(k) \tag{E36}$$

and

$$-\mu_{0s}^T = \frac{2ym_0^2}{\pi R_0^2}\int_0^\infty j_1^2(kR_0)S^T(k)\,. \tag{E37}$$

This leads to the total chemical potential given in Eq. (E29),

$$-\mu_{0s} = \frac{6ym_0^2}{\pi R_0^2(2\epsilon+1)}\int_0^\infty dk j_1^2(kR_0)\left[2\epsilon S^L(k)+S^T(k)\right]\,. \tag{E38}$$

In the continuum limit, we find

$$-\mu_{0s}^{\text{cont.}}(k\to 0) = \frac{m_0^2(\epsilon-1)}{R_0^3(2\epsilon+1)}\,, \tag{E39}$$

which is the Onsager result. Therefore, since the solvation chemical potential is generally given by

$$\mu_{0s} = -\frac{1}{2}\mathbf{m}_0\cdot\mathbf{R}\,, \tag{E40}$$

one finds the f–factor is given by

$$f = -\frac{2\mu_{0s}}{m_0^2} = \frac{12y}{\pi R_0^2(2\epsilon+1)}\int_0^\infty dk j_1^2(kR_0)\left[2\epsilon S^L(k)+S^T(k)\right]. \quad \text{(E41)}$$

Now, if one uses the reaction field dipolar tensor given in Eq. (E23), one finds for the components of the chemical potential

$$-\mu_{0s}^L = \frac{2m_0^2(\epsilon-1)}{9\epsilon R_0^3}\left[1-\left(\frac{R_0}{r_c}\right)^3\right]\left[1+R_{RF}\left(\frac{R_0}{r_c}\right)^3+\frac{R_{RF}^2}{4}\left(\frac{R_0}{r_c}\right)^3\right] \quad \text{(E42)}$$

and

$$-\mu_{0s}^T = \frac{m_0^2(\epsilon-1)}{9R_0^3}\left[1-\left(\frac{R_0}{r_c}\right)^3\right]\left[1-2R_{RF}\left(\frac{R_0}{r_c}\right)^3+R_{RF}^2\left(\frac{R_0}{r_c}\right)^3\right]. \quad \text{(E43)}$$

Putting these expressions into Eq. (E29), one finds

$$-\mu_{0s}^{RF} = \frac{m_0^2(\epsilon-1)}{R_0^3(2\epsilon+1)}\left[1-\left(\frac{R_0}{r_c}\right)^3\right]\left[1+\frac{1}{2}\left(\frac{R_0}{r_c}\right)^3 R_{RF}^2\right]. \quad \text{(E44)}$$

Finally, the correction the f–factor can be found by subtracting off the infinite part from Eq. (E44). This leads to

$$\begin{aligned} f^{corr} &= (f_{RF}-f^{\text{cont.}}) \\ &= -\frac{2\left(\mu_{0s}^{RF}-\mu_{0s}^{\text{cont.}}\right)}{m_0^2} \\ &= -\frac{2(\epsilon-1)}{(2\epsilon+1)r_c^3}\left\{1-\left[1-\left(\frac{R_0}{r_c}\right)^3\right]\frac{R_{RF}^2}{2}\right\}. \end{aligned} \quad \text{(E45)}$$

APPENDIX F

SIMULATION PROTOCOL

The simulations were performed under the standard Metropolis Monte Carlo (MC) algorithm for a constant NVT canonical ensemble. The initial configuration was constructed starting from an FCC lattice of solvent hard-spheres of diameter σ and density $\rho^* = 0.8$. Then the hard-sphere solute/cavity was 'grown' in the center starting from an initial diameter of 0.5σ increasing the diameter at each step by 0.002σ, adjusting σ as to ensure constant density, and moving (orienting) the solvent hard-spheres (dipoles) according to the Metropolis algorithm. After the solute/cavity was constructed, the initial configuration was equilibrated for approximately $10^5 - 10^6$ steps in parallel (using OpenMPI) assuring that each processor started from a different point along the Markov Chain. The parallel part of the program was implemented by running the same MC program on different processors separately therefore making the communications between processors minimized. This way of running the parallel MC code assures a linear scaling for a fixed number of particles meaning that it takes ten times more time to generate 10^7 configurations then it does to generate 10^6 configurations. This implementation does not, of course, effect the overall N–scaling produced by the Reaction Field and Ewald geometries, but does allow for the production of many more configurations in a fixed amount of time assuming the availability of processors. To guarantee the preservation of the Markovian nature of the configurations between each processor, the random number generators used in the MC moves were seeded independently. The production runs were then performed on 10 processors per $(m*)^2$ per cavity size consisting of $(1-5)\times 10^6$ steps assuring adequate sampling of the phase space.